POLITECNICO DI MILANO

Dipartimento di Ingegneria Meccanica

Mechanical characterization and comparison between structural and free-cutting steels

Supervisor: Prof. Marco V. Boniardi

Co-Supervisor: Ing. Andrea Casaroli

Author:

Andrea Cardillo Matr: 899154

Academic year 2018/2019

Ringraziamenti

Un grazie di cuore ai miei genitori Simona e Giuliano per avermi permesso di raggiungere questo traguardo ed avermi sempre sostenuto.

Un ringraziamento particolare al mio relatore, il Prof. Marco V. Boniardi e al mio co-relatore, l'Ing. Andrea Casaroli, ma anche a tutti i collaboratori che mi hanno seguito durante il mio lavoro di tesi.

Ringrazio anche i miei ex-professori che hanno sempre creduto in me e soprattutto la Prof.sa Rizzolini, perché senza di lei quest'avventura non avrebbe avuto inizio.

Tra tutti i ragazzi conosciuti in università e con cui ho condiviso questi ultimi anni spicca sicuramente AJ che ci tengo a ringraziare per tutto il tempo passato insieme anche al di fuori dello studio.

Un ruolo fondamentale lo hanno avuto gli amici di sempre Benz, Mare, e Valerio perché con loro "non si molla mai un c***o!".

Infine, devo ringraziare Luca, Maldo e Monfre, perché senza di loro non avrei superato nemmeno il primo esame. Abbiamo formato un gruppo di studio per puro caso, ma è diventato molto di più. In questi anni abbiamo affrontato di tutto insieme, tra i vari "Io" da ritrovare, le pareti da scalare, gli strumenti da suonare, i droni da pilotare e quell'insensata voglia di capire quello che stavamo studiando, perché diciamolo, in fondo a noi le cose facili fanno un po' schifo.

Index

List of figures

List of tables

Sommario

Questo lavoro di tesi aveva come obiettivo la caratterizzazione meccanica e il confronto tra diversi tipi di acciaio, in particolare sono stati analizzati due acciai per impiego strutturale e quattro acciai automatici. Le prove meccaniche effettuate sono state scelte per ottenere le principali caratteristiche di resistenza meccanica, mentre le analisi chimiche e metallografiche sono servite per comprenderne la loro composizione e le strutture presenti. È quindi stato possibile confrontare i risultati ottenuti dai differenti materiali e gli effetti portati dall'aggiunta di elementi chimici necessari per conferire attitudini tecnologiche completamente diverse.

Parole chiave: acciai da costruzione; acciai automatici; caratterizzazione meccanica.

Abstract

This thesis work had as objective the mechanical characterization and the comparison between different kind of steels, in particular two structural steels and four free-cutting steels have been analysed. The mechanical tests performed have been chosen in order to retrieve the principal mechanical properties, while the chemical and metallographic analysis allowed to understand their effective composition and which structures were present. At the end, it was possible to compare the results obtained from different material and the effects derived from the addition of chemical elements, that have to provide to these materials completely different technological attitudes.

Keywords: structural steels; free-cutting steels; mechanical characterization.

1 Chapter 1

1.1 Steel metallurgy mentions

Steel is an iron alloy containing carbon till a concentration in weight equal to 2,11%, over this value of carbon concentration the alloy takes the name of cast iron.

The knowledge of the metallurgical structure that characterizes each type of steel takes a very important role in the designing phase, leading to the choice of the most appropriate material, also considering all the possible thermal treatments that can be used to enhance its characteristics. For this reason, it is appropriate to start with a recap of metallurgical mentions about this alloy.

In the Fe-C diagram the equilibrium structures of the iron carbon alloy are represented, for our purposes the attention can be focused on the alloys in which the carbon concentration belongs to the range that goes from 0,008% to 2,11% in weight.

Before entering in detail, a differentiation among phase and structural constituent must be done; the first one is referred to thermodynamics or equilibrium conditions, while the second one is referred to the structure and the characteristics of the alloy.

Looking at the diagram the phases that are present are:

- liquid phase;
- α-phase (stable till 912°C);
- γ-phase (stable from 912°C till 1394°C);
- δ-phase (stable from 1349°C till 1538°C);
- Fe_3C.

Instead, the structural constituents are:

- Ferrite, that is a solid solution of carbon in the α-iron (homogeneous grains of α-phase);
- Austenite, that is a solid solution of carbon in the γ-iron (homogeneous grains of γ -phase);
- δ-ferrite, that is a solid solution of carbon in the δ-iron (homogeneous grains of δ -phase);
- Cementite, that corresponds to the alloy Fe_3C with a carbon concentration of 6,69% in weight;
- Pearlite, that is the eutectoid ferrite-cementite;
- Ledeburite, that is the eutectic austenite-cementite.
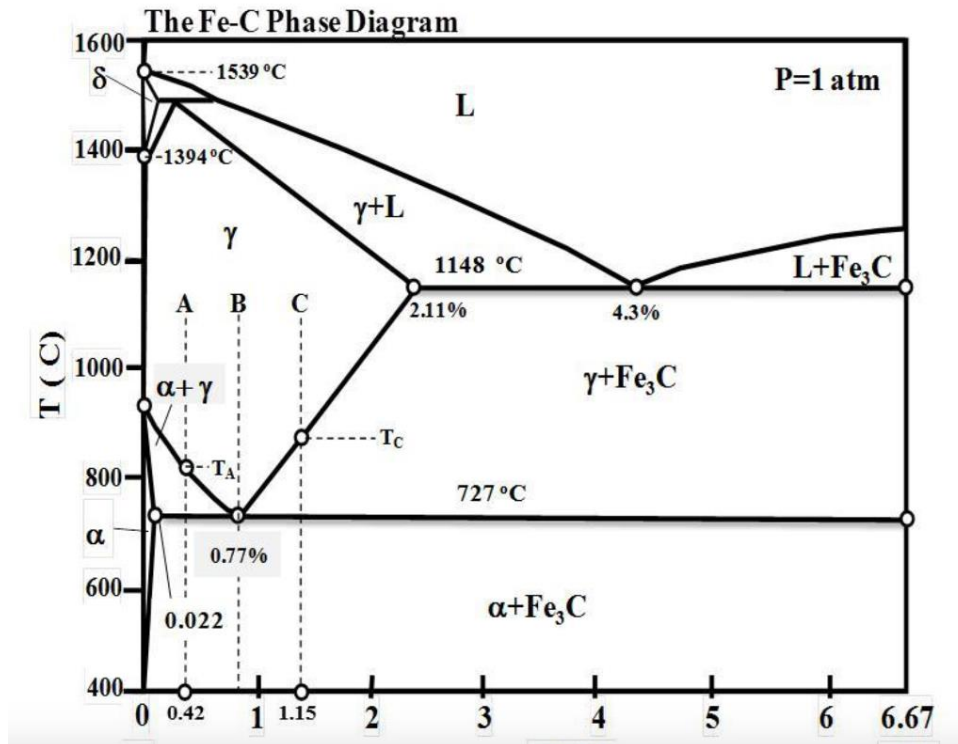
Figure 1 - Fe-C diagram.

Looking at the diagram, steels can be divided in respect to the carbon content present in the alloy having:

- hypoeutectoid steels (A), with a carbon content between 0,022% and 0,77%;
- eutectoid steel (B), with a carbon content equal to 0,77%;
- hypereutectoid steels (C), with a carbon content higher than 0,77% (lower than 2,11%).

In order to understand the differences among these three types, the structure that they present at ambient temperature must be considered. To do that let's see what happens to each of these alloys during the cooling from liquid to ambient temperature.

It can be seen that for every steel there is a temperature in which only γ-phase is present, so the part of the diagram above this point can be neglected, in which the liquid solidifies and the obtained solid structure changes until it is constituted only by austenite. Furthermore, it is better to start analysing the eutectoid steel in order to better understand what happens for the others.

1.1.1 Eutectoid steel structure

Considering a carbon content equal to 0,77% means dealing with the eutectoid alloy, this implies that after complete solidification, the structure is constituted only by homogeneous grains of γ-phase (austenite) up to an infinitesimal of degree above the eutectoid temperature (727°C). Cooling down the alloy, the structure undergoes a solid-state transformation and from an infinitesimal of degree under the eutectoid temperature, all the austenite transforms into lamellar grains, this structural constituent takes the name of pearlite.

Pearlite is formed by lamellar grains of α-phase lamellae alternated with lamellae of Fe₃C organized in different direction in each grain. This configuration guarantees a higher strength of the structure in respect to homogeneous grain.

1.1.2 Hypoeutectoid steels structure

Dealing with a steel characterized by a carbon content lower than 0,77% the structure obtained at ambient temperature is slightly different due to the excess in iron content in respect to the eutectoid alloy. The starting point is again a structure completely formed by austenite, but in this case, it must reduce the content of iron present in the γ-phase in order to reach the same concentration present in the eutectoid alloy. This is done by the segregation of homogeneous grains of α-phase, rich in iron, at the grain boundaries, obtaining so homogeneous grains of γ-phase surrounded by homogeneous grains of α-phase. The segregation goes on till an infinitesimal of degree above the eutectic temperature, then the solid-state transformation takes place and, from an infinitesimal of degree under this temperature, the structure is composed by pearlite surrounded by ferrite. As said before, lamellar grains are stronger than homogeneous grains, for this reason hypoeutectoid steels are not so strong and therefor easier to be machined.

1.1.3 Hypoeutectoid steels structure

In this latter case, with a carbon content higher than 0,77%, there is an excess of carbon in respect to the eutectoid alloy, so during the cooling the austenite must segregate plates of Fe₃C, that is the phase rich in carbon, at the grain boundaries. The segregation goes on till an infinitesimal of degree above the eutectic temperature, then the solid-state transformation takes place and, from an infinitesimal of degree under this temperature, the structure is composed by pearlite surrounded by cementite. This structure can seem similar to the previous one, but it isn't. In fact, we are no more dealing with homogeneous grains rich in iron, but with fine plates rich in carbon that are very hard. This is the reason why a higher carbon content leads to a higher strength of the steel.
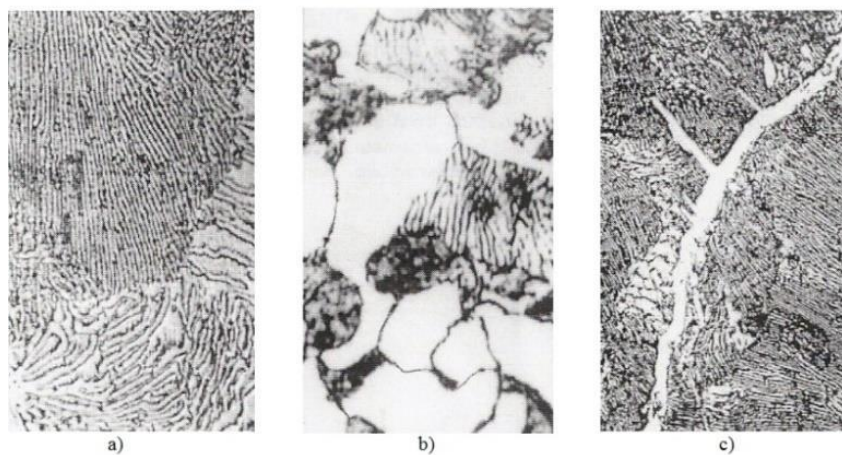
Figure 2 - a) pearlite 800x; b) pearlite & ferrite 500x; c) pearlite & cementite 500x.

As said before, steel is an alloy between iron and carbon, but at the end of the production process other chemical elements are generally present, that could be intentionally added or that are not easily removable from the steel. These elements have different effects on the phase diagram in relation to their concentration in the alloy. There are some elements, like: Ni, Mn; C; N and Cu, that cause the enlargement of the γ-phase field, reducing that of α-phase. On the contrary, other elements like Cr; Mo; V; Si; B; Al; P and Ti, tend to enlarge the α-phase field, reducing the γ-phase one. With a concentration of an element greater than the 12%, the diagram could become very different from the original one.

Usually some of these chemical elements can be added in order to enhance some properties of the steel, but there are also elements that are considered as pollutants due to their negative effects on the steel properties, such as S; P; O; H and N;

1.2 Steel designation

There are a lot of possible methods to classify all the existing types of steel present on the market, following the standard UNI EN 10027 we can divide them in two macro groups

1.2.1 Category 1

In the first group, steels are classified on the base of their purpose of use and their mechanical or physical characteristics. This designation is composed by a letter that indicates the type of steel and a number indicating a property, then can be eventually present other letters or numbers that are used in order to specify other characteristics of the material. Usually these materials are used without applying any particular thermal treatment and for static or quasi-static applications. They are characterized by a carbon concentration around 0,12-0,18% in mass and generally do not contain other alloying elements, however usually Mn is added in order to improve the toughness.

Table 1 - Designation for steels of the first group.

Category 1		
Application symbol	Mechanical property	Additional indications
S (structural steel)	Minimum yield strength	N (normalised)
P (steel for pressure lines and vessels)		C (cold worked)
		Q (quenched)
L (steel for pipe and tube)		JR (toughness >27J at 20°C)
E (engineering steel)		JO (toughness >27J at 0°C)
		J2 (toughness >27J at -20°C)
B (steel for reinforced concrete)		KR (toughness >40J at 20°C)
R (steel for rail use)	Minimum UTS	KO (toughness >40J at 0°C)
		K2 (toughness >40J at 20°C)
H (high tensile strength flat products)		LR (toughness >60J at 20°C)
		LO (toughness >60J at 0°C)
D (flat product for cold forming)		L2 (toughness >60J at 20°C)
T (tin-mill products)		
M (magnetic steel)		

1.2.2 Category 2

In the second group, steels are classified on the base of their chemical composition and divided in four subgroups: carbon steels; low-alloyed steels, alloyed steels and rapid steels.

Carbon steels are characterised by a content of Mn <1%, they are indicated by the letter C (carbon) followed by the carbon content multiplied by 100 (e.g. C40, contains 0.4 carbon).

Steels of the second subgroup are featured by a content of Mn >1% and a content of the other elements lower than 5%. They are indicated by a number that represents the carbon concentration multiplied by 100, followed by the symbols of the principal alloying elements and numbers that divided by proper factors will return their real concentration (e.g. 30NiCrMo4-2).

Table 2 - Characteristic factors for low-alloyed steels.

Chemical element	Factor
Cr, Co, Mn, Ni, Si, W	4
Al, Be, Cu, Mo, Nb, Pb, Ta, Ti, V, Zr	10
Ce, N, P, S	100
B	1000

The alloyed steels contain at least one alloying elements with a concentration higher than 5%. Their designation starts with X followed by the carbon content multiplied by 100, then there are the symbols of the principal alloying elements followed by numbers that indicate their real concentration (e.g. X5CrNi1810).

The last subgroup contains those steels that will undergo specific thermal treatment before being used, this allows to improve their properties thanks to the presence of the alloying elements. Their designation starts with HS (high speed), followed by numbers that indicate the concentration of the alloyed elements in this order: W; Mo; V and Co (e.g. HS18-0-1).

2 Chapter 2

This work concerns the mechanical characterization of different steel grades, that could be divided in two groups considering their designation.

2.1 Materials under study

In particular there are two structural steels (S235JR; S355J2) and four free-cutting steels (11SMn30; 11SMn37; 11SMnPb30 and 11SMnPb37).

2.1.1 Structural steels

These materials are generally used for static application, when particular characteristics are not required and the most important property is the strength of the steel. From the designation some mechanical properties of the material can be directly retrieved and then verified with different tests.

- S235JR: structural steel characterized by a minimum yield strength of 235 MPa and a minimum toughness of 27 J at room temperature;
- S355J2: structural steel characterized by a minimum yield strength of 355 MPa and a minimum toughness of 27 J at -20°C.

Considering that in these steels the presence of alloying elements is very low, the difference between their properties is primary due to the carbon concentration. We will see how the carbon content affects the results of the tests.

2.1.2 Free-cutting steels

While the first two were alloys of mainly iron and carbon, these materials are featured by the presence of other elements added in order to modify the behaviour of the steel during the manufacturing processes. The designation allows to see that they are low-alloyed steels, so with some alloying elements, but each of them with a concentration lower than the 5% in mass.

- 11SMn30: low-alloyed steel with 0,11% in mass of C, 0,3% in mass of S and Mn;
- 11SMn37: low-alloyed steel with 0,11% in mass of C, 0,37% in mass of S and Mn;
- 11SMnPb30: low-alloyed steel with 0,11% in mass of C, 0,3% in mass of S, Mn and Pb;
- 11SMnPb37: low-alloyed steel with 0,11% in mass of C, 0,37% in mass of S, Mn and Pb.

All these steels are featured by the addition of sulphur and lead; indeed, they are more or less the same material characterized by fairly different contents of these elements. The aim of our tests will be also to verify the effects, if any, of such different concentrations.

S and Pb are both added with the purpose of increasing the machinability of the steel and so to allow higher cutting speed. Free-cutting steels are indeed mainly used to produce small metal parts, like bolts, used in mass

production fields like automobile industry and household appliances. Increasing the cutting speed, it is possible to reduce the production time maintaining low the cost, that is an important factor for those small metal parts.

Lead is added to the steel because it doesn't take part in the solution, it remains at the grain boundaries absolving, thanks to its low melting point, a lubricating action on the tool during machining operations allowing higher cutting speeds.
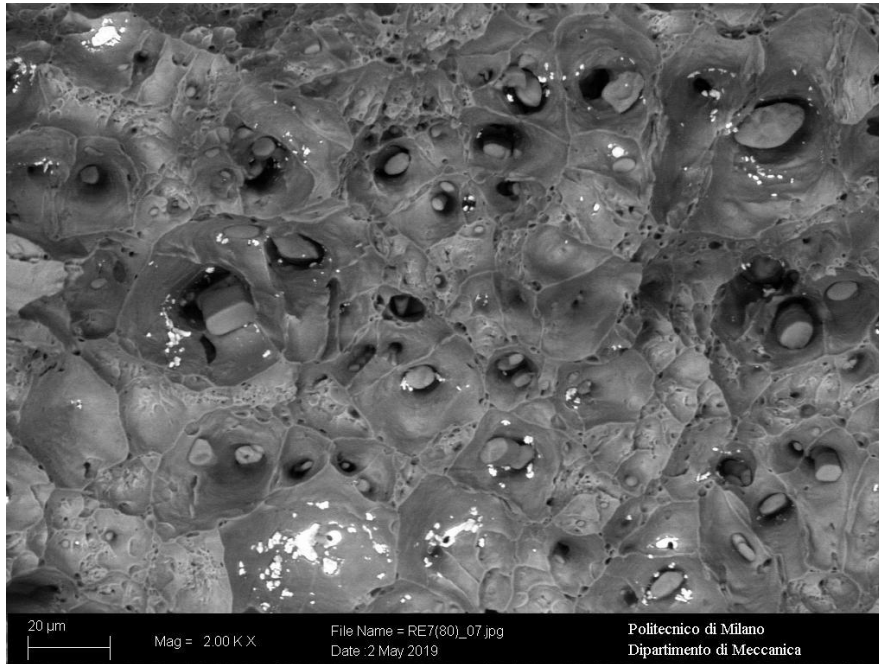
Figure 3 - Backscattered SEM image of 11SMnPb30.

In the figure, the lighter parts indicate the presence of lead in the material, it can be seen that it is easily distinguishable from the metal matrix that appears with an almost homogeneous grey colour.

Generally, sulphur is considered as a detrimental element due to the embrittlement caused by its presence in the steel, so during the steelmaking it is removed as much as possible. However, for the purpose of free-cutting steels, the presence of sulphur is important, because it forms manganese sulphides at the grain boundaries. These inclusions are very brittle in respect to the steel grains and during machining operations are useful for the chip breakage. Reduction of the chip's length means reduction in the friction on the tool surface, so leading to a lower consumption of the tool and possible higher cutting speed.

In order to obtain the proper content of sulphur and the desired effect on the material the procedure is a little bit complicated in respect to that of lead. The presence of sulphur in the metal bath at the beginning of a steelmaking process is due to its presence in the used raw materials. Its concentration is very high dealing with iron-ores and coke, so in case of a process that involves a blast furnace and converters, while it is lower when steel scraps are used, so in case of a process that involves an electric arc furnace. In any case the sulphur content must be kept under control, this harmful element has to be removed from the liquefied metal and, in case of free-cutting steels, it must be re-added to the steel bath at the end of the steelmaking process in order

to ensure its correct concentration and to be sure that it would form manganese sulphides and no other unwanted compounds.

2.2 Chemical analysis

Before starting with any test, chemical analysis has to be performed in order to be sure that the provided materials respect their designation in terms of chemical species and their concentrations.

To do that, a quantometer was used, that is an instrument able to recognize and quantify the presence of chemical elements in a specimen of the alloy under study exploiting the optical emission of the material.

Materials were provided in cold drawn bars from "Tre Valli Acciai s.p.a.", while reference value from chemical concentrations are reported by EN 10277-2/08 for structural steels and by EN 10277-3/08 for free-cutting steels.

Table 3 - Chemical composition.

Material	Designation	% C	% Si	% Mn	% P	% S	% Cu	% Pb
Structural steels	S235JR	0,102	0,0236	0,60	0,012	0,0068	0,32	-
	Reference	≤ 0,17	-	≤ 1,4	< 0,04	< 0,04	≤ 0,55	-
	S355J2	0,19	0,17	1,50	0,010	0,018	0,12	-
	Reference	≤ 0,20	< 0,55	≤ 1,60	< 0,030	< 0,030	≤ 0,55	-
Free-cutting steels	11SMn30	0,065	0,036	1,31	0,062	0,22	-	-
	Reference	≤ 0,14	< 0,05	0,9 - 1,3	< 0,11	0,27 – 0,33	-	-
	11SMn37	0,081	0,0070	1,62	0,072	0,29	-	-
	Reference	≤ 0,14	< 0,05	1 - 1,5	< 0,11	0,34 – 0,40	-	-
	11SMnPb30	0,084	0,0050	1,34	0,057	0,23	-	0,25
	Reference	≤ 0,14	< 0,05	0,9 - 1,3	< 0,11	0,27 – 0,33	-	0,2 - 0,35
	11SMnPb37	0,085	0,016	2,14	0,061	0,3	-	0,29
	Reference	≤ 0,14	< 0,05	1 - 1,5	< 0,11	0,34 – 0,40	-	0,2 - 0,35

Chemical analysis returns that for the free-cutting steels the quantity of manganese exceeds the interval recommended by the standard, it is a little bit higher than the maximum limit for each material apart for the last one in which we have a very high concentration. Instead, the sulphur's concentration is always a bit lower than the minimum recommended by the standard. These concentrations could derive from a choice and a consolidated method of this steelmaker that allows to have in any case the characteristic behaviour of a free-cutting steel during machining operations, but with lower general brittleness due to lower presence of sulphur and higher toughness due to a higher concentration of manganese. In fact, when the required concentration of S is higher, the difference between the actual quantity of Mn and the required one increases.

However, these differences from the standards in the chemical composition can be accepted due to the fact that manganese-sulphides are present, giving anyway their contribution during machining operations and the increased quantity of Mn will not affect negatively the mechanical properties, on the contrary it will return an higher toughness that will compensate the embrittlement caused by the presence of sulphur.

2.3 Metallographic analysis

After the chemical analysis, also metallographic analysis were done in order to detect the structures present in the materials, so testing the correct state after the production process.

All the materials were provided in bars as cold drawn, so without undergoing any thermal treatment exactly as they are generally used in order to make an analysis on samples that are as much as possible similar to the pieces that are industrially used. Bars were cut in small disks and for all of them the analysis was done for both the longitudinal and the orthogonal plane in respect to the drawing direction. These disks were incorporated in a resin cylinder of 40 mm in diameter to be easily handled during the polishing of the surface. Polishing is a mandatory operation for metallographic analysis because it allows to remove all the superficial defects. To see the metallographic structure of the material it is needed a planar surface without scratches or indentation that are for sure provided during cutting operations, for this purpose a sequence of abrasive papers was used decreasing gradually the dimension of the abrasive particles. Between one paper and the successive one the orientation of the sample must be changed in order to recognise with an optical microscope the scratches made during polishing and their direction, so assuring that with the finer abrasive the scratches made by the previous paper were completely removed. This is the sequence of papers used for this purpose, graded using the number of holes present in a linear inch for the sieve used to sort the abrasive particles: 120; 180; 320;800; 1200; 2500.

After the abrasive papers, the samples were polished using a synthetic cloth on which an abrasive in suspension with a particle size of 1μm was applied. This allowed to obtain a mirror finish that assured that the surface was completely free of defects.

Figure 4 - Metallographic specimens before (left) and after (right) polishing

To be able to see the metallographic structure this is not enough, before looking at the sample on the microscope, it has to undergo a chemical etching that allows to distinguish the different structural compounds. It has been done with a solution of alcohol (98%) and nitric acid (2%), that is able to oxidize the pearlite, making it recognizable from the ferrite.

Figure 5 - S355J2 longitudinal 500X.
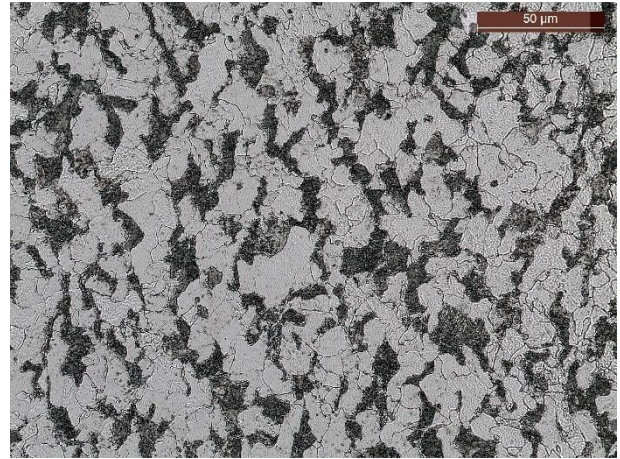
Figure 6 - S355J2 transversal 500X.

Both the structural steels present the same structure composed by ferrite (white grains) and pearlite (black lamellar grains), the only difference between the two materials lies in the ratio of these structural components that could be obtained looking at the Fe-C diagram. In fact, the S235JR presents a higher amount of ferrite and a lower amount of pearlite in respect to the S355J2 due to the lower carbon content present in the alloy.

Figure 7 - 11SMn30 longitudinal 500X.
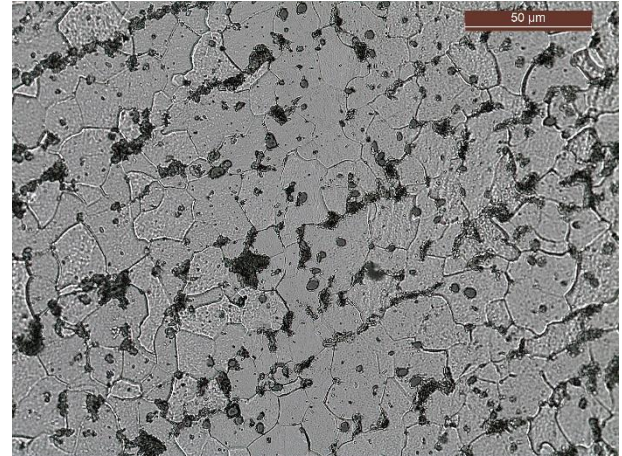
Figure 8 - 11SMn37 transversal 500X.

All the materials under study are hypoeutectoid steels, so also the free-cutting steels are mainly composed of ferrite (white grains) and pearlite (black lamellar grains), with manganese-sulphides as inclusions that can be seen as grey compounds, elongated in the longitudinal direction and almost circular in the transversal one.
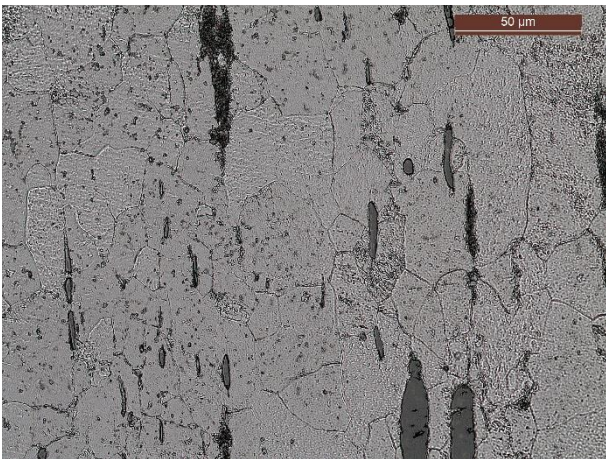
Figure 9 - 11SmnPb37 longitudinal 500X.
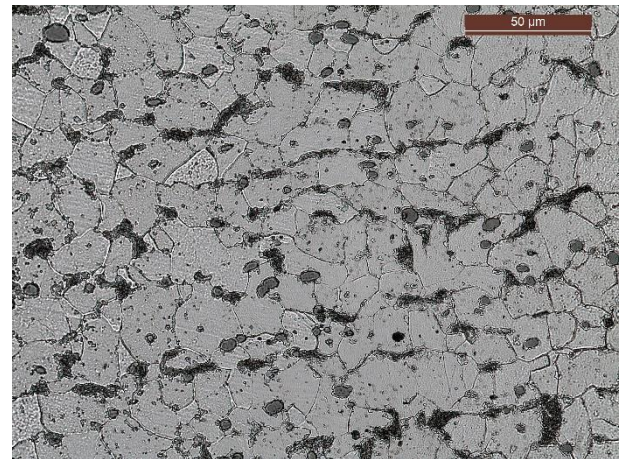
Figure 10 - 11SMnPb37 transversal 500X.

The free-cutting steels with the addition of lead present this element as scattered points all over the surface, but they are hardly detectable by metallographic images, it is easier to see them thanks to a backscattered acquisition with a scanning electron microscope or SEM (figure 3).

Due to the deformations applied during drawing operations, the structure of each material presents a preferential direction along the bar's axis, feature visible in the longitudinal section.
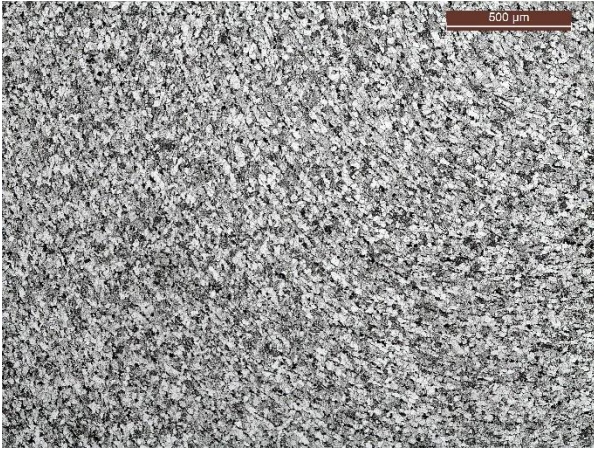
Figure 11 - S235JR transversal 50X.

Figure 12 - S235JR transversal 100X.

From the images taken at lower magnification it can be noticed that the deformations applied during cold drawing operations altered the structure orientation also in the transversal section of the bar.

In appendix A it is possible to see a series of metallographic pics, in order to compare directly the different steel grades analysed.

3 Chapter 3

Investigation methods for the identification of mechanical properties are of primary importance for the mechanical characterization of a material not only from the scientific point of view, but also considering all the checks and inspections needed for its applications. These methods are divided in two groups easily distinguishable that are the "destructive" tests and the "non-destructive" ones.

As the name says, the tests belonging to the first group are based on the destruction of a sample made by the material under examination, the breakage of this sample is needed in order to obtain a value for a specific mechanical property, the non-rupture of the specimen is considered as a fail for the test. In order to obtain comparable results, these tests must be done following standard prescriptions that provide all the conditions under which the test has to be executed, considering also the characteristics of all the used devices and the characteristics of the sample.

For what concerns the "non-destructive" methods, they are usually used directly on the final component in order to verify if the production process or a specific treatment has been successful. These tests are not only used to calculate some mechanical properties related to the material, but also to detect internal or very small defects that should affect the resistance of the piece.

During this characterization some investigation methods were used for all the materials under study in order to obtain an almost complete overview of the behaviour and capabilities of these steel grades under different points of view.

Destructive methods:

- tensile test;
- Charpy pendulum impact test;
- rotating bending fatigue test.

Non-destructive methods:

- Vickers hardness test.

3.1 Fracture analysis

Before analysing in depth the different methods, it is important to understand how the different materials behave during these tests and what is possible to deduce, besides the provided numerical results, looking at the specimen after its breakage.

Fracture is that phenomenon caused by a too high load sustained by the piece in respect to its resistance in that condition and consists macroscopically in the separation in two or more scraps. It results from the rupture of the bonds present between the atoms, that constitute the structure of the material, due to the energy provided by the external load applied to the specimen.

In mechanical applications there are many different types of load at which a component can be subjected to, they can differ in terms of action applied to the piece, like in case of tensile loads rather than torsional loads, or in terms of speed of application like in case of stationary loads rather than alternated loads or impacts.

Different loads applied to the same piece can cause different fracture modality, the result depends on the behaviour of the material structure when it is subjected to such excitation. Steels can exploit two different kind of fracture modalities: ductile fracture and brittle fracture. In general, the specimen can present both the two types of fracture at the same time according to the applied loads.

3.1.1 Ductile fracture

This type of failure is featured by plastic deformations of the component before the complete breakage, that are the macroscopic result of the dislocation's movement at microscopic level. It is an index of high toughness of the material because it is characterized by a high absorption of energy from the component before its breakage. The plastic deformation allows to have a "warning" before the complete failure, this can be an important factor in several occasions in order to avoid dangerous accident that could involve operators or other people.
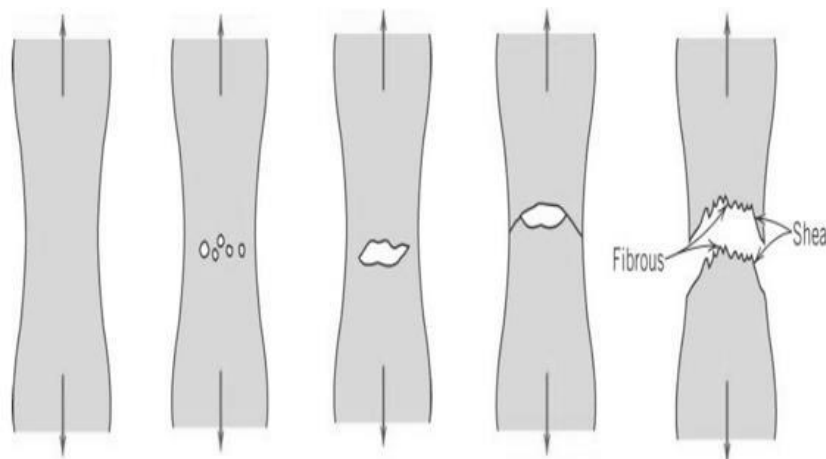
Figure 13 - Ductile fracture failure mechanism

In the figure it can be seen the ductile behaviour of the specimen at which a monoaxial tensile load is applied. The initial deformation lays in the elastic region, it means that the applied load is not able to break the links between the atoms and so to move the dislocation inside the structure. This deformation is called elastic due to the capability of the material to recover it when the load is removed. Increasing the load, dislocations' movement starts, causing plastic irreversible deformations that bring to the first stage of the failure consisting in the necking of the section. Dislocations' movement stops in correspondence of microstructural discontinuities and their grouping causes micro voids in the metallic structure. When these voids increase in number and dimensions, they coarse in a real tear in the specimen that would decrease its resistant area. The load exerted on the remaining material surrounding this tear increase again leading to its enlargement till the complete shearing that takes place along a plane inclined by 45° in respect to the loading direction.
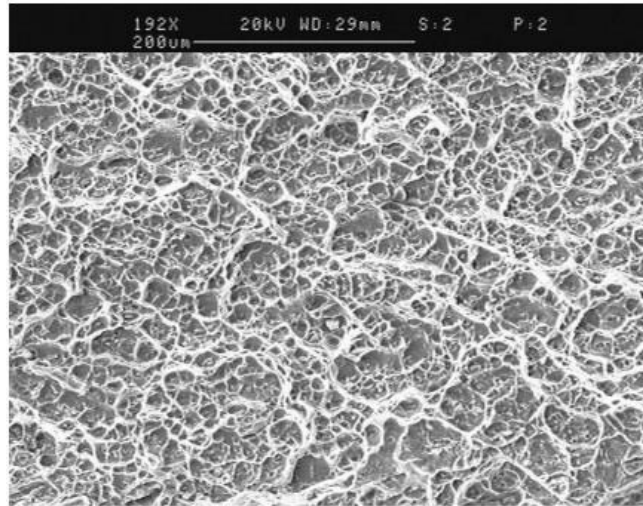
Figure 14 - Ductile fracture surface 190X

In the image are visible the "dimples", that are the characteristic feature of a ductile fracture. Dimples are the almost circular micro voids that appear on the surface in consequence of the tearing of the material. The shape depends on the deformation direction, it is symmetrical when the material flows only in the direction in which the load is applied.

3.1.2   Brittle fracture

On the other side there is the brittle fracture, that occurs without any macroscopic deformation. In fact, in case of brittle failure it would be possible to "reconstruct" the specimen simply putting together the scraps. This kind of failure occurs when the dislocations' movement is prevented, it could be due to factors depending on the microstructure of the material, but also to the conditions under which the load is applied.

There are two types of brittle fracture in the microscopic field: trans-granular and intergranular.

Macroscopically, the brittle fractures appear the same, but looking at the grain structure it can be possible to distinguish them.
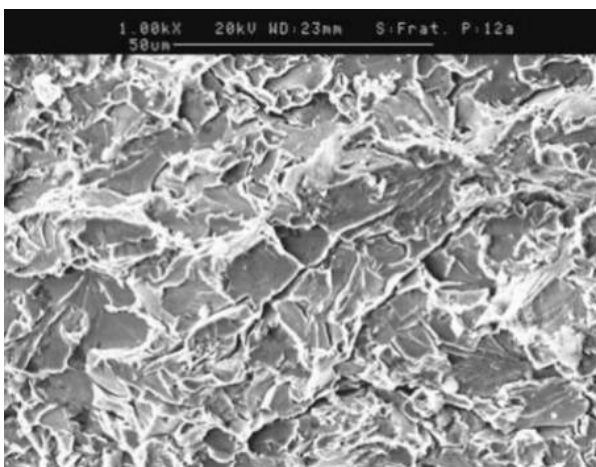
Figure 15 - Trans-granular fracture 1000X
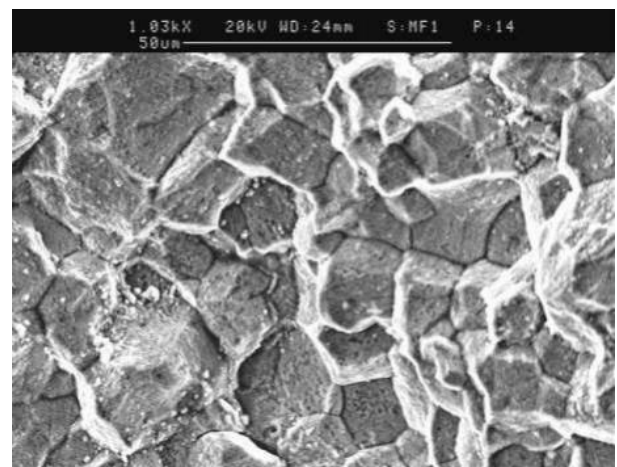
Figure 16 - Intergranular fracture 1030X

From the two pics above it can be seen the difference between the two kind of brittle fracture. The intergranular one presents a well-defined grain delimitation due to the fact that the crack propagates along the grain boundary, while in the trans-granular fracture the crack propagation happens into the grain along a metallographic plane till reaching the grain boundary and then in the next grain following its microstructure along another metallographic plain.
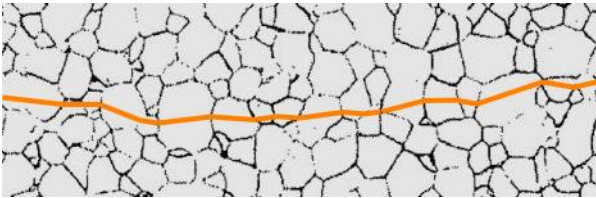
Figure 17 - Crack propagation in trans-granular fracture
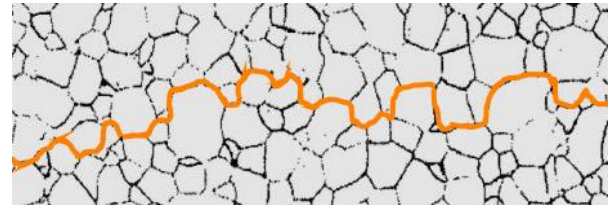
Figure 18 - Crack propagation in intergranular fracture

The intergranular fracture is typical of materials subjected to embrittlement phenomenon that tends to decrease the resistance of the atomic bonds in correspondence of the grain boundary, that in general is the part of the microstructure with the highest binding energy and so where it is more difficult to have crack propagation.
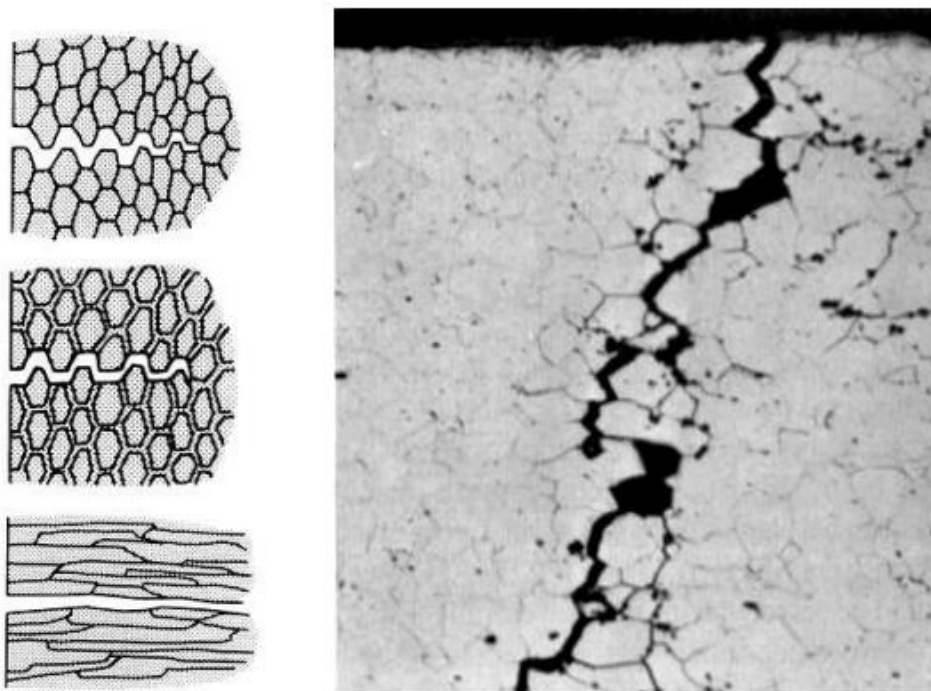
Figure 19 - Intergranular fracture appearance

For this reason it is not so common to have intergranular fractures, due to the fact that something has to occur to the piece in order to reduce the resistance of the bond between grains, as in case of chemical etching, but this could be not sufficient if the produced defect doesn't reach a certain deep in the specimen.
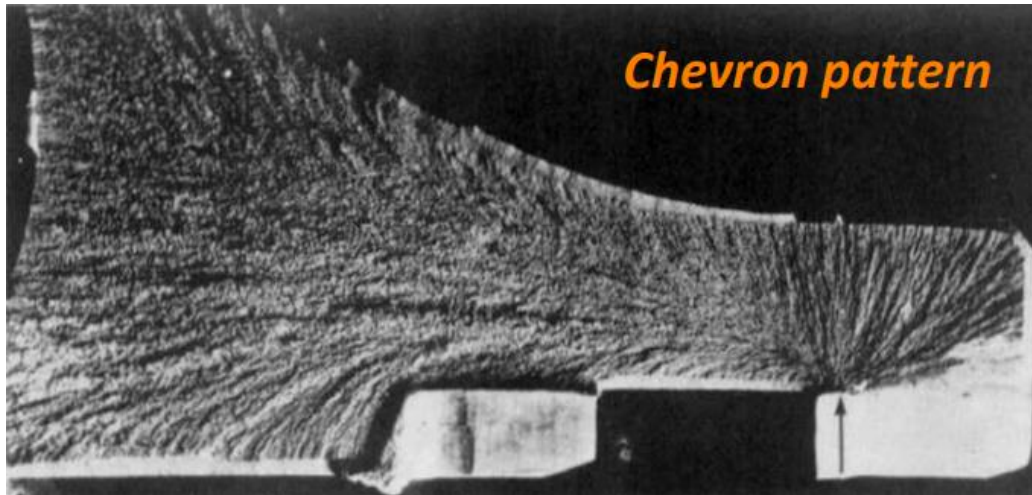
Figure 20 - Brittle failure of a component

As said before, brittle failure happens suddenly, without any macroscopic deformation, precisely the crack propagation happens at the velocity of sound in the same material. On the piece it can be observed the initiation point of crack propagation, one or more. This is due to the fact that cracks start from defects or discontinuities both of the material and of the component and then propagate. The dimension of the defect or the type of discontinuity able to become an initiation point for a crack depends on the extent of the applied stresses. With higher stresses the minimum critical dimension for a defect decreases and every little discontinuity in the piece or in the microstructure can laid to a brittle failure.

Besides the characteristics of the material that could make it brittle, also the conditions under which the load is applied have an important role, two conditions in particular are considered: temperature and speed of application.

The temperature at which the load is applied to the sample, like that at which the component is normally used, can change the behaviour of the material. In fact, it could be that testing a material at room temperature with a certain load result in a ductile fracture and testing the same material with the same load but at a lower temperature it results in a brittle fracture. This is due to the fact that at low temperatures the dislocations movement is prevented and, as said before, brittle fractures happen in this situation. The level of temperature at which a material starts to behave in a brittle way depends on the material itself.

The speed of application of the load acts in the same way of the temperature, enabling the movement of the dislocations. In reality, in this case the dislocations movements are not prevented, but when the speed of application is very high, like in case of an impact, the speed at which dislocations move is negligible and it is as if they were blocked.

3.2 Tensile test

This is one of the most important and so one of the most used tests, it is done in order to evaluate different characteristics of a material, as strength, deformability and elasticity. The related standard is the UNI EN ISO 6892-1.

Results obtained from the tensile test can be used to evaluate the state of the material under study and are commonly used during designing phase of a component as in the feasibility analysis for a technological process or as well during activities of "Failure Analysis".

The test consists in the application of a quasi-static monoaxial tensile load to a specimen increasing its value until the complete breakage. The specimen must respect exactly the standard in terms of geometry, dimensions and surface finish in order to obtain uniform and comparable results.

3.2.1   Test machine

It is constituted by a fixed structure and a moving part. The fixed structure is composed of a base in which takes place the control system, then there are the fixed traverse beam and two columns that act as a guide for the moving part. The other traverse beam constitutes the moving part of the machine, it moves along the two columns. The motion can be generated by an electric motor that puts in rotation the two columns and thanks to ball-screw connections is able to shift the mobile traverse, or by hydraulic actuators acting directly on the mobile traverse. Each traverse is equipped with jaws that allow to handle the sample during the application of the load. To measure the applied load, a load cell is placed in series to the specimen and to measure the elongation an extensometer is applied to the sample during the test, although the machine itself is equipped with a system that control the displacement of the moving crosshead.

Figure 22 - Control devices for a tensile test

Figure 21 - Schematic of a tensile test machine

3.2.2 Specimens

As said in advance specimens must respect standards imposed by the UNI EN ISO 6892-1, this allow to carry out the test every time in similar conditions and so to obtain results that are comparable between several tests but also between different materials. Usually the specimen is circular, but in case of plates or flat products in general there is also the possibility to use a rectangular sample. In any case the sample is usually characterised by two wider sections at the ends, that are the parts that will be inserted in the jaws. The central section has a thinner constant section and the transition parts between the sections must be as gradual as possible. All these features are studied and applied in order to assure that the breakage occurs in the central part of the specimen. In fact, in case of very small specimen, where also the force applied by the jaws could alter the obtained results, particular grips are used coupled with specimens that present threaded endings.
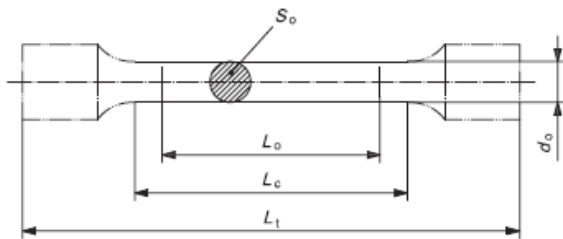
Figure 23 - Circular specimen for tensile test
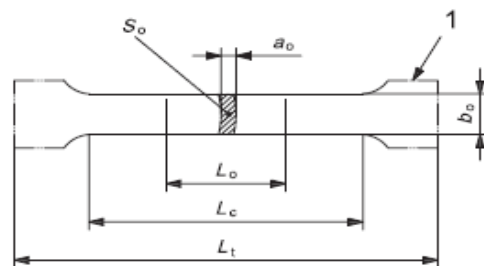
Figure 24 - Rectangular specimen for tensile test

The fundamental characteristic for these specimens is the length L_0 that can be calculated using the following formula:

$$L_0 = k \cdot \sqrt{S_0}$$

L_0 is called "original gauge length" and it is used to calculate the elongation reached at the end of the test, while S_0 is the "original cross-sectional area" of the parallel length L_c. "K" is a constant given by the standards, as for the relation between L_0 and L_c, because it depends on the considered type of sample.

The original gauge length is of great importance because in order to retain valid the test, the fracture has to occur within this section of the specimen. It is also the section at whose ends has to be applied the extensometer, for these reasons its length and its position are very important. Before the test, L_0 is marked with a pen and divided in intervals of 5-10 mm that are used to evaluate the elongation at the end of the test.

3.2.3 Analysis of the tensile test

The result provided from this test is the stress-strain curve, obtained coupling data registered by the load cell and the extensometer. The shape of the curve depends on the tested material, but it is possible to divide it in: elastic deformations region; plastic deformations region; necking and breaking.
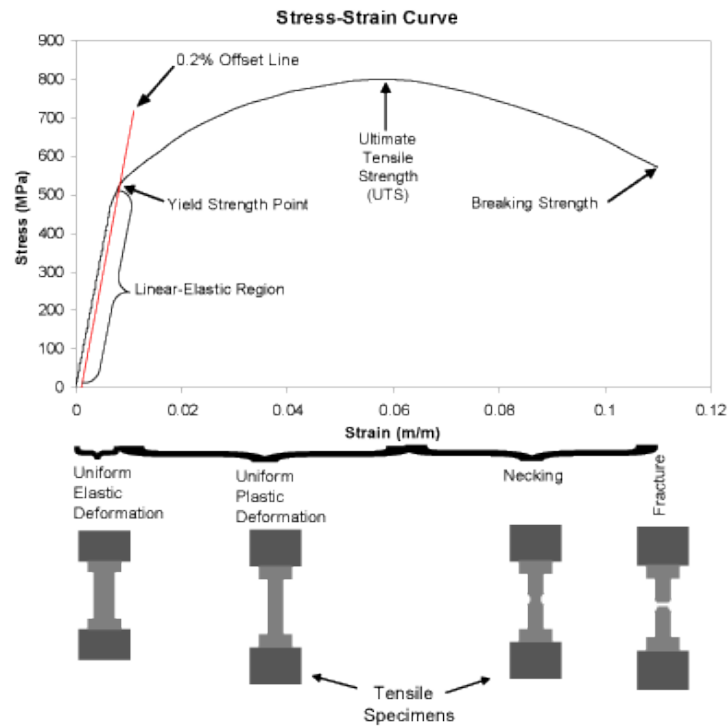
Figure 25 - Stress-strain curve

In the first part the slope of the curve is constant, its value is given by the elastic modulus E of the material, in fact this interval represents the elastic behaviour of the material. Here the deformations are considered reversible, so removing the applied load the specimen will return to its initial length. In reality, the deformation to which the microstructure is subjected in this region are not completely reversible but are evaluated with a maximum value equal to the 0,001% of the initial length, so are considered negligible.
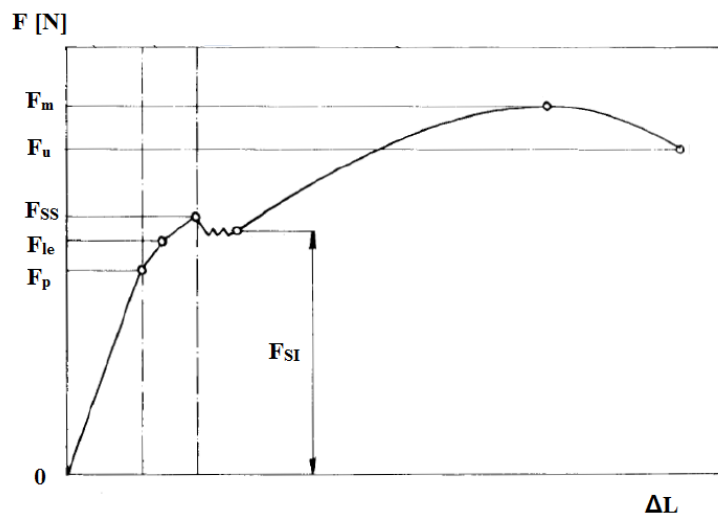
Figure 26 - Force-elongation diagram

This behaviour takes place till the limit proportional load F_P, exceeding this value the speed of deformation starts to increase in respect to the speed of application of the load, leading to non-reversible deformations. This is the elastic-plastic region where the curve is no more linear but removing the load the length of the specimen

will return almost to its initial value. The elastic plastic region continues till the higher yield strength value F_{SS} but from the elastic limit value F_{le} the curve starts to depart a lot from the linear behaviour. Yielding is that phenomenon in which the material undergoes through a deformation keeping constant the applied load. In the graph it is clearly detectable, it starts with the decreasing of the load due to a sudden deformation and goes on with a "plateau" abound the lower yielding value F_{SI}. Not all the materials present a so well-defined yielding area, in those cases there is a method used to calculate the yielding stress value considering the value of stress that imply a deformation of the 0,2% called R_{p02}, this method is also used in case of brittle materials.
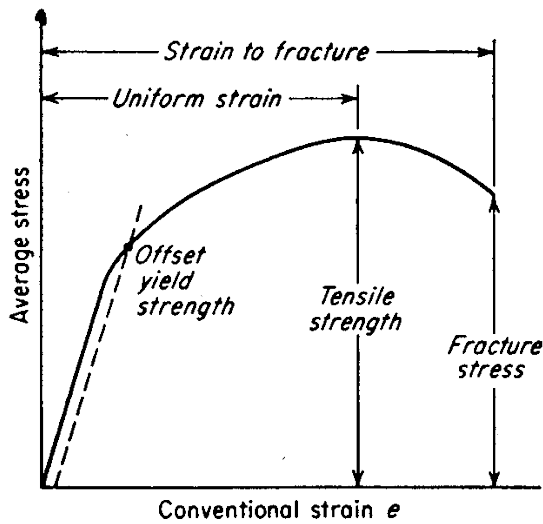
Figure 27 - R_{P02} method
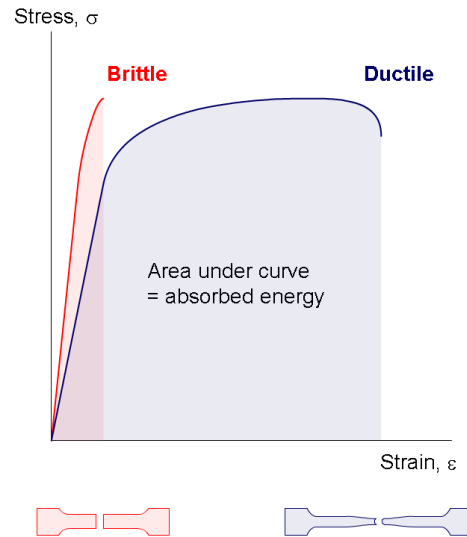
Figure 28 - Brittle vs ductile material

Continuing from F_{SI} the curve presents an increasing of the load, this is due to the strain hardening phenomenon due to the grouping of the dislocation within the crystallographic structure that reduces their mobility. The applied load increases till the maximum value F_M corresponding, considering the nominal section of the sample, to the ultimate tensile stress UTS in the stress-strain diagram. From this point the necking phenomenon takes place, that brings the sample to the complete fracture. It consists in the sudden reduction of the specimen's transversal section in a specific point and no more along all the length of the specimen. The point in which the necking happens is random, but for a well-done test it must belong to the central section of the sample. The breaking load F_U corresponds to the ultimate load value applied to the sample before its breakage, the correspondent stress R_U is calculated considering the original section S_0 and not that one subjected to the necking phenomenon, for this reason the last part of the curve has a descendant parabolic profile. In reality, using the effective section, the applied stress tends to increase, but the so called "engineering curve" is preferred for designing purposes for safety reasons.
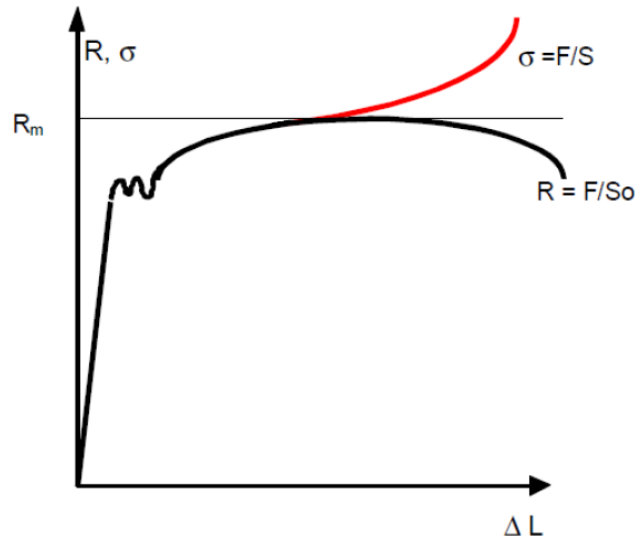
Figure 29 - True (red) vs engineering (black) curve

3.2.4 Tensile test resulting properties

As said before, there are many properties of engineering interest that could be retrieved from this test:

- Elastic modulus E [MPa]

  It can be calculated from the elastic region of the curve using the Hook's law

$$\sigma = \frac{F}{S_0} \quad \text{with} \quad F < F_P \quad \rightarrow \quad E = \frac{\sigma}{\varepsilon}$$

- Yielding strength σ_Y or R_{P02} [MPa]

$$\sigma_Y = \frac{F_S}{S_0} \; ; \qquad R_{P02} = \frac{F_{P02}}{S_0}$$

- Ultimate tensile strength σ_{UTS} or R_m [MPa]

$$\sigma_{UTS} = \frac{F_M}{S_0}$$

- Elongation at break A

$$A\% = \frac{L_F - L_0}{L_0} \cdot 100$$

- Necking coefficient Z

$$Z\% = \frac{S_0 - S_F}{S_0} \cdot 100$$

(where 0 means the initial condition and F the final one, after the break)

3.3 Charpy pendulum impact test

This test is very important for designing purposes because it returns an index of the toughness of the material. Toughness is the attitude of a material to absorb energy when subjected to impulsive loads like in case of an impact.

This test follows the standard UNI EN ISO 148-1 for what concerns the machine and the specimen characteristics, the obtained numerical result corresponds to the energy dissipated by the sample during the impact. This value is comparable only with other samples of the same material, in order to see when it has a brittle or ductile behaviour dependently on the conditions under which the test is done. Between different materials, the only thing that can be compared is the transition temperature in order to detect which material is the best for a certain situation.

The test consists in breaking the sample with a unique impact, so if the specimen doesn't break the test is not valid. Impact is provided by an oscillating pendulum on a rectangular sample engraved in a proper way in order to facilitate the fracture.

3.3.1 Test machine

The machine used for this test is the Charpy's pendulum, that takes his name from the french engineer, Augustin Albert Charpy, who invented the test in the 1905. It is composed by a heavy basement, made in cast iron, that sustains a frame at which a rod is connected by means of a pin joint. The pendulum consists in a rod with a mass fixed at the end. This mass has a precise geometry that allow to hit the sample in the correct way, all the characteristics are provided in the standard of the test.
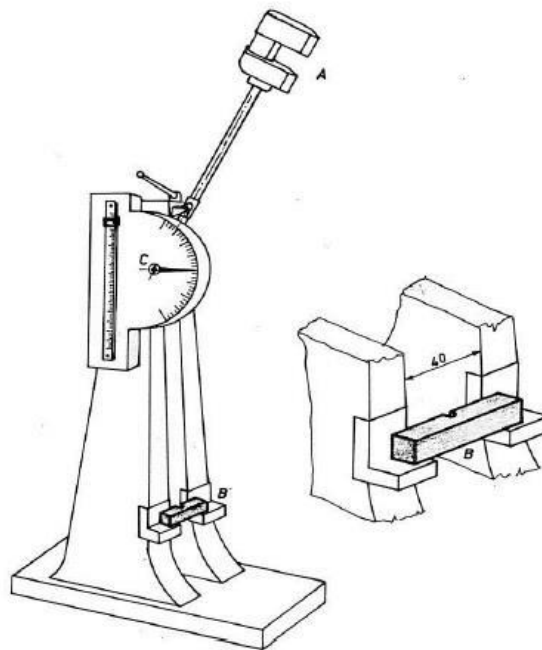
Figure 30 - Charpy pendulum

3.3.2 Specimens

There are essentially two kind of specimens for this test, it depends on the geometry of the carving present on it that could be a "V" type or a "U" one.
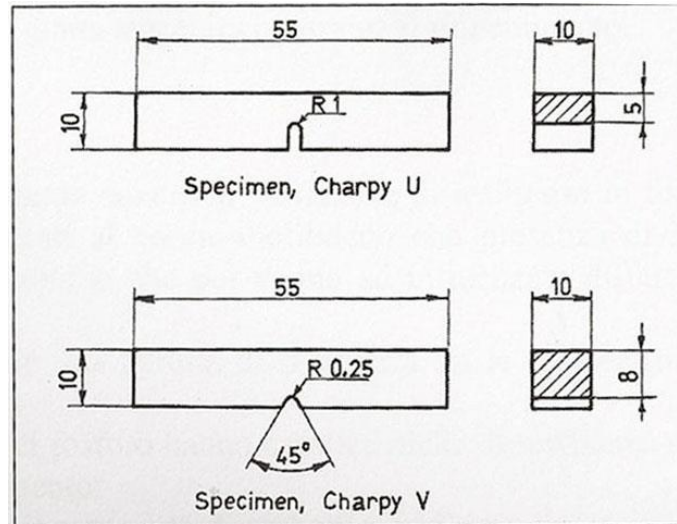
Figure 31 - Charpy specimens

Both are characterized by a square section with a side of 10 mm and by a length of 55 mm. The engraving is placed in the middle of the sample and it is usually obtained by milling. The type of specimen depends on the characteristics of the material under study, there are also specimens with other standardized dimensions, but those reported above are the most used.

3.3.3 Analysis of the test

The procedure for this test is very simple, it starts bringing the pendulum to its top position, positioning the specimen on its support and then leaving the pendulum that impacting against the specimen will transfer him part of its energy.
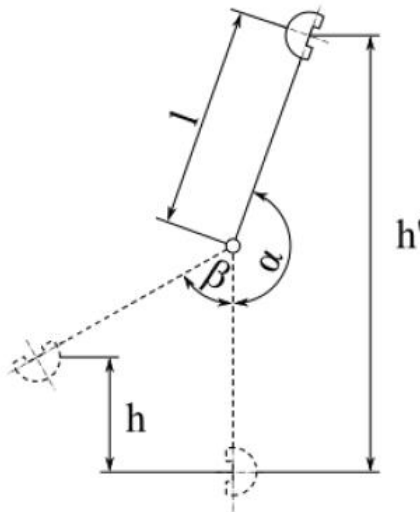
Figure 32 - Schematic of a Charpy pendulum

When the hammer is in its top position (h') it has a potential energy equal to 300 ± 10 J, leaving it free it would transform it in kinetic energy till the moment in which it will impact the specimen. At this point the pendulum moves with a speed equal to 5 m/s, the impact would deform and break the sample, the higher the deformation the higher the amount of energy dissipated (K) during the impact. This value of energy can be calculated using the maximum height (h) reached by the hammer after the impact, point in which the hammer has again only potential energy.

$$K = (m \cdot g \cdot h') - (m \cdot g \cdot h)$$

In the formula above the energy absorbed by the specimen K [J] is calculated considering the difference of the potential energy owned by the hammer before and after the impact, where "m" is the mass of the hammer in kg, "g" is the gravity acceleration in m/s^2, "h'" and "h" are the maximum heights of the hammer respectively before and after the impact in m considering as reference the position of the specimen.

This test is in appearance very simple due especially to the speed of execution and the relatively easy calculation standing behind the result. In reality, there are a lot of critical issues that could affect the results and must be taken into account, as the type of engraving on the sample, but also the method used to obtain it. From literature it is confirmed that the Charpy pendulum test cannot provide any quantitative indication for designing purposes, the obtained results must be used in a qualitative way to understand the behaviour of a material at a certain temperature subjected to impulsive stresses. An interesting result obtainable is the presence or not of a transition in the behaviour of the material as the temperature of the specimen decreases.

Most of the used steels are characterized by a body centred cube (BCC) structure that shows a sharp decline of the absorbed energy when the temperature decreases. This feature brings to a transition from a ductile behaviour, with higher energy absorption, to a brittle one, with lower amount of absorbed energy.
There are other materials characterized by a face centred cube (FCC) structure that doesn't show such transition in its behaviour. In this case the amount of absorbed energy is almost the same despite the

lowering of temperature. It doesn't mean that a material presenting a FCC structure is better than one with a BCC one, it depends from the conditions in which these materials has to be used.

The ductile-brittle transition temperature (DBTT) curves are those curves that show the results obtained by varying the temperature during the Charpy pendulum impact test on a material, in the following figure is clearly visible the drop in the value of absorbed energy in correspondence of the transition temperature in case of BCC structures. These curves are used during the designing phase in order to detect the possible materials for a determined situation, considering the temperature under which the component has to operate and the behaviour that it has to show. In some cases it is needed a material that also at very low temperature maintains high toughness values, but in other situations it would be better to have a material that shows a brittle behaviour, so it can break without important deformations that could damage other components.
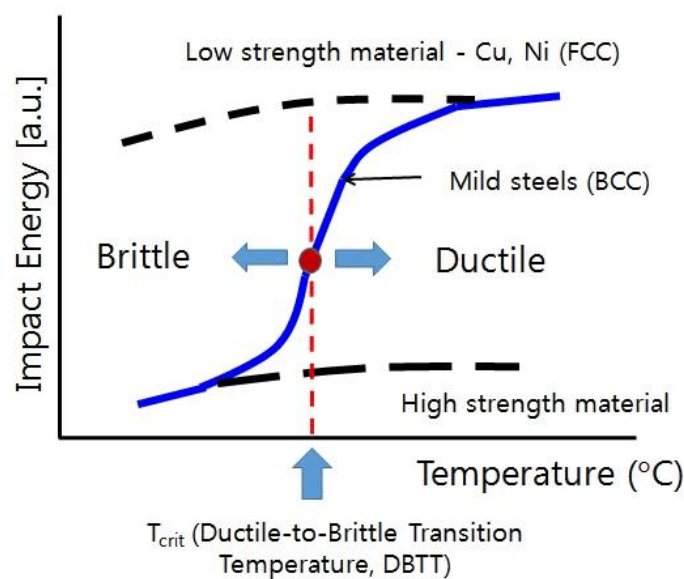
Figure 33 - DBTT curve

As it can be seen from the diagram above, the presence of a FCC structure doesn't mean higher values of absorbed energy and these values are usually inversely proportional to the strength of the material.

3.4 Fatigue test

3.4.1 Fatigue phenomenon

Mechanical components are usually subjected to variable loads repeated in time that can bring to its fracture even with a much lower value of applied stress in respect to the static limit of the material. This phenomenon takes the name of "fatigue" and consists in a progressive damaging of the material that starts at a microscopic level and extends progressively till reaching defect dimensions that can bring to the complete fracture of the component. Studies on the fatigue phenomenon started in 1800, first interesting results relating applied stresses and life of the component were obtained in 1850 by August Wöhler (Wöhler's curves).

Statistically about 75% of fractures in mechanical components are caused by fatigue phenomena, so it takes a very important part during the designing phases. In any case the fracture is composed by three different phases:

- nucleation, where the defect's dimensions are comparable to those of some grains;
- propagation, in which the defect enlarges till a macroscopic level;
- breakage.

Usually the nucleation phase doesn't occur due to the fact that defects are already present on the components, provided by previous operations or during the production process.

The fracture's surface presents two distinct parts, the "smooth" one is generated during the crack propagation and it is characterized by concentric lines with respect to the initiation point of the crack called "beach-marks" or "clamshell pattern". The "rough" surface part is generated in correspondence with the breakage of the component. The smoothness of the propagation zone is due to the fact that during the life of the component the crack is opened and closed by the acting alternated stresses, This lead to several contacts between the two sides of the crack that smooth out, while during final breakage the resistant zone yields quickly.
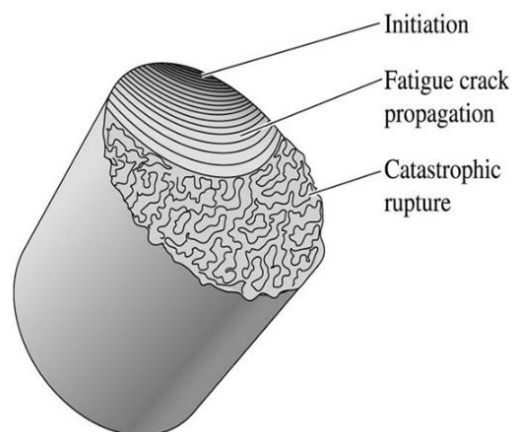
Figure 34 - Fatigue fracture surface

The analysis of the fracture surface will return important indications about the conditions to which the component was subjected and its failure modalities. Particular attention must be deserved to the propagation area and to the defect that originated the fracture, that could be an intrinsic fault of the material or due to specific loading conditions. From the extension of the propagation area it can be evaluated the level of the stresses applied, for example with a wider propagation area the resistant part remaining just before the complete failure will be very small, this imply a much lower applied stress in respect to the static limit of the material. When, on the contrary, the crack propagates less is because the applied stress is very high and is able to cause the breakage also with a larger resistant area.

The behaviour of a material subjected to fatigue phenomena is reported by experimental campaigns in terms of applied stress and number of cycles carried out with that value of stress on a specimen. With higher values of applied stress, the "life" of the component will be lower, while with a lower enough applied stress it can be

considered as infinite. Usually in the last case the stress can cause the nucleation of defects, but it isn't enough to cause their propagation.

S-N Curve for steel:
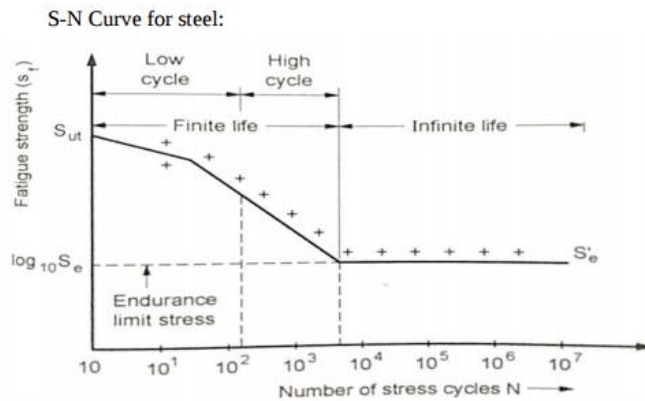
Figure 35 - Wöhler curve example

As reported in the diagram, a load repeated in time can bring to the failure of a component after a certain number of repetitions (cycles) even with a lower value in respect to the critical load in the static case. The finite life region is divided in two parts, the so called "low" and "high" cycle regions. In the low cycle fatigue the component is subjected to high stresses for a low number of cycles, this situation promotes the nucleation of several defects, while the high cycle fatigue is characterized by lower stresses repeated for a high time duration that will promote the propagation of the cracks. With very high stresses, any microscopic defect present in the material could generate a crack, for this reason is easy to find more than one nucleation point when the applied stresses are consistence.

The represented curve is typical of a steel, in which the decreasing in the applied stress finds an asymptote in correspondence of the fatigue limit σ_f from which the life of the component is considered infinite. This is not true in case of non-ferrous materials, that show a continuous decreasing behaviour of the curve.
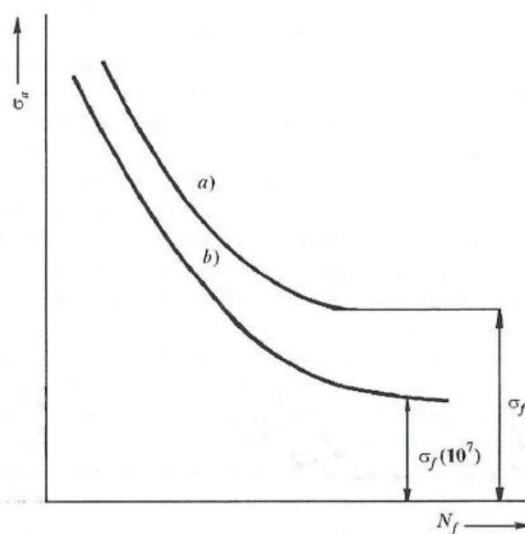
Figure 36 - a) steel typical fatigue behaviour; b) non-ferrous material typical fatigue behaviour

In case the fatigue limit is not easily detectable, it is arbitrary chosen the stress value corresponding to a high enough number of cycles (usually 10^7 cycles), considering negligible the further decreasing in the curve behaviour.

3.4.2   Repeated and/or variable loads

Fatigue phenomena are caused by the application of loads that are variable in time or with a constant value, but that are repeatedly applied following a cyclical trend over time. Applied stresses can be of any kind, as in case of tensile, compressive, torsional or bending loads, but acting on the component in a dynamic way. Usually, in mechanical applications, the stresses do not follow a precise path, they are randomly applied, but this is not possible to be reproduced during testing campaigns due to their complexity. So, the behaviour of the stresses is simplified and represented with sinusoidal trends in time. The stress cycle can be alternating, so with a stress that changes not only in its value but also in its direction (e.g. from a tensile stress to compressive one), or it can be pulsating, when the action on to which the component is subjected is always the same changing only in its amplitude.

In any case, for a stress cycle it is possible to recognize some fundamentals parameters:

- σ_{max} and σ_{min}, respectively the maximum and the minimum stress values of the cycle;
- $\sigma_M = \frac{\sigma_{max} + \sigma_{min}}{2}$, mean stress;
- $\sigma_a = \frac{\sigma_{max} - \sigma_{min}}{2}$, amplitude of the cycle;
- $R = \frac{\sigma_{min}}{\sigma_{max}}$, loading ratio.
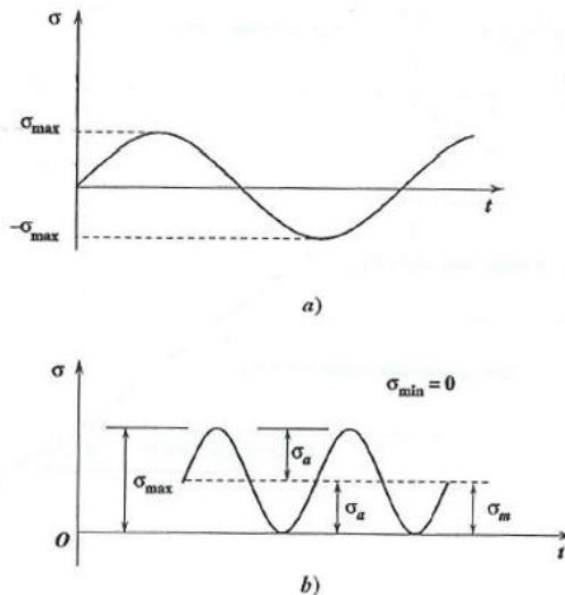
Figure 37 - a) alternating cycle; b) pulsating cycle

3.4.3 Nucleation and growth of a crack

It is easier to have a crack initiation in correspondence of a point on the component in which stresses concentrations are present. For this reason, a component with sharped features or engraves is more easily subject to fatigue failures and the surface finish has a very important role for its resistance, in fact with high loads every little defect can bring to the nucleation of a crack, while with lower applied stresses it takes more time. The fatigue life of a component calculated in number of cycles can be divided in two parts, the time needed for the initiation of the crack N_i and that needed for its propagation N_p, there would also be the time of elapsed during the breakage, but the complete fracture happens in such a sudden way that it is negligible. Generally cracks nucleate on the surface of the piece, where little defects in the material or discontinuities are always present. In the very first phase, a crack propagates at grain level in the direction of maximum shear stresses, usually inclined by 45° in respect to the direction of application of the load. After this microscopic propagation it will increase its propagation velocity and change inclination moving on a plane orthogonal to the direction of application of the load, interesting a wider section of the component.
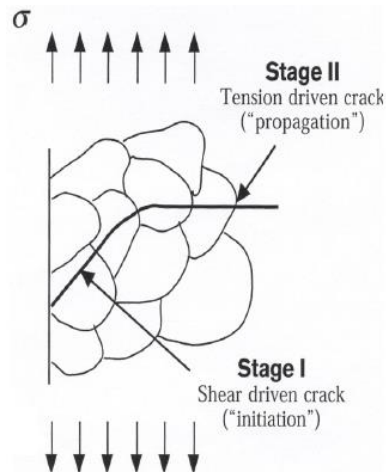
Figure 38 - Crack propagation

This behaviour generates particular signs on the fracture surface, the so called "beach-marks", concentric lines starting from the initiation point and visible by eye. These signs are due to different stages of oxidation of the crack's surfaces, due to the cyclic stops occurred during the life of the component. On a specimen used for fatigue test these signs are not present because it is subjected to a continuous test, it doesn't stop until its complete fracture, while in general application a component or a mechanical system doesn't work continuatively for all its life. During the stress cycles the crack propagates and at each stop a new portion of the crack surfaces is oxidized by the environment, the oxidation level decrease going from the nucleation point to the last portion of the crack before the complete fracture. The remaining part of the section breaks in a macroscopic brittle way, perpendicular to the direction of application of the load and without large plastic deformations, but here the fracture appears "rough" due to microscopic plastic deformations of the structure, in fact, here the fracture is microscopically ductile. The fracture macroscopic morphology depends on which type of load is applied to the component, in the next image are represented the more general cases.

34
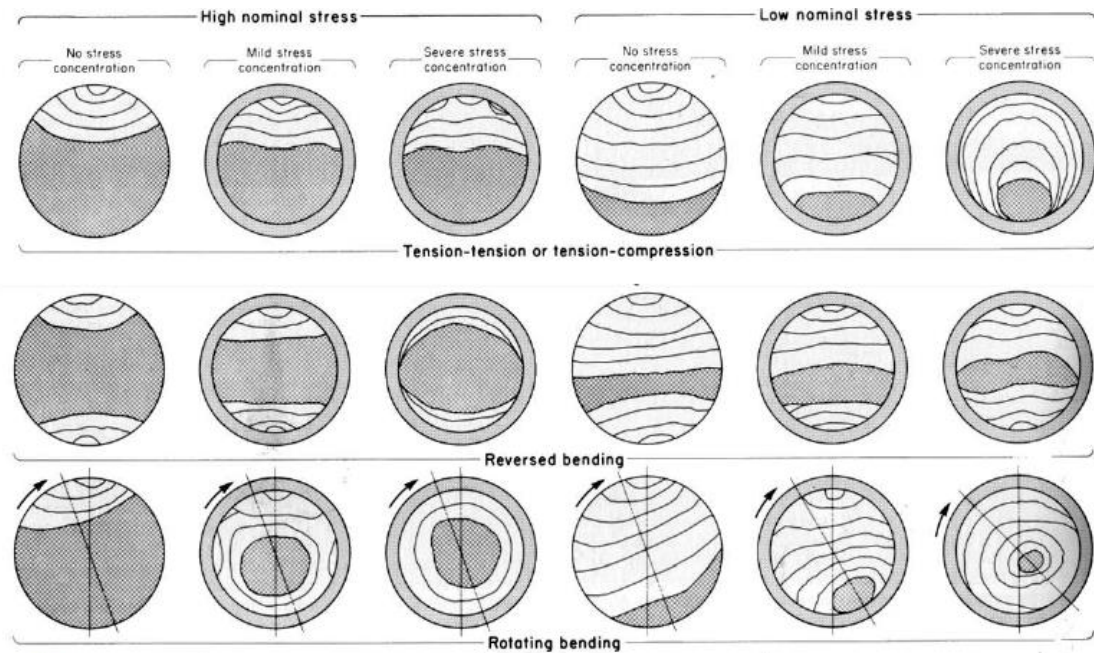
Figure 39 - Macroscopic morphology of fatigue fracture surfaces

3.4.4 Analysis of the test

There isn't a unique fatigue test, due to the different possible applicable loads it can be a tensile or compressive test, a bending test or also a rotating bending one. The machine used is different according to the type of fatigue limit that has to be evaluated. All these tests are usable for different purposes, but for all of them the results can be used to create the diagrams relating the applied stresses with the number of loading cycles (Wöhler diagram). During fatigue tests the parameters that have to be defined are:

- the number of cycles N at which occur the breakage of a specimen;
- the value of the stress in correspondence of the number of cycles N;
- the fatigue limit, that is the stress value in correspondence of a number of cycles between 10^6 and 10^7.

In order to obtain an estimation of the Wöhler curve, it is needed a large number of experimental data. These data are affected by a very large dispersion due to the several factors that could affect the result of a fatigue test, for this reason they are usually analysed with statistical methods. Usually the "Staircase" method is used for this purpose, that allows to determine that value of applied stress in correspondence of which there is the 50% of possibility to have the fracture of the sample.

The Staircase method involves an initial estimation of two stress levels, one lower and one higher than the expected fatigue limit. The gap between these two limits must be divided by many intermediate levels with equal intervals between them. The test campaign is carried out with an odd number of samples increasing the stress level when the specimen doesn't break in the considered number of cycles (run-out) or decreasing it in case of failure. The number of breakages will be different from that of undamaged samples, than the stress values belonging to the less frequent event are taken into account and their mean has to be calculated. In case that the considered series is that of broken samples, to the obtained mean it has to be subtracted a half of the

35

gap between two subsequent stress levels. On the contrary, if the considered series is that of the undamaged samples, this value must be added to the obtained mean stress.

Less frequent event

$$\sigma_e = \frac{3\sigma_2 + 2\sigma_3}{5} - \frac{\Delta\sigma}{2}$$

failure

5 broken specimens (3 at σ_2 and 2 at σ_3)
6 run out specimens (2 at σ_2, 3 at σ_1 and 1 at σ_0)

• run-out
✕ failure
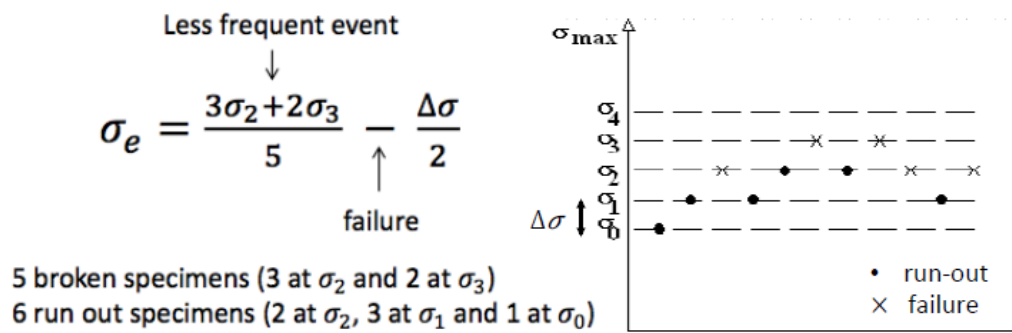
Figure 40 - Staircase method example

3.4.6 Specimens

As for the testing machine, also the specimen's characteristics varies according to the kind of fatigue test. For all the type of specimen particular attention must be deserved to the surface finish, because as said before any kind of defect can behave as initiation point for a crack. All the characteristic dimensions for the specimens are reported in the related standard, that varies for any type of tested fatigue.
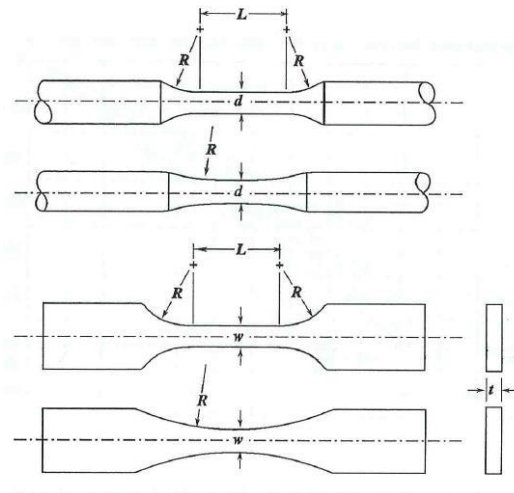
Figure 41 - Examples of cylindrical and rectangular specimens for fatigue tests

3.4.7 From the specimen to the component

Following the indication reported by the standards, both for what concerns the procedure and the characteristics of the specimen to be tested, it is possible to calculate the fatigue limit of a material. The problem is that for a generic component made by that material, its fatigue limit would be lower or at maximum equal to the value obtained for the material itself. This difference is caused by several factors having the same effect, all of them make the piece more prone to cracks formation in respect to the tested specimen. The principal reductions of the fatigue resistance are caused by the presence of notches and by the quality of the surface finish, but also the dimensions of the component play an important role in this field. There are coefficients that can be used in order to correct the value of the fatigue limit considering these characteristics, let's see how they work.

- Notch effect: coefficient "K_f", that allow to evaluate the reduction of the fatigue resistance caused by possible notches present on the component.

$$K_f = 1 + q \cdot (K_t - 1)$$

   It is in general lower than the theoretical notch coefficient "K_t" and to calculate it the notch sensitivity "q" is needed. The value of "q" lays between 0 and 1, it is reported in diagrams that consider the stress gradient, the fillet radius and the material, but it can also be calculated using the following formulas

$$\text{Peterson: } q = \frac{1}{1+\frac{a}{r}}; \qquad \text{Neuber: } q = \frac{1}{1+\sqrt{\frac{\rho}{r}}}.$$

Where "r" is the fillet radius in the correspondence of the notch, while "a" is a parameter depending on the material and "ρ" another characteristic of the material that depends on its resistance.
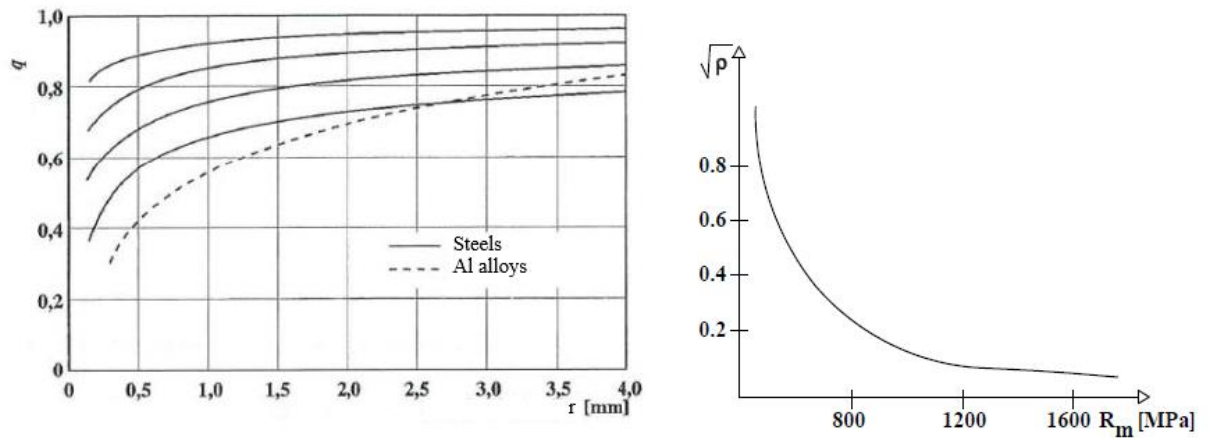
Figure 42 - Notch sensitivity diagrams

- Dimensional effect: coefficient "b_2", that allows to take into account the reduction of the fatigue limit caused by higher dimensions in respect to the specimen used in the test. In fact, wider is the component, higher is the probability of finding superficial defects, furthermore, on a wider section, the stress gradient is lower so determining a higher mean stress over a single grain. This coefficient can be calculated referring to the diameter or the thickness of the component by experimental observations:
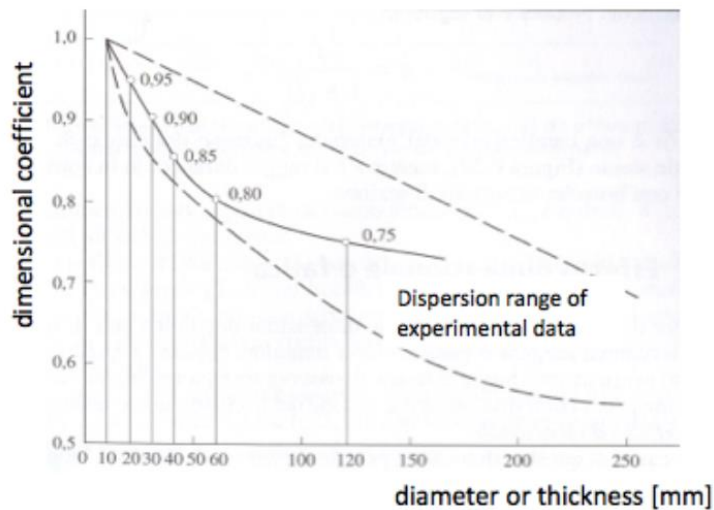
Figure 43 - Dimensional coefficient diagram

- Surface finish effect: coefficient "b_3", it is referred to the roughness of the component, so to the technological process used, and the resistance of the material. It is reported on a diagram that relates it to the roughness of the surface and to the maximum tensile strength of the material:
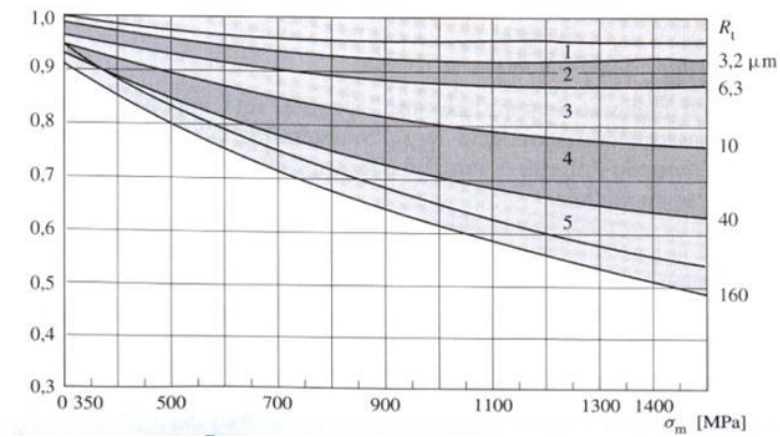
Figure 44 - Surface finishing coefficient diagram

These three coefficients are applied to the fatigue limit of the material, obtained by the fatigue test or evaluated from the tensile strength, in order to calculate the fatigue limit of the component:

$$\sigma_{lim,component} = \frac{\sigma_{lim,material} \cdot b_2 \cdot b_3}{K_f}$$

3.5 Vickers hardness test

Hardness is a mechanical property of a material that expresses the resistance it opposes to the penetration of a harder material according to a localized compression carried out by a properly shaped penetrator. Unlike the previous ones, the hardness test is a non-destructive one and can be directly done on the real component. There are many types of hardness tests, differentiated according to the shape and the material of the penetrator, characteristics that determine the maximum hardness detectable and therefor the material to be tested. This test is featured by low costs and very short execution time, most common tests are: Brinell; Vickers; Knoop and Rockwell.

Table 4 - Hardness tests characteristics

4 Chapter 4

4.1 Preparation of the specimens

All the materials were provided in cold drawn bars from "Tre Valli Acciai s.p.a.", these bars were 18 mm in diameter and 1,5 m length for all the materials except for the 11SMn37 that was provided in bars with a diameter of 20 mm. Bars were marked using the chosen encoding and cut in order to obtain raw specimens for all the tests. There were 18 raw specimens (3 for each material) with a length of 180 mm for the tensile test, 48 raw specimens (8 for each material) with a length of 180 mm for the fatigue test and 31 raw specimens (5 for each material except the 6 obtained for the S355J2) with a length of 200 mm for the Charpy's pendulum test. For tensile and fatigue tests, a final specimen was obtained from each raw specimen, while each raw specimen for the toughness test corresponded to a set of three final samples, due to easily operation in their manufacturing process.

Figure 45 - Raw specimens obtained for the material 11SMnPb30 and 11SMnPb37

From the remaining parts of the bars were obtained the samples for the metallographic and chemical analysis. The hardness tests were carried out taking advantage of the samples made for metallographic analysis.

Figure 46 - Samples for chemical analysis

4.1.1 Specimens encoding

Each specimen was marked with the corresponding code in order to simplify their identification. The same code applied with a pencil before machining operations, were punched using shaped penetrators on the final specimens. Each code used for mechanical tests contains a letter representing the type of the test, a progressive number indicating the single specimen and another letter representing the material.

Table 5 - Tests encoding

Test	Coding letter
Tensile test	T
Toughness test	R
Fatigue test	F

Table 6 - Materials encoding

Material	Coding letter
S235JR	A
S355J2	B
11SMn30	C
11SMn37	D
11SMnPb30	E
11SMnPb37	F

4.1.2 Drawings of the specimens

Raw specimens were processed by the company "Ready for test s.r.l" ("R4t s.r.l.") in order to obtain the final specimens. Drawings of the specimens were made following the indications reported in the standards for each kind of sample and then provided to the company.

For the tensile test, the specimen has to follow the standard UNI EN ISO 6892-1.
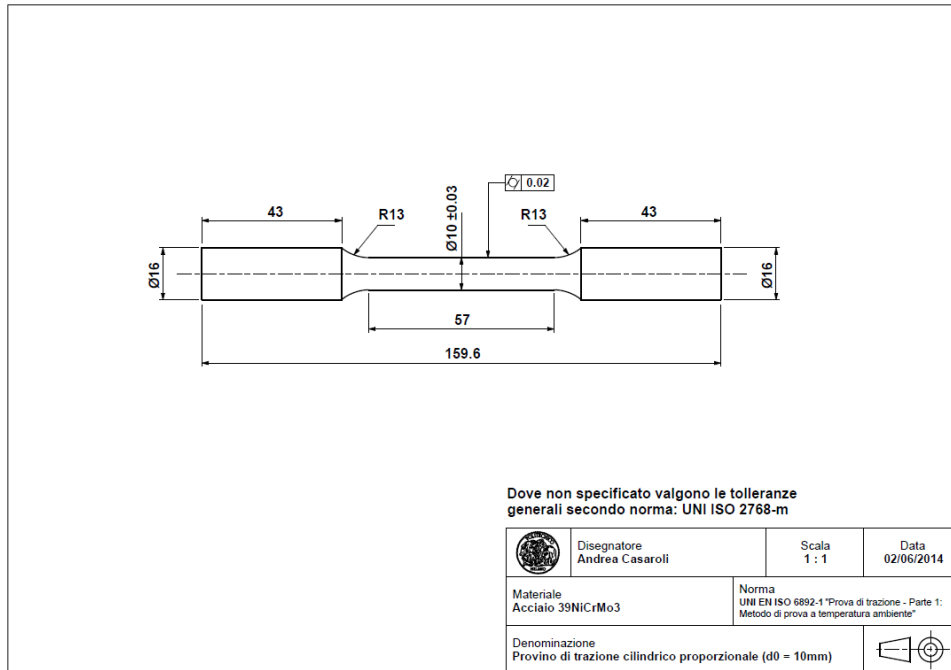
Figure 47 - Drawing of the specimen for tensile tests

Before proceeding to the test, the central part has been marked with a pen and divided in intervals of 5-10 mm, this operation allows to evaluate the elongation at the end of the test.
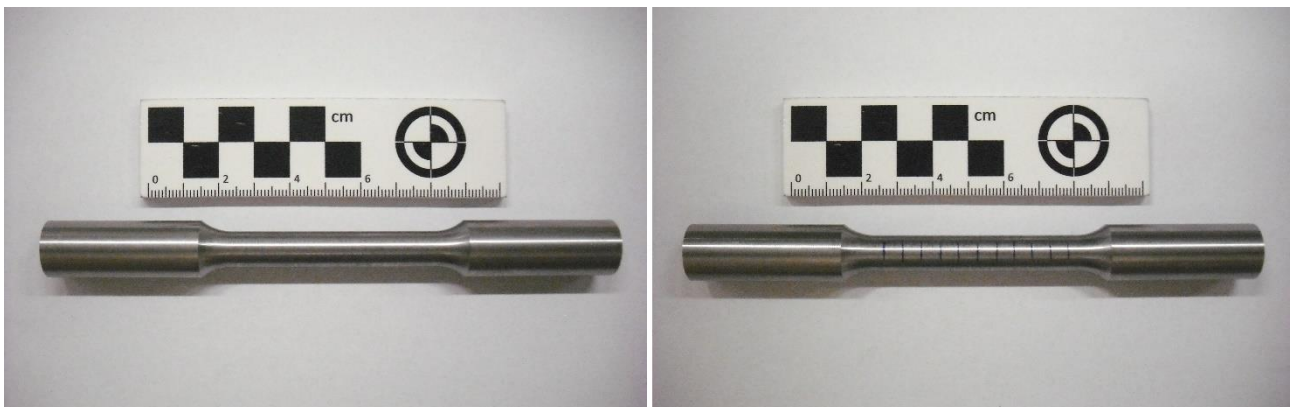
Figure 48 - Tensile test's specimen as delivered (left) and marked (right)

For the Charpy's pendulum impacting test, the specimen has to follow the standard UNI EN ISO 148-1.
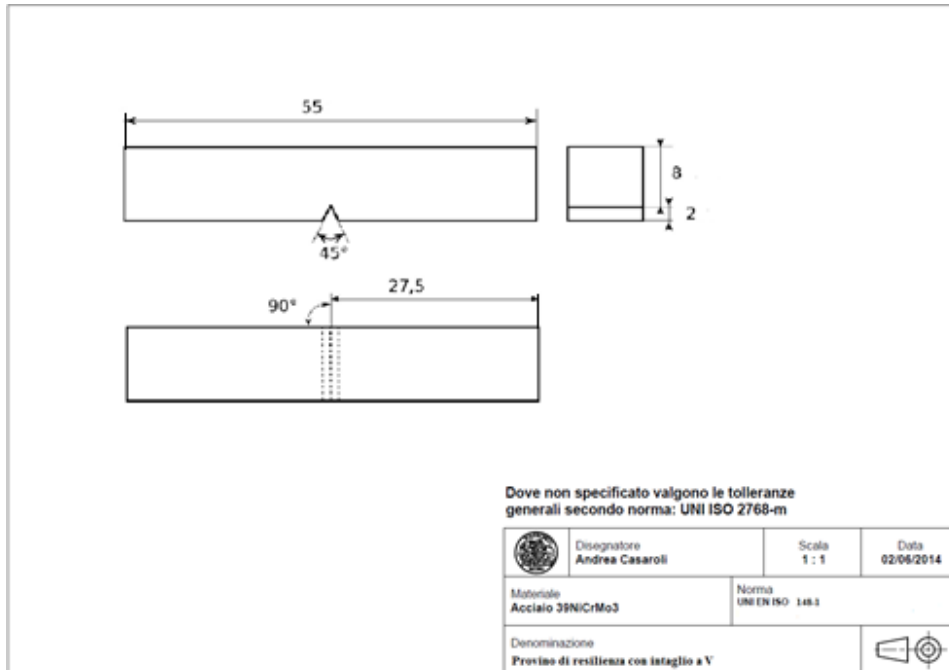
Figure 49 - Drawing of the specimen for toughness tests

Specimens were manufactured in sets of three specimens each, then they were divided by the company, this procedure allows to machine them easily and in a faster way.
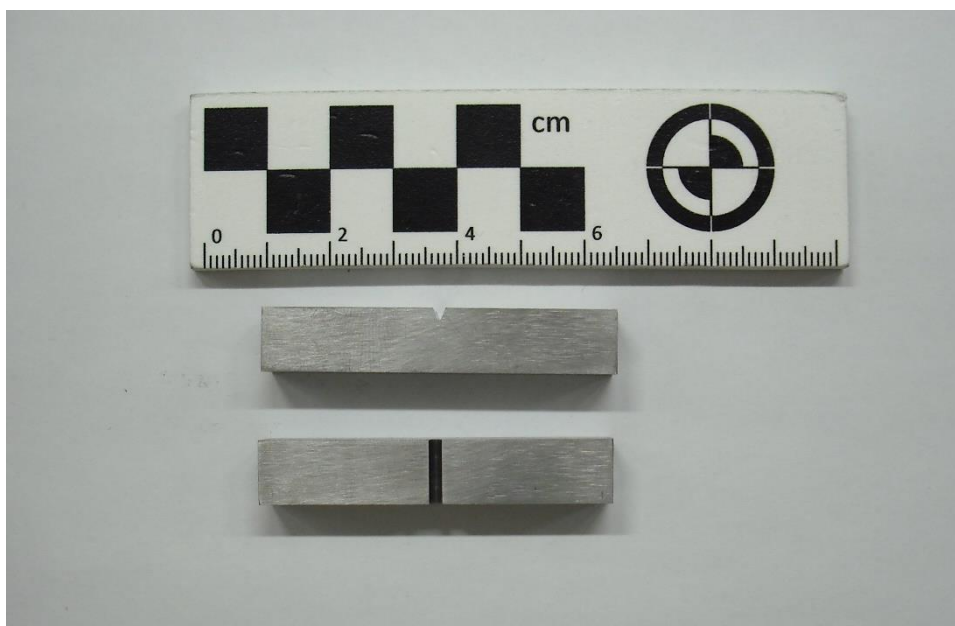
Figure 50 - Toughness test's specimens

For the rotating bending fatigue test, the specimen has to follow the standard ISO 1143.
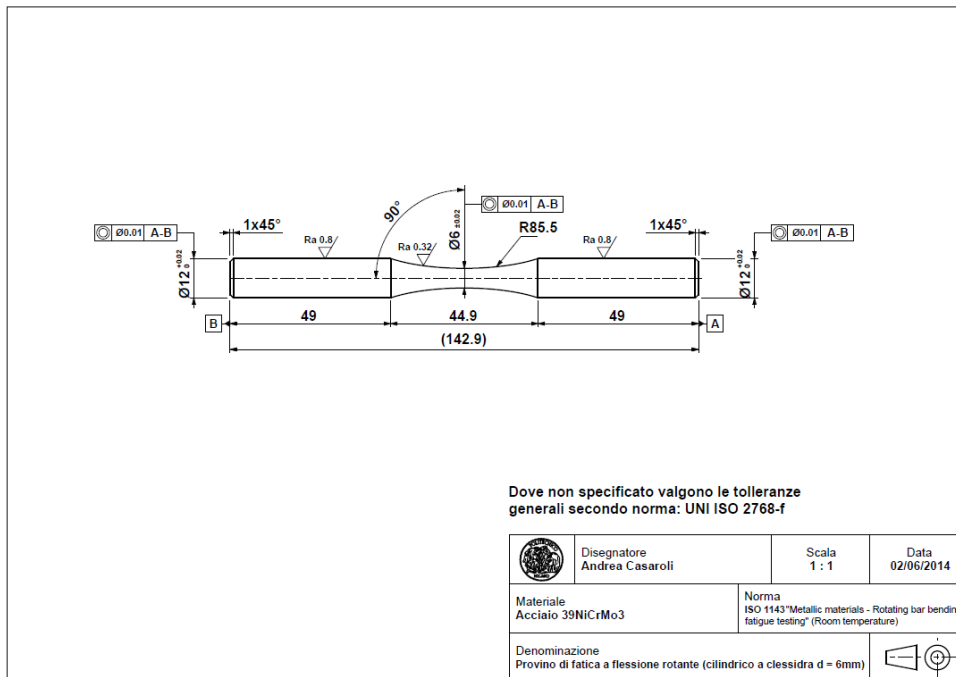
Figure 51 - Drawing of a specimen for rotating bending fatigue tests

Figure 52 - Rotating bending fatigue test's specimen

4.2 Tensile test

Tensile tests were performed at the laboratories of Politecnico di Milano following the standard UNI EN ISO 6892-1. First of all, specimens were measured, not only to control the correctness of the machining operations, but also because these measurements are fundamental for the evaluation of the necking phenomena at the end of the test. Measurements of the diameter in correspondence of the central part of the specimens were taken using a calibre.

4.2.1 Test's execution and analysis

After measuring its diameter, each specimen was clamped in the jaws of the machine paying attention to maintain its axis as vertical as possible. Then the extensometer was applied to the specimens positioning his grips at both ends of the "original gauge length" (L_0), that is that section marked with a pencil. After resetting the extensometer and the loading cell, the characteristics of the specimen were uploaded in the program controlling the machine. The fundamental characteristics are the initial diameter d_0, the original gauge length L_0 and the speed at which the machine has to increase the applied load. This last characteristic is provided by the standard that, for a material with an elastic modulus E higher than 150000 MPa as a steel, must be between 6 and 60 MPa/s.

Figure 53 - Tensile test machine
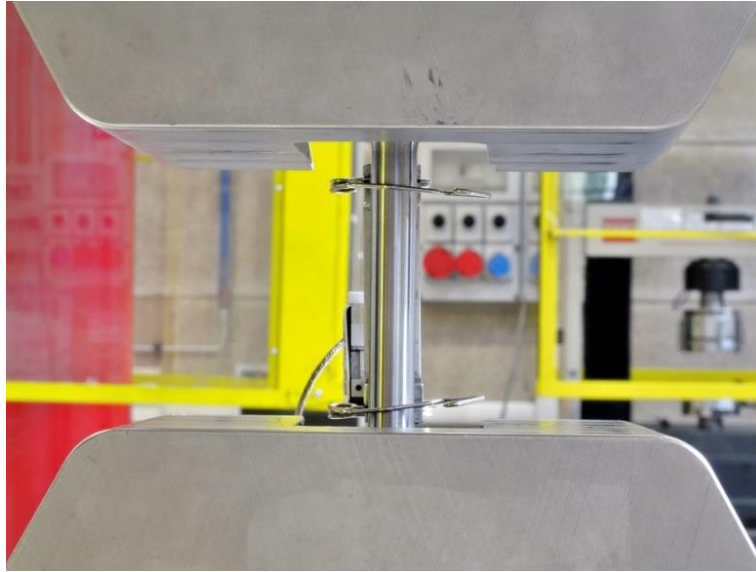
Figure 54 - Tensile test machine particular (extensometer)

At the end of the test, the program requires the values of the "final gauge length" (L_U) and of the minimum diameter after the fracture (d_F) in order to calculate some properties of the material. So the specimen has been removed from the machine and with a calibre the required measurement were taken matching the fracture surfaces of the two pieces.
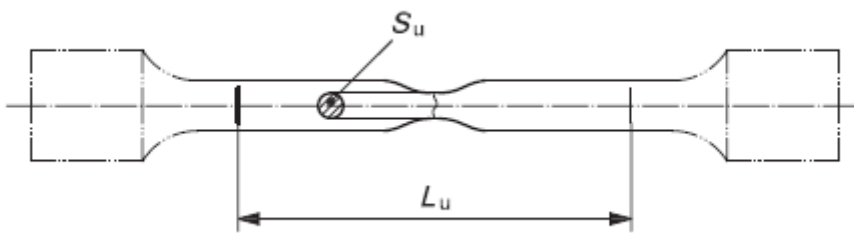
Figure 55 - characteristics of the specimen after the tensile test

Figure 56 - Specimen of S235JR after the tensile test

At the end of the test, the machine returns the principal characteristics of the material in a report and the values of the stress-strain curve obtained during the test. The curve of the tests carried out are shown below.
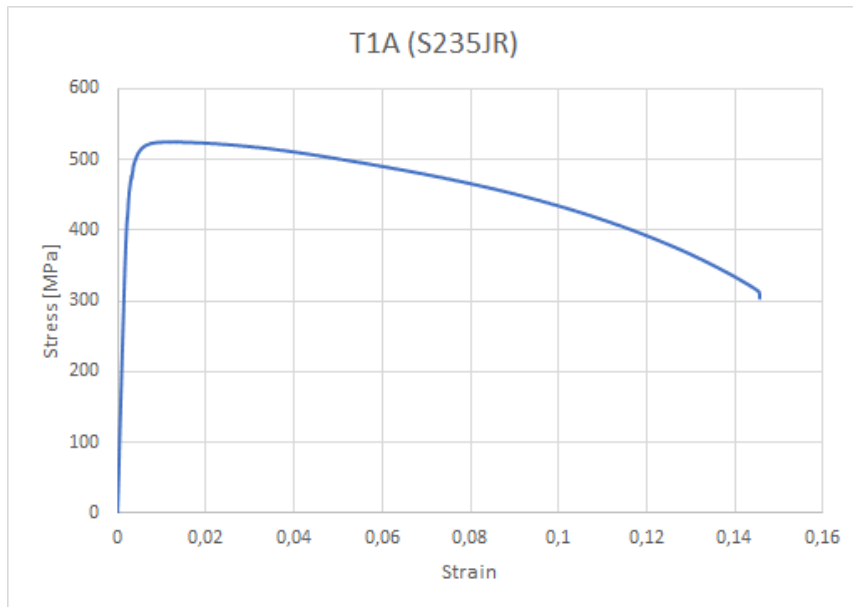
Figure 57 - Stress-strain curve specimen T1A (S235JR)
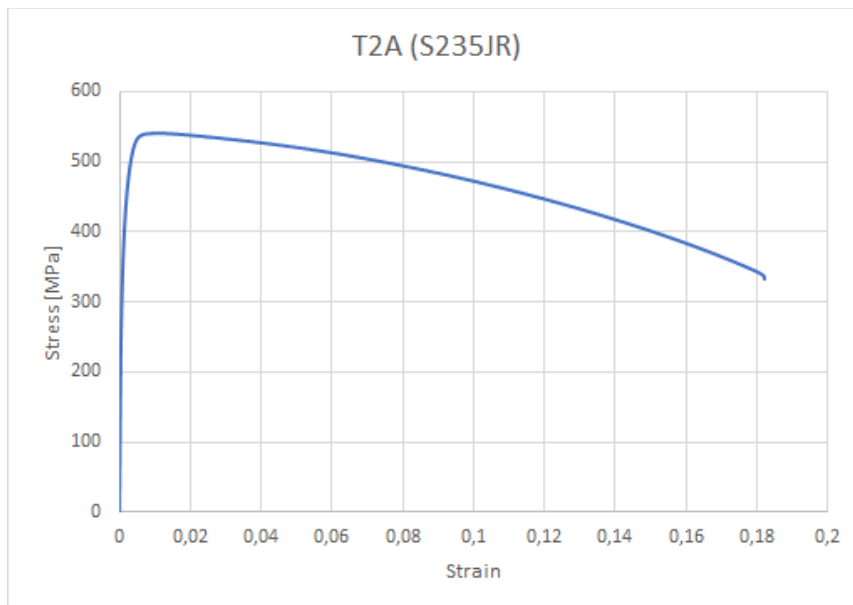
Figure 58 - Stress-strain curve specimen T2A (S235JR)
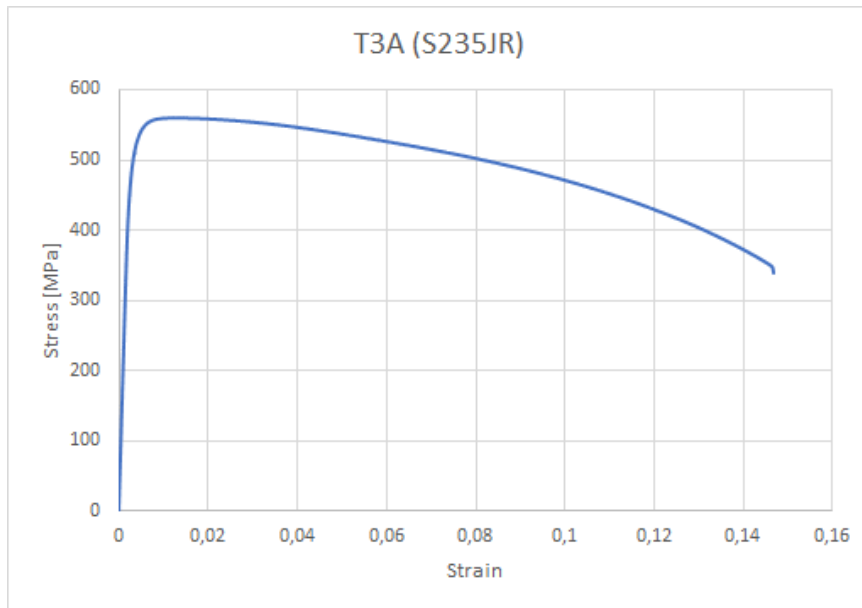
Figure 59 - Stress-strain curve specimen T3A (S235JR)
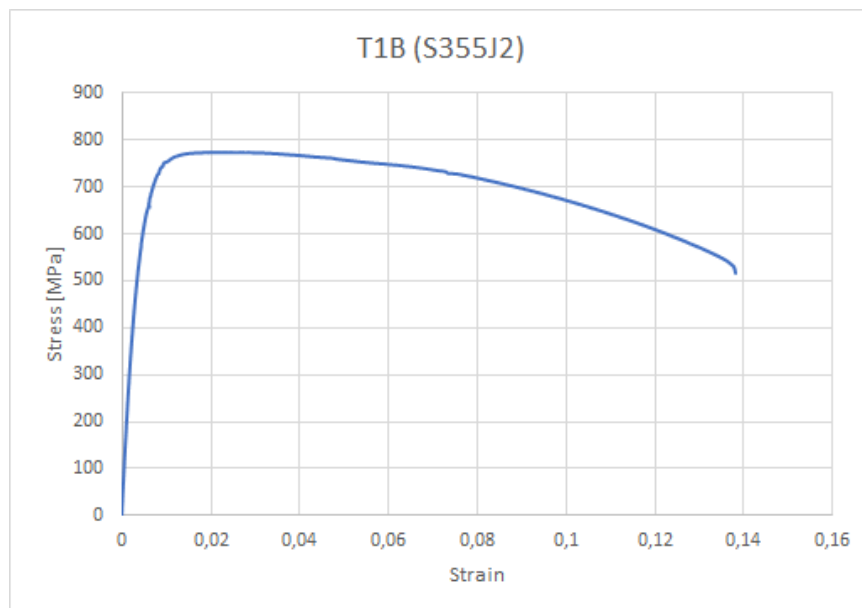
Figure 60 - Stress-strain curve specimen T1B (S355J2)
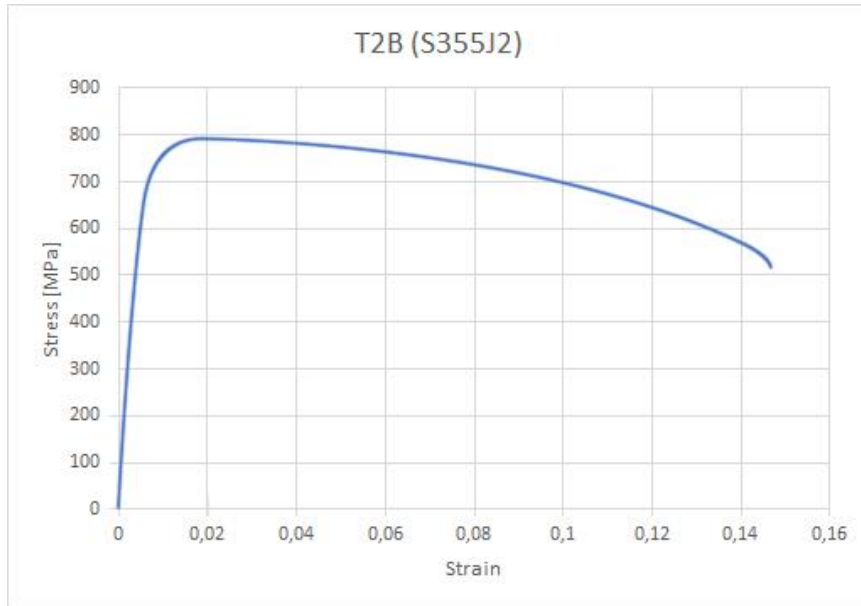
Figure 61 - Stress-strain curve specimen T2B (S355J2)
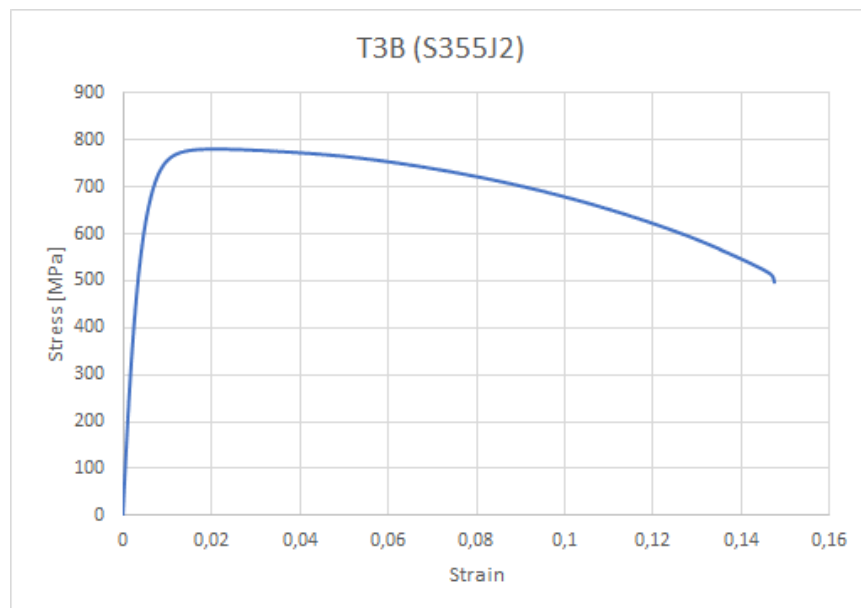
Figure 62 - Stress-strain curve specimen T3B (S355J2)
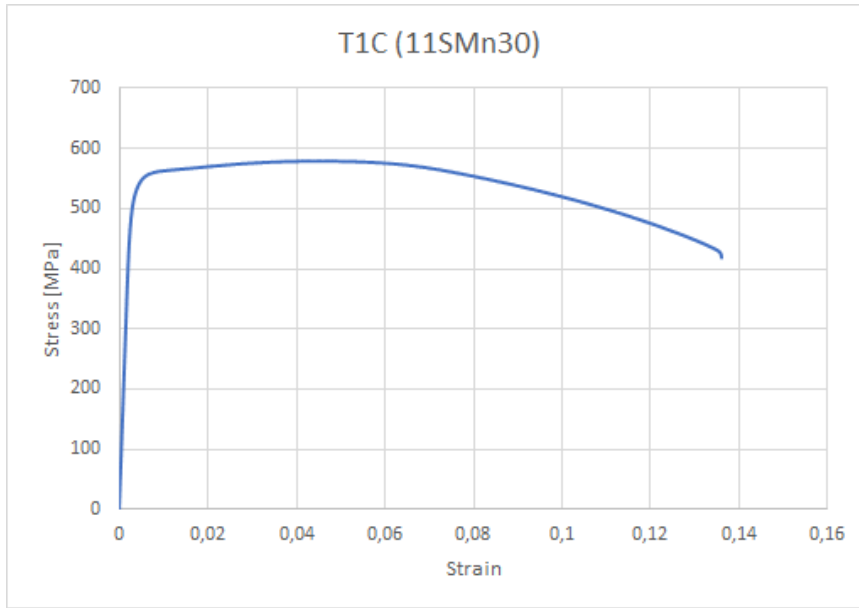
Figure 63 - Stress-strain curve specimen T1C (11SMn30)
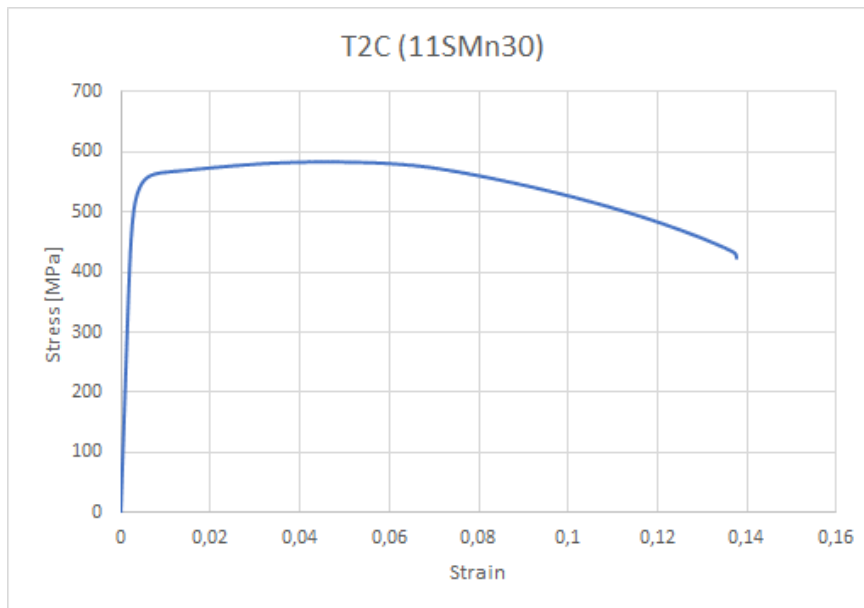
Figure 64 - Stress-strain curve specimen T2C (11SMn30)
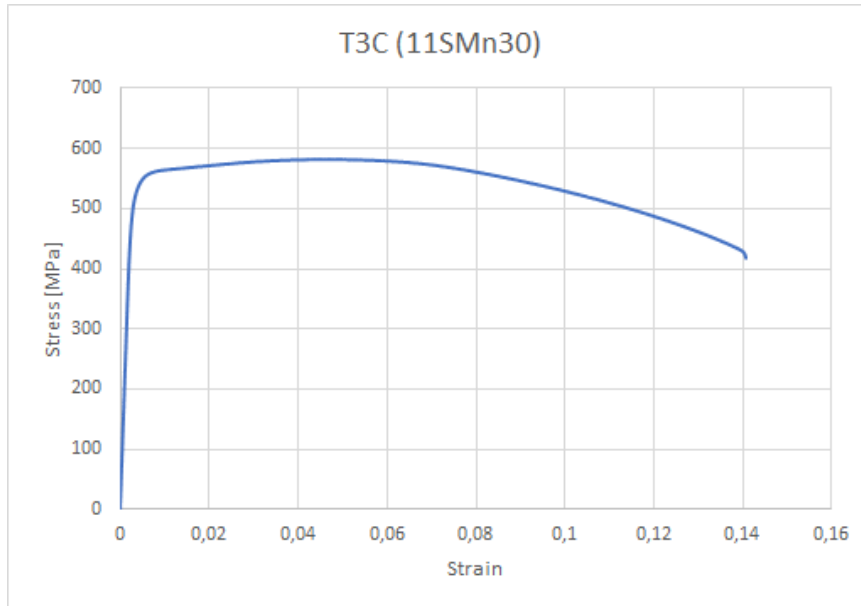
Figure 65 - Stress-strain curve specimen T3C (11SMn30)
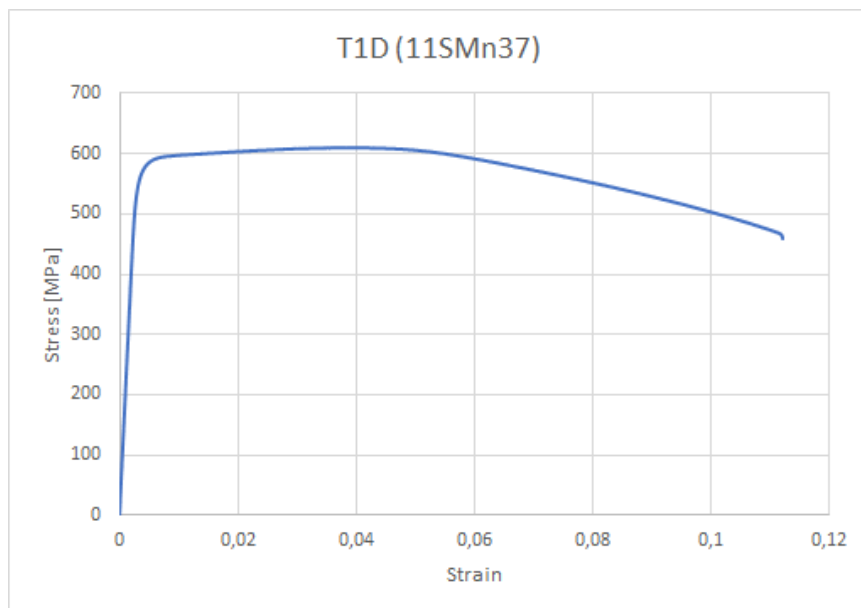
Figure 66 - Stress-strain curve specimen T1D (11SMn37)
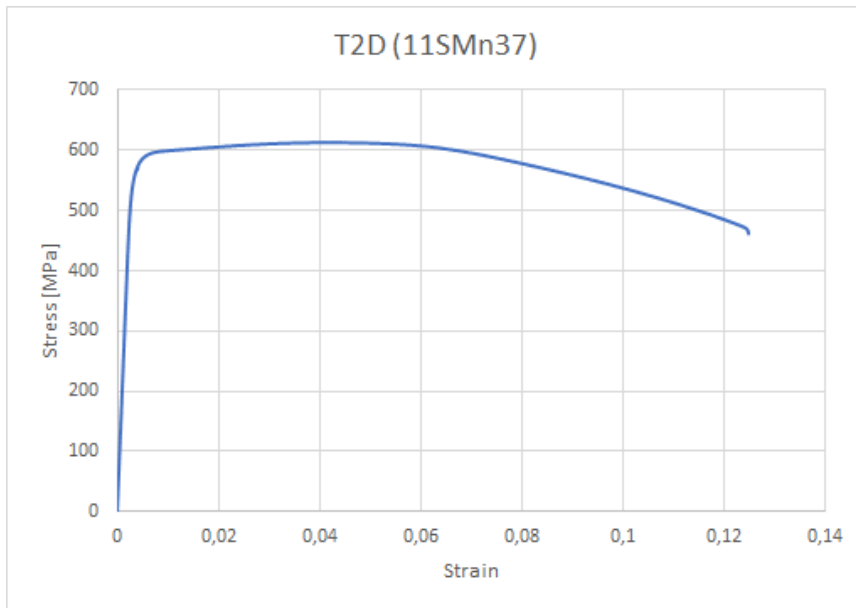
Figure 67 - Stress-strain curve specimen T2D (11SMn37)
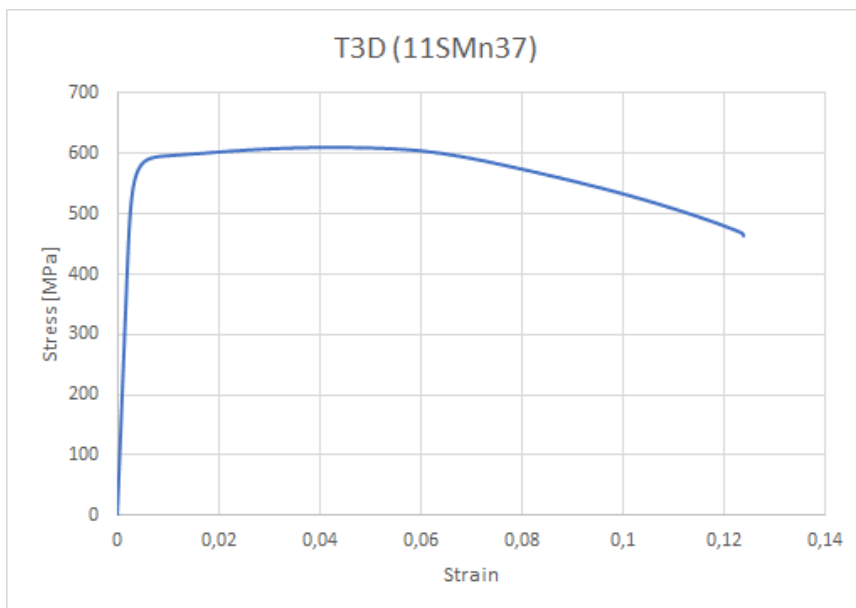
Figure 68 - Stress-strain curve specimen T3D (11SMn37)
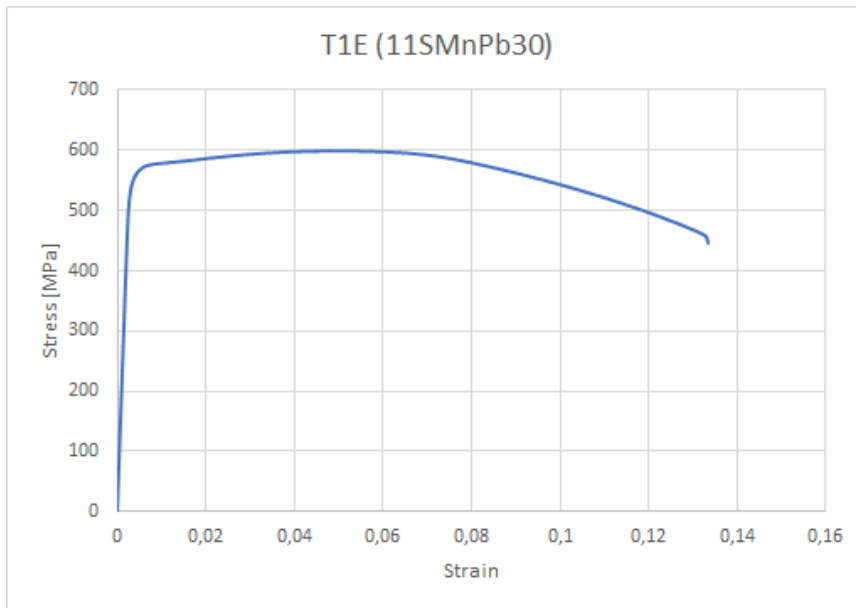
Figure 69 - Stress-strain curve specimen T1E (11SMnPB30)
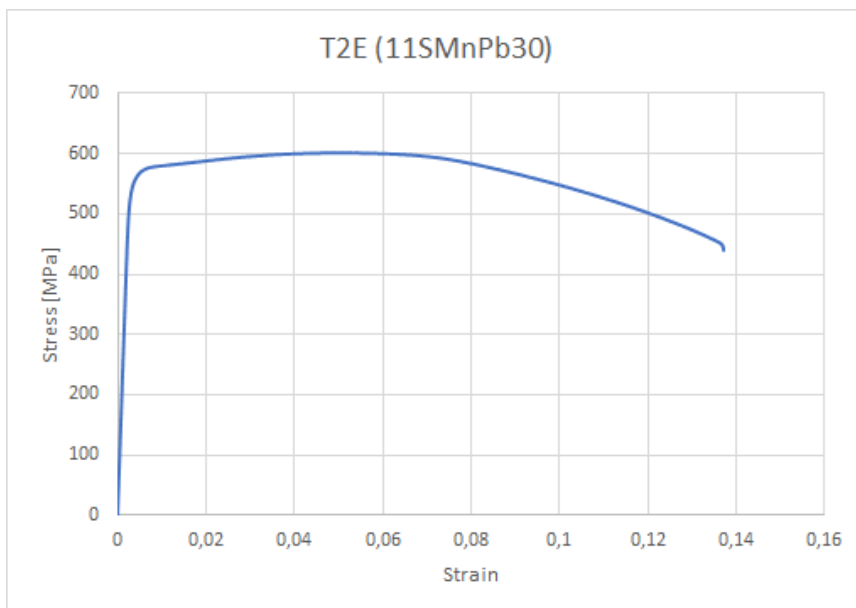
Figure 70 - Stress-strain curve specimen T2E (11SMnPB30)
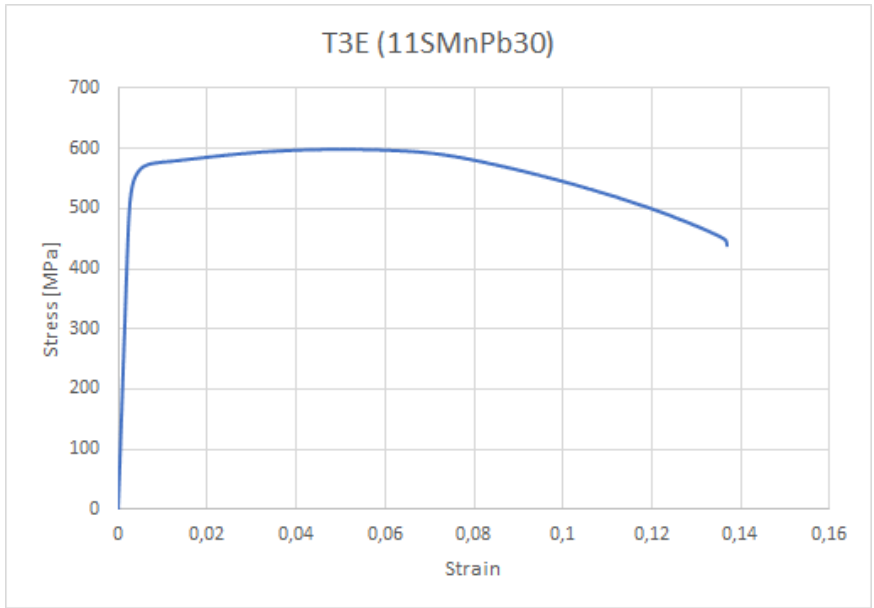
Figure 71 - Stress-strain curve specimen T3E (11SMnPB30)
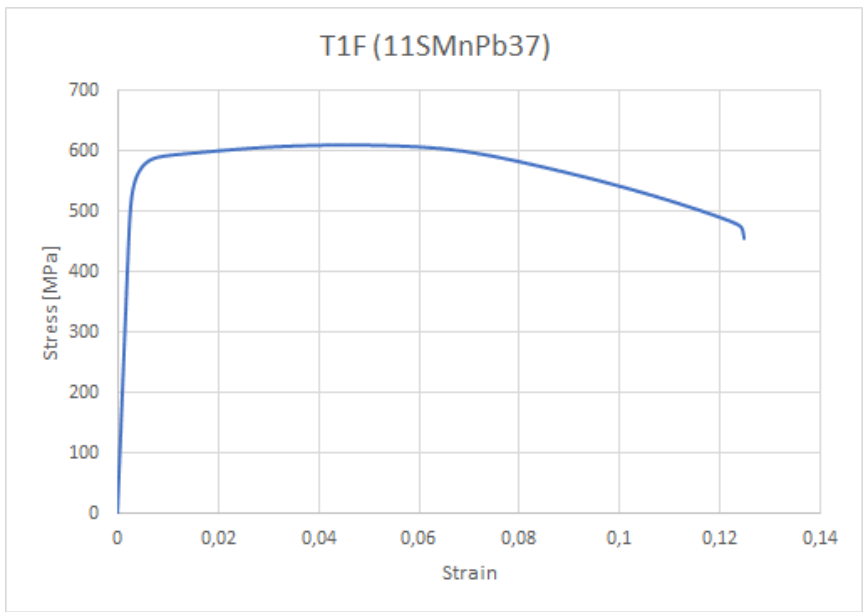
Figure 72 - Stress-strain curve specimen T1F (11SMnPB37)
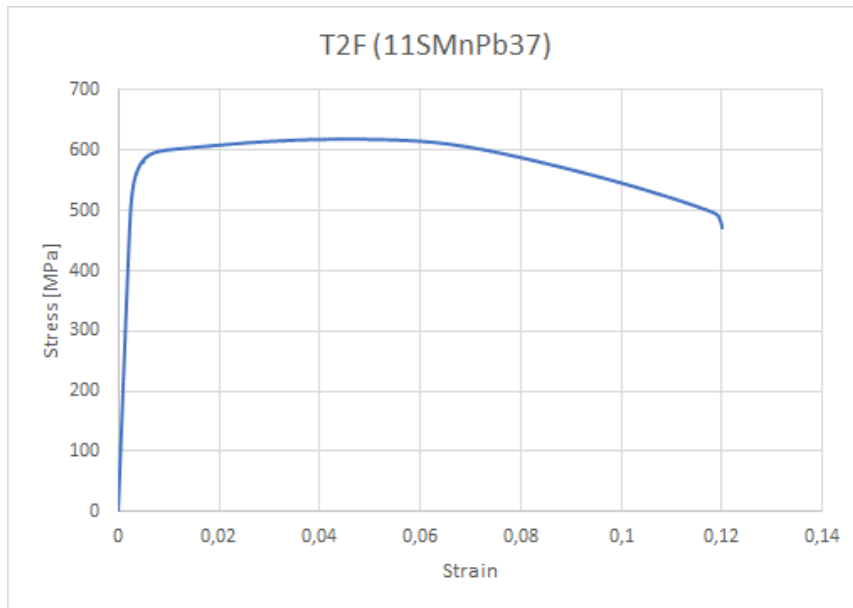
Figure 73 - Stress-strain curve specimen T2F (11SMnPB37)
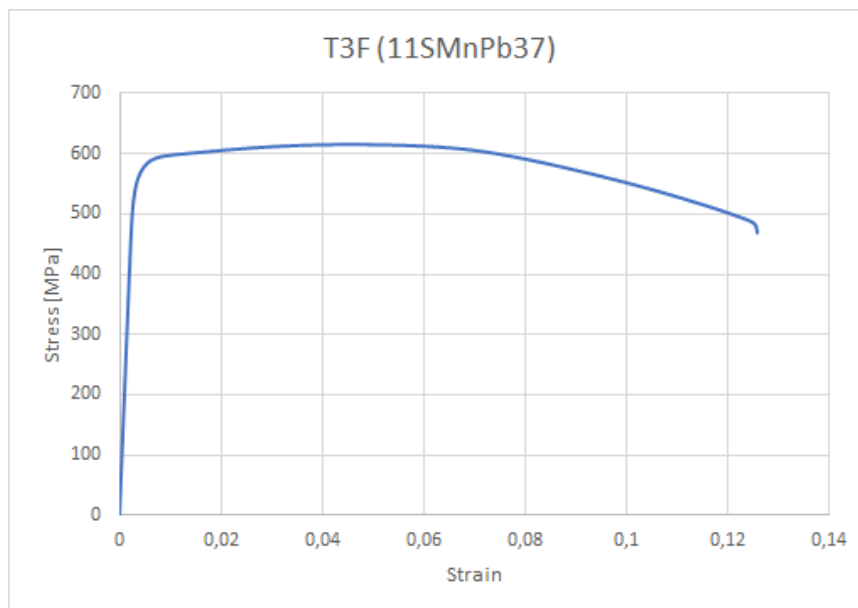
Figure 74 - Stress-strain curve specimen T3F (11SMnPB37)

As it can be seen from the graphs, the tensile test is repeatable, in fact for the same material the values of stress and strain along the tests are similar. This can be easily seen looking at the tables and graphs reported below where a comparison between specimens of the same material can be done. The values of elongation (A%) reported in the tables were calculated using the "final gauge length" on the specimens after the test, in this way the values can differ by those reported on the curves, mainly due to the elastic recovery of the material.

Table 7 - Tensile test results for material S235JR

Specimen	d0 [mm]	L0 [mm]	S0 [mm2]	du [mm]	Lu [mm]	Su [mm2]	Rp0.2 [MPa]	Rm [MPa]	A %	Z %
T1A	9,95	50	77,76	6,15	57,86	29,71	500	525	15,72	61,80
T2A	9,94	50	77,60	6,05	59,7	28,75	515	541	19,4	62,95
T3A	9,95	50	77,76	6,02	57,7	28,46	535	560	15,4	63,39

For the S235JR steel, the obtained mean value for the R_{P02} and R_m are:

$$\overline{R_{P02}} = \frac{\sum_{i=1}^{3} R_{P02_i}}{3} = 517\ MPa;$$

$$\overline{R_m} = \frac{\sum_{i=1}^{3} R_{m_i}}{3} = 542\ MPa.$$
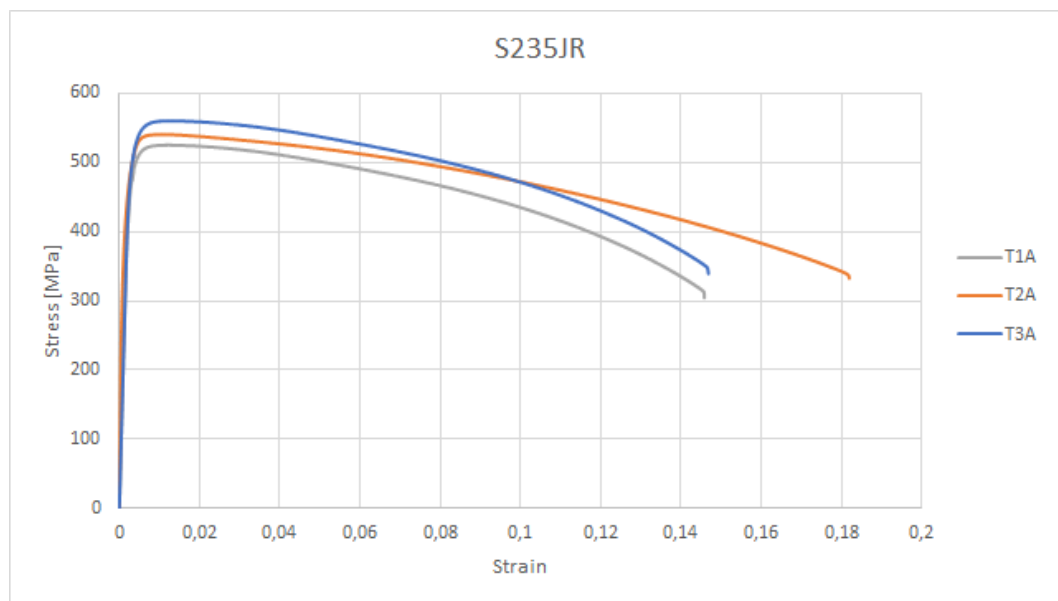
Figure 75 - Stress-strain curves for material S235JR

Table 8 - Tensile test results for material S355J2

Specimen	d0 [mm]	L0 [mm]	S0 [mm2]	du [mm]	Lu [mm]	Su [mm2]	Rp0.2 [MPa]	Rm [MPa]	A %	Z %
T1B	9,94	50	77,60	6,3	56,56	31,17	634	773	13,12	59,83
T2B	9,93	50	77,44	6,2	57,8	30,19	651	792	15,6	61,02
T3B	9,9	50	76,98	6,14	57,57	29,61	634	780	15,14	61,53

For the S355J2 steel, the obtained mean value for the R_{P02} and R_m are:

$$\overline{R_{P02}} = \frac{\sum_{i=1}^{3} R_{P02_i}}{3} = 640 \; MPa;$$

$$\overline{R_m} = \frac{\sum_{i=1}^{3} R_{m_i}}{3} = 782 \; MPa.$$
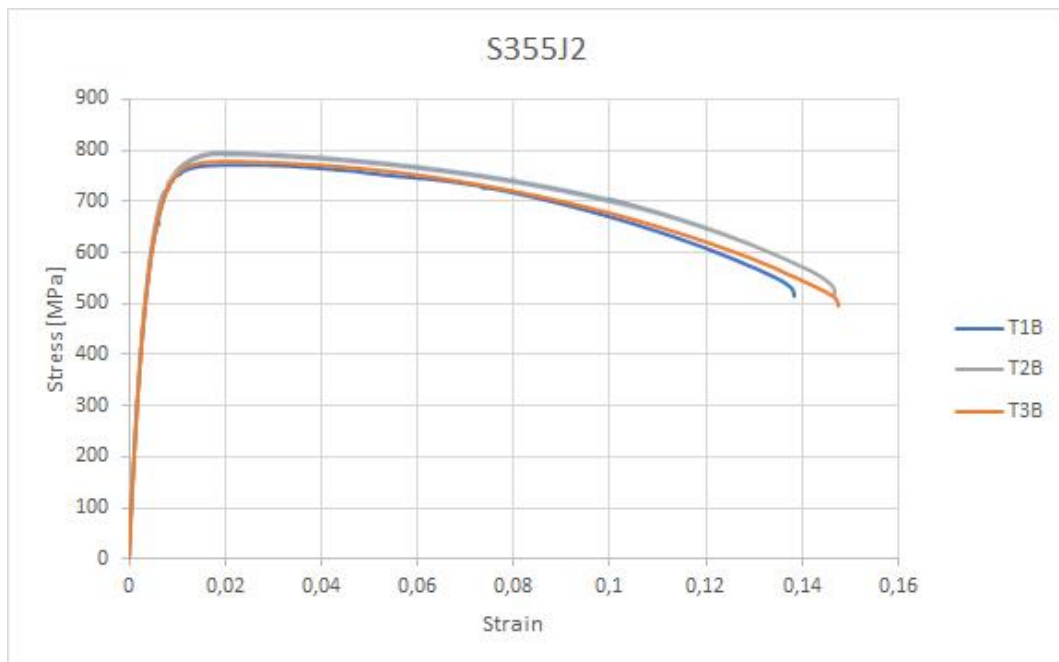
Figure 76 - Stress-strain curves for material S355J2

Table 9 - Tensile test results for material 11SMn30

Specimen	d0 [mm]	L0 [mm]	S0 [mm2]	du [mm]	Lu [mm]	Su [mm2]	Rp0.2 [MPa]	Rm [MPa]	A %	Z %
T1C	9,95	50	77,76	7,4	57,15	43,01	543	579	14,3	44,69
T2C	9,94	50	77,60	7,2	57,2	40,72	548	585	14,4	47,53
T3C	9,93	50	77,44	7,14	57,8	40,04	545	583	15,6	48,30

For the 11SMn30 steel, the obtained mean value for the R_{P02} and R_m are:

$$\overline{R_{P02}} = \frac{\sum_{i=1}^{3} R_{P02_i}}{3} = 545 \; MPa;$$

$$\overline{R_m} = \frac{\sum_{i=1}^{3} R_{m_i}}{3} = 582 \; MPa.$$
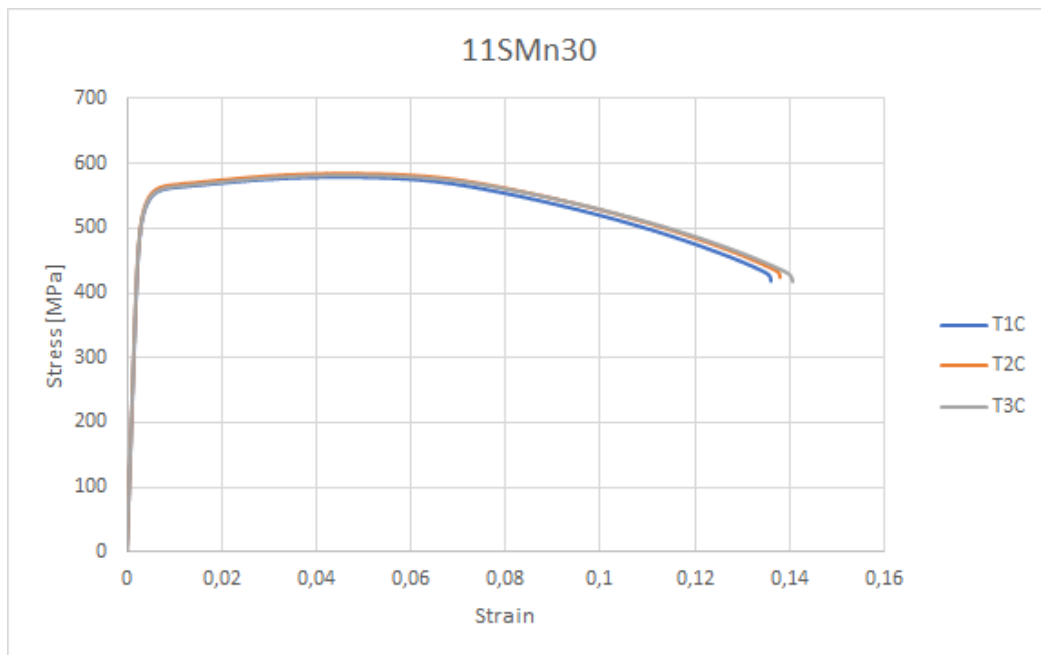
Figure 77 - Stress-strain curves for material 11SMn30

59

Table 10 - Tensile test results for material 11SMn37

Specimen	d0 [mm]	L0 [mm]	S0 [mm2]	du [mm]	Lu [mm]	Su [mm2]	Rp0.2 [MPa]	Rm [MPa]	A %	Z %
T1D	9,95	50	77,76	7,58	55,07	45,13	583	609	10,14	41,96
T2D	9,94	50	77,60	7,44	56,2	43,47	585	613	12,4	43,98
T3D	9,93	50	77,44	7,35	56,1	42,43	583	612	12,2	45,21

For the 11SMn37 steel, the obtained mean value for the R_{P02} and R_m are:

$$\overline{R_{P02}} = \frac{\sum_{i=1}^{3} R_{P02_i}}{3} = 584\ MPa;$$

$$\overline{R_m} = \frac{\sum_{i=1}^{3} R_{m_i}}{3} = 611\ MPa.$$
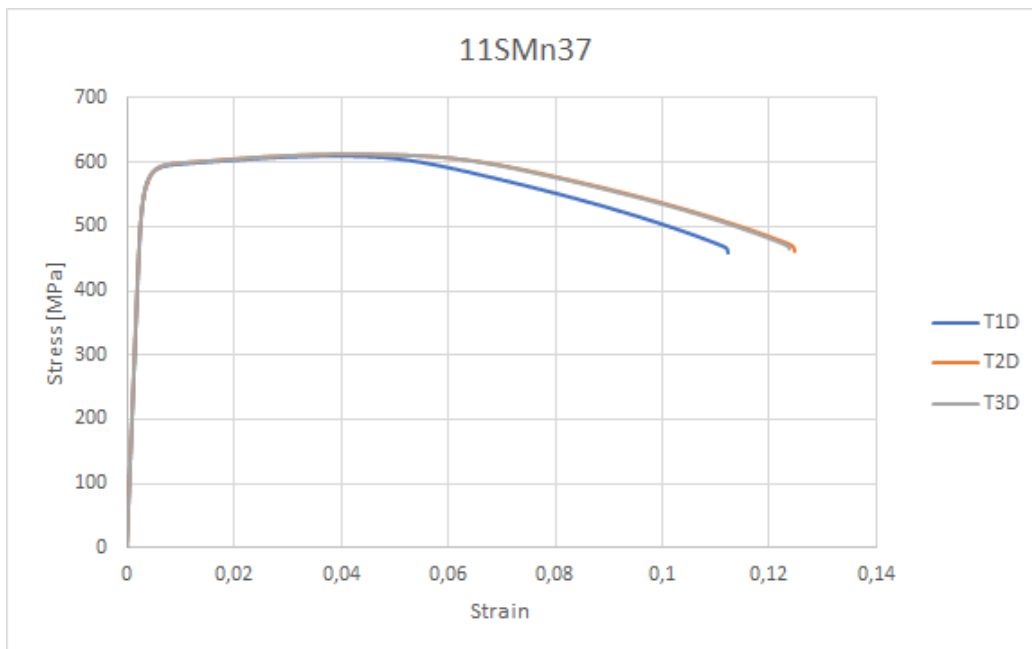
Figure 78 - Stress-strain curves for material 11SMn37

Table 11 - Tensile test results for material 11SMnPb30

Specimen	d0 [mm]	L0 [mm]	S0 [mm2]	du [mm]	Lu [mm]	Su [mm2]	Rp0.2 [MPa]	Rm [MPa]	A %	Z %
T1E	9,94	50	77,60	7,3	56,7	41,85	565	599	13,4	46,06
T2E	9,93	50	77,44	7,3	57,2	41,85	566	601	14,4	45,96
T3E	9,93	50	77,44	7,4	56,7	43,01	564	599	13,4	44,47

For the 11SMnPb30 steel, the obtained mean value for the R_{P02} and R_m are:

$$\overline{R_{P02}} = \frac{\sum_{i=1}^{3} R_{P02_i}}{3} = 565\ MPa;$$

$$\overline{R_m} = \frac{\sum_{i=1}^{3} R_{m_i}}{3} = 600\ MPa.$$
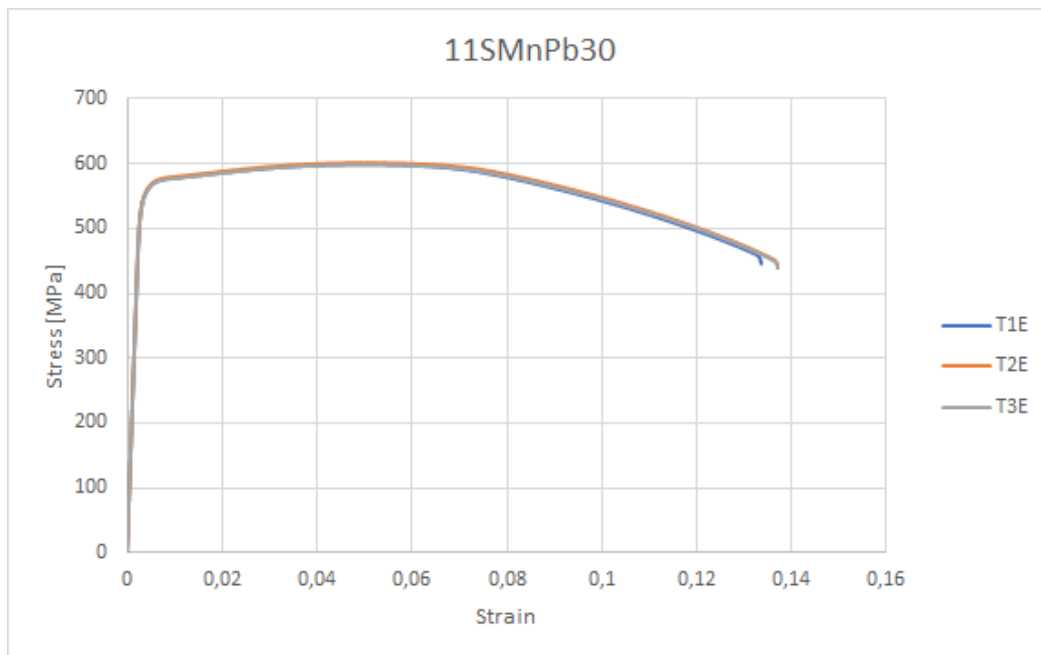
Figure 79 - Stress-strain curves for material 11SMnPb30

61

Specimen	d0 [mm]	L0 [mm]	S0 [mm2]	du [mm]	Lu [mm]	Su [mm2]	Rp0.2 [MPa]	Rm [MPa]	A %	Z %
T1F	9,95	50	77,76	7,6	56,45	45,36	574	611	12,9	41,66
T2F	9,95	50	77,76	7,7	56,2	46,57	581	618	12,4	40,11
T3F	9,94	50	77,60	7,6	56,15	45,36	577	615	12,3	41,54

For the 11SMnPb37 steel, the obtained mean value for the R_{P02} and R_m are:

$$\overline{R_{P02}} = \frac{\sum_{i=1}^{3} R_{P02_i}}{3} = 577 \ MPa;$$

$$\overline{R_m} = \frac{\sum_{i=1}^{3} R_{m_i}}{3} = 615 \ MPa.$$
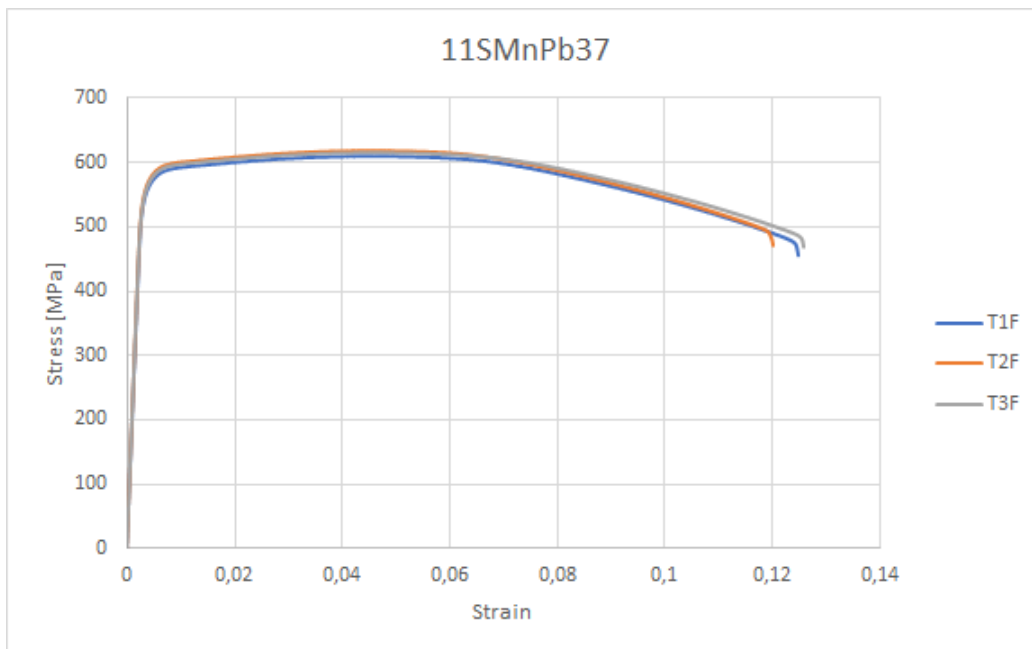
Figure 80 - Stress-strain curves for material 11SMnPb37

Comparing the curves obtained from all the tested material it can be seen the difference between them. All the considered steels showed a ductile behaviour but characterized by different values of maximum stress and strain.
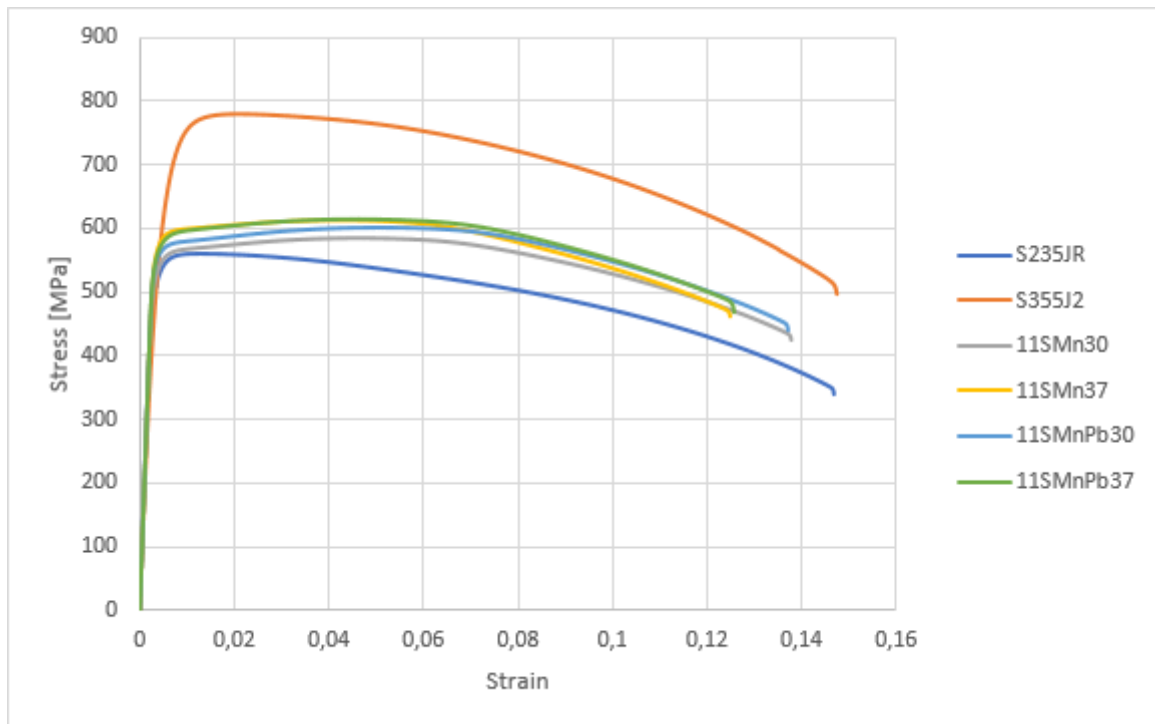
Figure 81 - Tensile tests results

Looking at the structural steels, it can be seen that they show almost the same elongation and, looking at the reported tables, a fairly similar decreasing of section during necking before complete fracture. The difference among these two materials stays in the values of stress reached during the test. The higher content of carbon present in the S355JR gives it a higher strength implying higher yielding and maximum stresses.

For what concerns the free-cutting steels, they show an almost identical behaviour both in terms of stress and strain. It can be seen that a higher content of sulphur leads to a lower ductility of the steel, showed in the graph by a lower elongation and in the tables by a lower decreasing of the cross-section during the necking phenomenon. Another interesting thing that can be noticed is that the presence of lead does not alter the result of the test.

Comparing now the two different kind of steels it is easy to see the differences among their behaviours. The free-cutting steels present a strain hardening phenomenon that isn't detectable in the structural steels. The presence of manganese-sulphides leads to a lower ductility and so a smaller elongation, while the large amount of manganese allows to compensate the lower content of carbon in terms of maximum applied stresses. In fact, all the free-cutting steels present a higher strength in respect to the S235JR, despite a lower carbon concentration.

Following the standard for the tensile test, the fracture has to occur within the marked section in order to consider valid the results. Considering the initial gauge length divided in three equal parts we can have two cases of correct fracture position. If the rupture occurs in the central section of the gauge length, the elongation can be calculated simply measuring the final gauge length and calculating the difference in respect to the original one. On the contrary, if the rupture occurs in one of the two side thirds of the gauge length the procedure is a little bit tricky.

Before proceeding with calculations, some references have to be defined:

- X is the side reference of the gauge length on the shorter piece of the specimen;
- Y is the reference of the gauge length on the longest piece of the specimen at the same distance of X from the fracture;
- N is the total number of intervals marked in the gauge length;
- n is the number of intervals within the references X and Y.
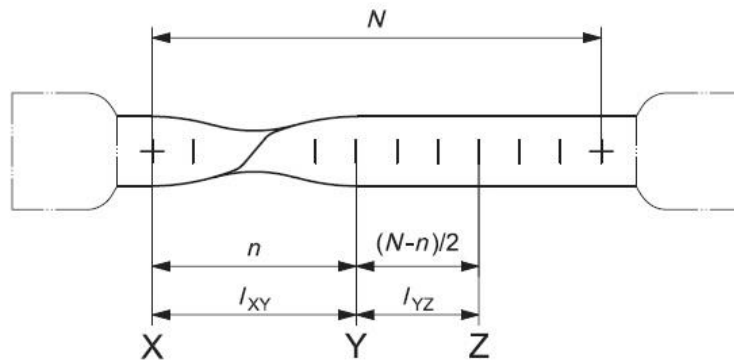
a) $N - n$ is an even number
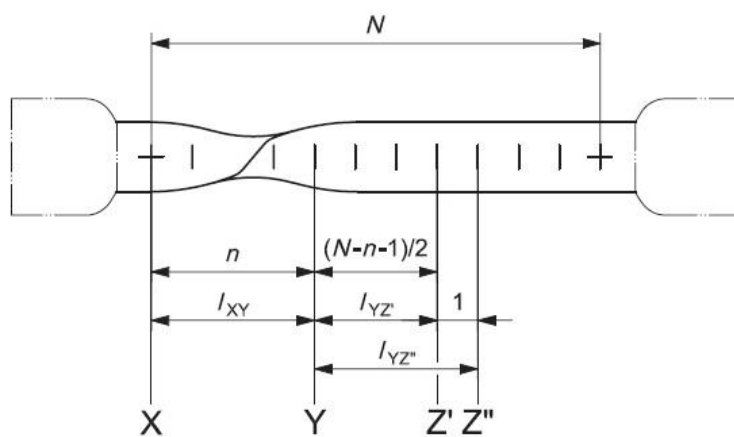
b) $N - n$ is an odd number

Figure 82 - Scheme for calculating the elongation

$$A\% = \frac{l_{xy} + 2l_{yz} - L_0}{L_0} \cdot 100 \qquad\qquad A\% = \frac{l_{xy} + l_{yz'} + l_{yz''} - L_0}{L_0} \cdot 100$$

<div align="center">

case a)   case b)

</div>

For what concerns this study, all the fractures occurred within the central third of the gauge length, as can be seen in the next pic, so this kind of calculations were not necessary.

Figure 83 - Specimen after the tensile test

4.2.2   Macroscopic analysis of the fractures

Visual inspection of the fracture surfaces is of great importance in order to understand how the specimen behaved during the test. After taking the necessary measurement for the calculations, the specimens were cut in order to obtain smaller samples and then the fracture surfaces have been photographed.

From the samples, it can be seen also by eyes that the necking occurred in the free-cutting steels is smaller than that occurred for the structural ones.

Figure 84 - Fracture surfaces S235JR

Figure 85 - Fracture surfaces S355J2

Figure 86 - Fracture surfaces 11SMn30

Figure 87 - Fracture surfaces 11SMn37

Figure 88 - Fracture surfaces 11SMnPb30

Figure 89 - Fracture surfaces 11SMnPb37

4.2.3 Microscopic analysis of the fractures

The same samples obtained for the macroscopic inspection were used also for the microscopic analysis acquiring pics with the SEM. All the samples have been cleaned in order to remove the possible oxides deposited on the surface. The main target for this analysis was to see how the material deformed during the test and in which way the particles present in the free-cutting steels modify this behaviour.

Some of the following pics are reported also in appendix B with other ones in order to better compare the different analysed materials.

Pics of the fracture surfaces were taken at different magnifications and in different positions in order to have an overview of the surface and some details demonstrating the behaviour of the material.

For what concerns the analysis of the structural steels they do not present anything in particular and can be taken as example to see the behaviour of a ductile material during the tensile test.
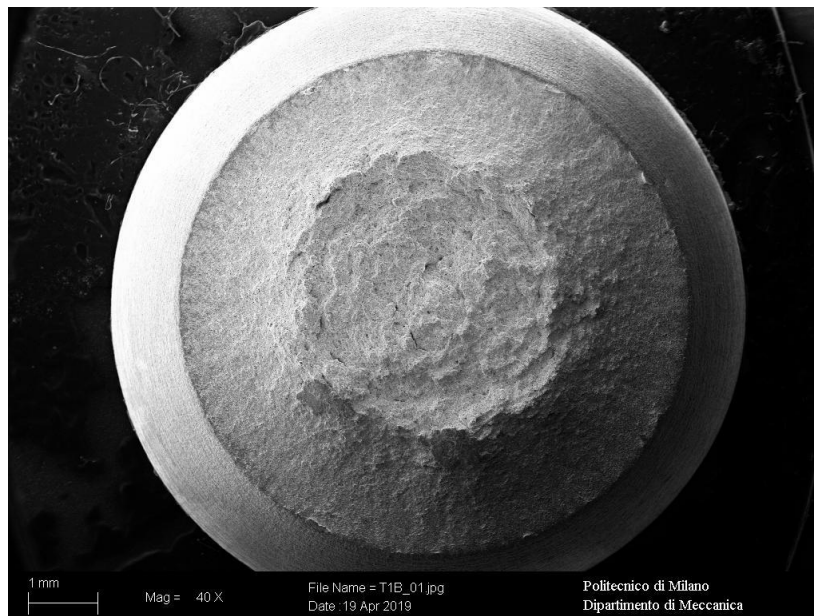
Figure 90 - S355J2 sample 40X

In the figure above it can be seen the typical "cone shape" assumed by a ductile material during the tensile test. The central almost plane part is constituted by the last resistant section of the specimen, while the surrounding one is inclined of almost 45° in respect to the axle of the specimen and is the part in which the material yields and flows during the necking phenomenon. Both the two parts present dimples, so the characteristic features of a ductile fracture, but it is possible to see that these dimples appear different looking in a position rather than the other.
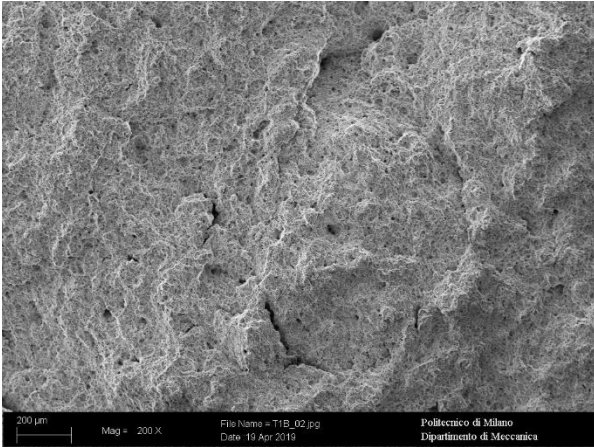
Figure 91 - S355J2 sample 200X
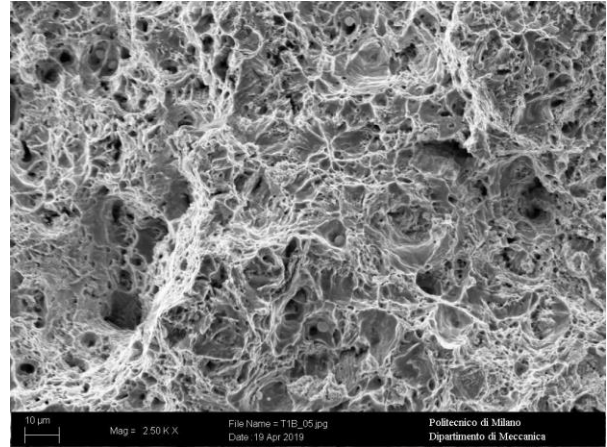
Figure 92 - S355J2 sample 2500X

As it can be seen from the above pictures, in the central part of the fracture, dimples appear regular, without any particular direction of elongation.
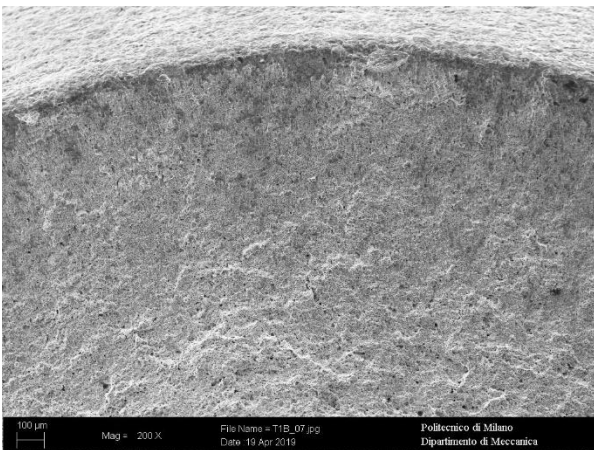
Figure 93 - S355J2 sample 200X
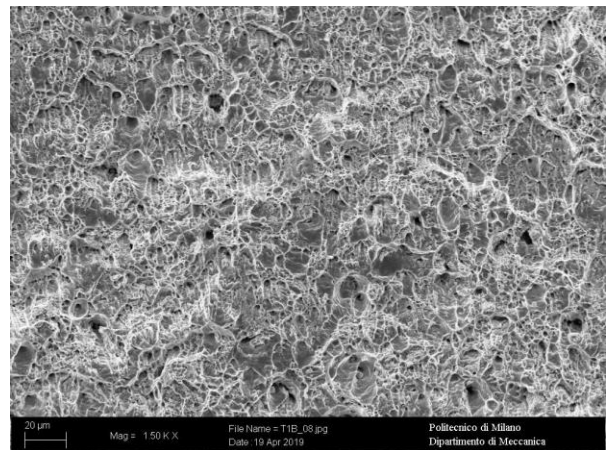
Figure 94 - S355J2 sample 1500X

Dimples present in the surrounding part, on the contrary, appear elongated in the radial direction, especially the most external ones, that are in the area where the necking phenomenon occurs more intensely.

In both the structural steels are present some grey particles visible in the dimples. The microscope used to take the pictures allows also to execute an analysis of the materials present in the material similar to that obtained with the quantometer. This analysis revealed that these inclusions are composed by Ca in its oxidized form. Its presence is helpful for different reasons, in fact adding it to the molten steel, it is possible to decrease the concentration of oxygen forming calcium oxides and this helps also in the refining of the grains during the solidification, obtaining so a more resistant material.
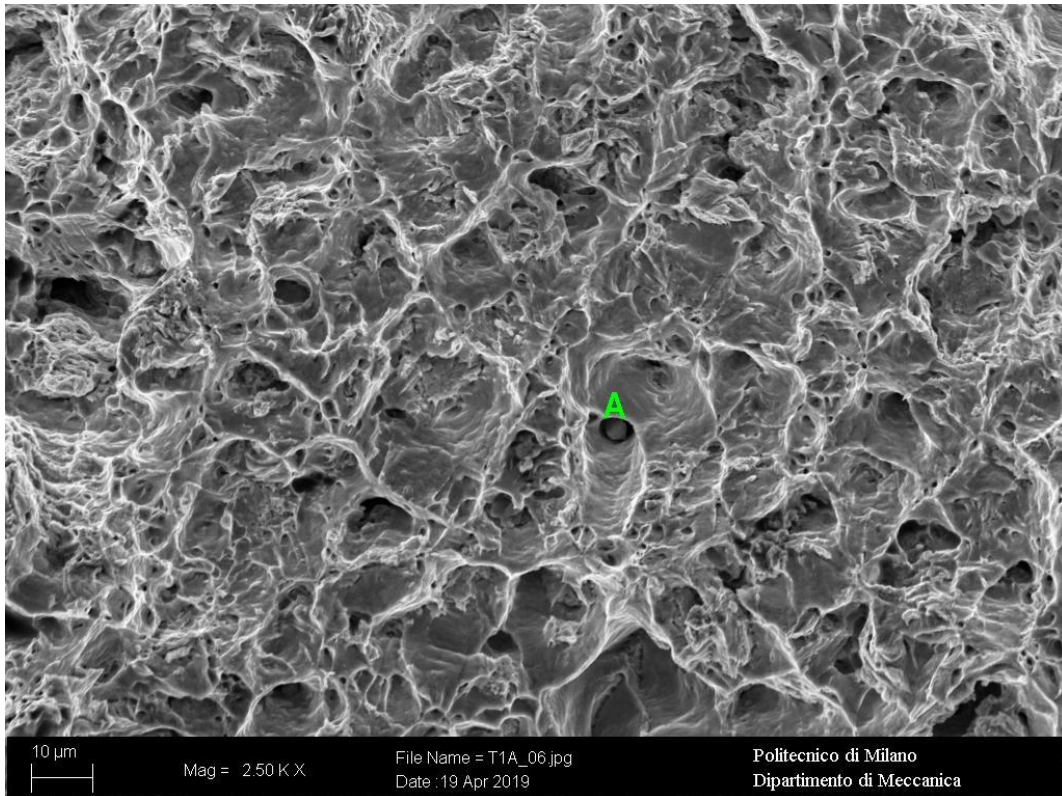
Figure 95 - S235JR sample 2500X

The particle marked with the letter "A" has been analysed and the following graph shows the chemical element found by the SEM.
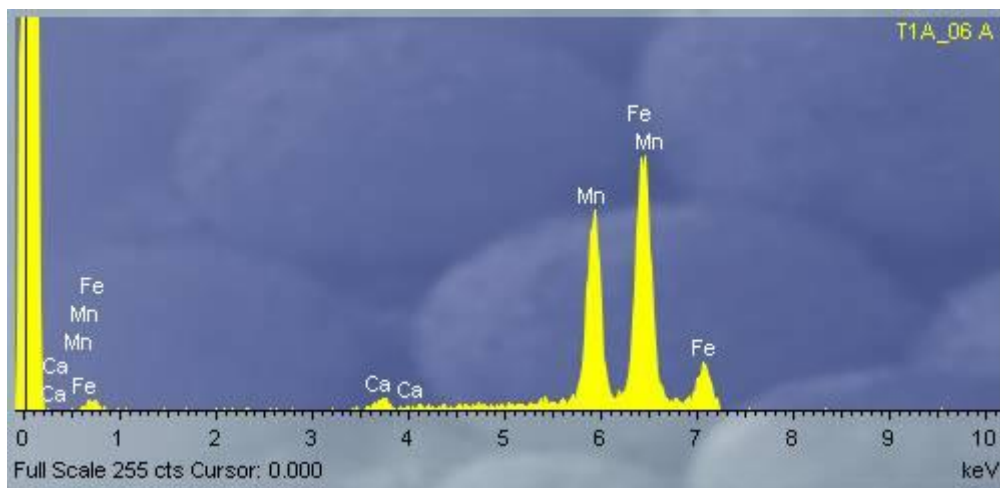
Figure 96 - Chemical analysis S235JR

As it can be seen the principal elements present are Fe; Mn and Ca. Fe and Mn are present in that they are the main chemical elements of the steel matrix, while Ca is present in form of inclusions.

Considering now the free-cutting steels, it can be seen that they present the same ductile behaviour, but the samples are characterized by a wider plane part and so a wider resistant section at the end of the necking phenomenon due to their lower ductility. This is due to the presence of a large number of inclusions (manganese sulphides) and is detectable also looking at the morphology of the surface. In fact, it presents always dimples, but those in the central part are very regular and they didn't slide between them, as opposed to the structural steels' ones. For this reason, in the central part the fracture appears more brittle from a macroscopic point of view than the other cases, in that the material showed a lower deformation.

Figure 97 - 11SMn37 sample 37X
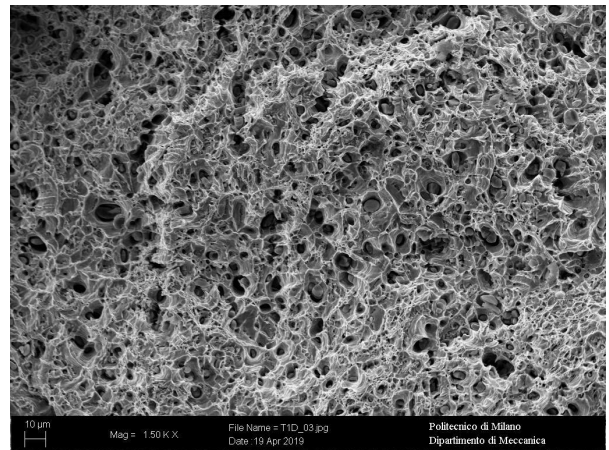
Figure 98 - 11SMn37 sample 1500X

Looking at the external part of the surface it is possible to see the same radial elongation of the dimples seen for the other materials.
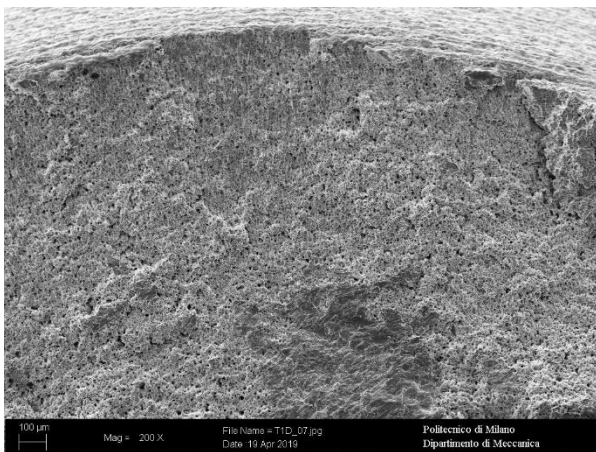
Figure 99 - 11SMn37 sample 200X
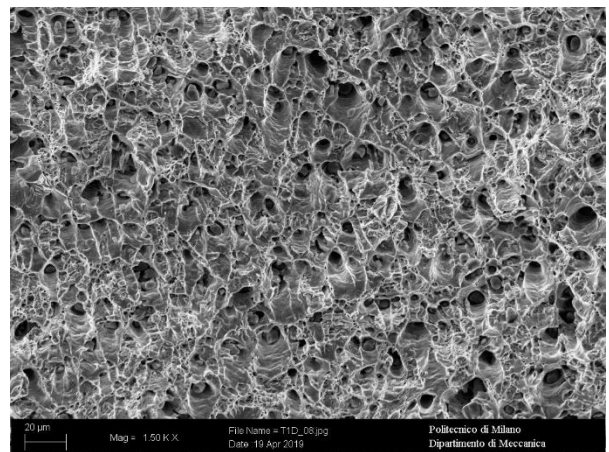
Figure 100 - 11SMn37 sample 1500X

Manganese sulphides are widely present in the material and it is possible to see them in the dimples as grey compounds with almost the same dimension of the occupied "hole".
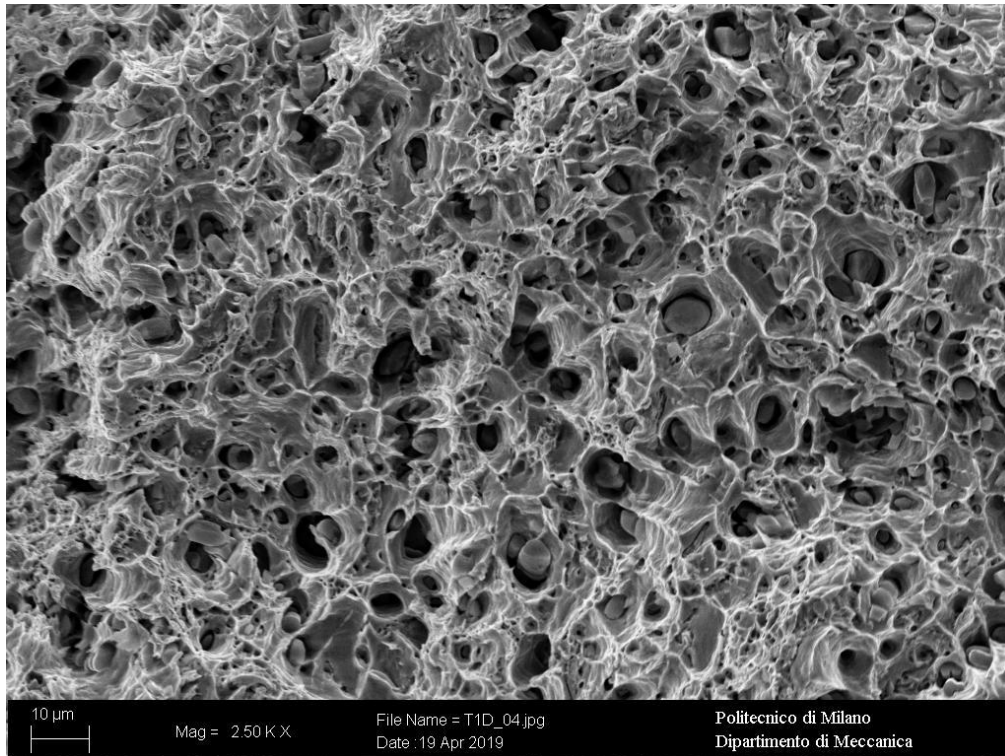
Figure 101 - 11SMn37 sample 2500X

The same picture was also acquired with the backscattered modality, that allow to better identify if are present or not different compounds and chemical elements but loosing information about the morphology of the surface. In the next picture, the particle marked with the letter "A" is a manganese sulphide as all the particles similar to it that seem to be encrusted in the surface.
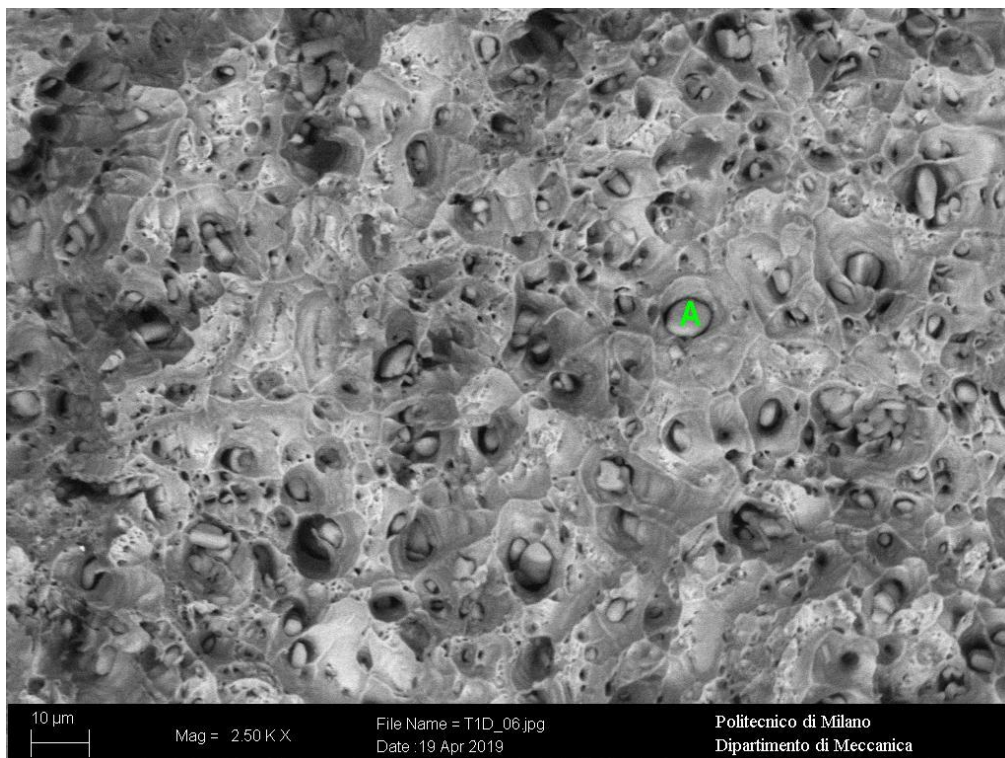
Figure 102 - 11SMn37 sample 2500X (backscattered)

All the free-cutting steels appear similar, the only difference stays in the presence of lead. This feature is visible only using the backscattered acquisition in which the lead appears in brighter colour spread over the surface or in scattered points.
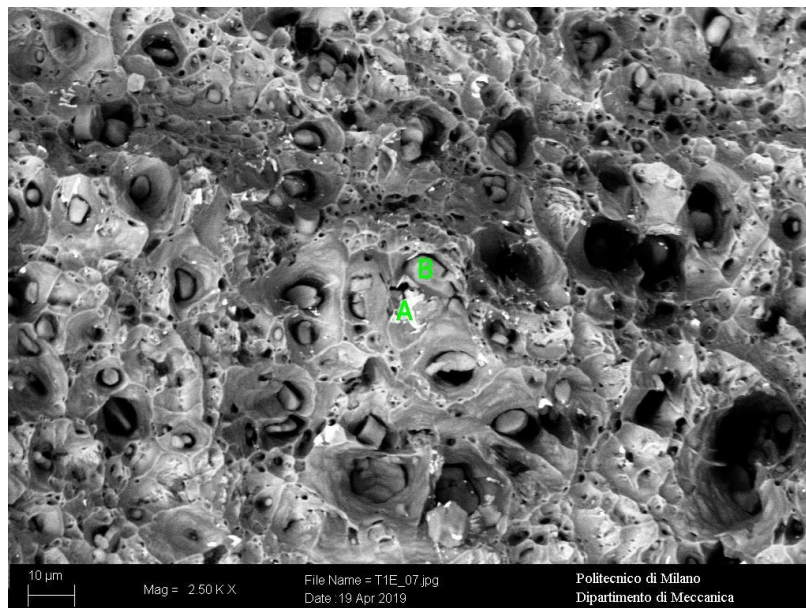
Figure 103 - 11SMnPb30 sample 2500X (backscattered)

In the picture above it can be seen the central area of the fracture, where lead is present in scattered points as that marked with letter "A" and manganese sulphides are widely present in the material as that marked with letter "B".

Instead, in the next figure, it is possible to see how the lead follows the direction of sliding of the dimples. Lead is more spread where the material had slide more, so in the external part of the fracture. This is due to the fact that lead is very malleable and being present at the grain boundary it deforms with the steel structure.
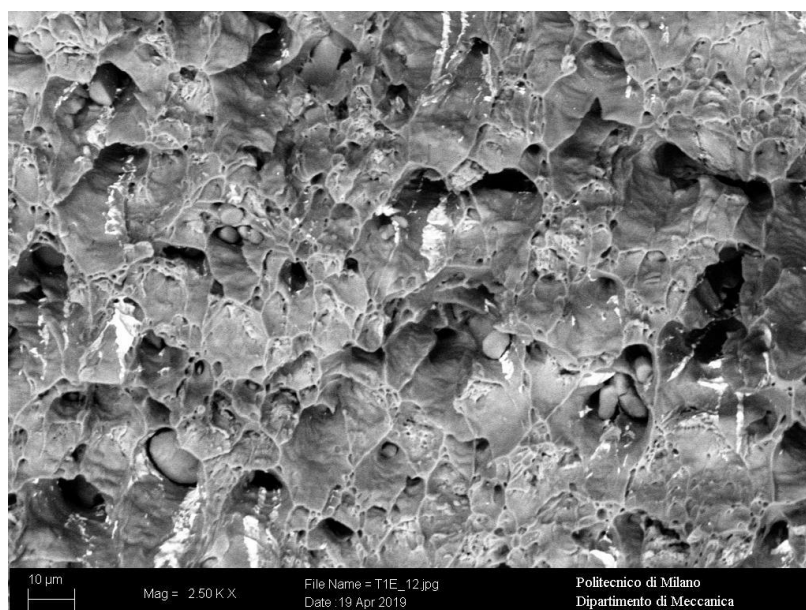
Figure 104 -11SMnPb30 sample 2500X (backscattered)

4.3 Charpy's pendulum test

Toughness tests were performed in the Hammer laboratory in Rho, using the Charpy's pendulum and specimens with a "V" shaped engrave following the standard UNI EN ISO 148-1.

Figure 105 - Charpy's pendulum

4.3.1 Test's execution and analysis

First of all, the specimens have been measured in order to check the correctness of the specific dimensions, while the engraves have been looked at a microscope in order to check the state of the internal fillet and the surface finishing.

For all the materials there were five sets of three specimens, apart from the steel S355J2 for which there were six sets. Each set of specimens were tested at a specific temperature, having so three replicates for each condition. For what concerns the structural steels they were tested at room temperature and at lower temperature levels till -80°C. Instead, the free-cutting steels were tested at temperature levels ranging from -20°C till 80°C. Negative temperatures have been reached immersing the specimens in "melting pot" containing a solution of ethanol and solid CO_2, while for temperatures higher than 20°C the specimens have been immersed in a tub containing water to which heating was provided with an heating system. Once reached the test temperature, the specimens have to be put quickly on the support of the machine, for this operation particular tongs are needed to handle the specimens avoiding errors in its positioning.
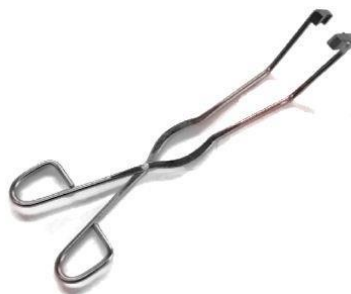
Figure 106 - Tongs for specimens handling

In the next tables are reported the results provided by the Charpy's pendulum for all the materials.

Table 13 - Toughness test results for material S235JR

Specimen	Temperature [°C]	KV [J]
R1A	20	156
R2A	20	150
R3A	20	142
R13A	10	147
R14A	10	142
R15A	10	148
R10A	0	22
R11A	0	20
R12A	0	18
R7A	-20	6
R8A	-20	8
R9A	-20	11
R4A	-80	4
R5A	-80	4
R6A	-80	3

Table 14 - Toughness test results for material S355J2

Specimen	Temperature [°C]	KV [J]
R1B	20	156
R2B	20	148
R3B	20	158
R10B	0	148
R11B	0	152
R12B	0	156
R13B	-10	130
R14B	-10	131
R15B	-10	133
R16B	-20	56
R17B	-20	46
R18B	-20	50
R7B	-30	40
R8B	-30	34
R9B	-30	36
R4B	-80	9
R5B	-80	7
R6B	-80	8

Table 15 - Toughness test results for material 11SMn30

Specimen	Temperature [°C]	KV [J]
R7C	80	40
R8C	80	35
R9C	80	37
R10C	60	36
R11C	60	33
R12C	60	40
R13C	40	35
R14C	40	28
R15C	40	25
R1C	20	9
R2C	20	13
R3C	20	13
R4C	-20	4
R5C	-20	3
R6C	-20	4

Table 16 - Toughness test results for material 11SMn37

Specimen	Temperature [°C]	KV [J]
R7D	80	29
R8D	80	27
R9D	80	28
R10D	60	27
R11D	60	27
R12D	60	29
R13D	40	21
R14D	40	23
R15D	40	21
R1D	20	9
R2D	20	15
R3D	20	14
R4D	-20	4
R5D	-20	4
R6D	-20	3

Table 17 - Toughness test results for material 11SMnPb30 Table 18 - Toughness test results for material 11SMnPb37

Specimen	Temperature [°C]	KV [J]
R7E	80	31
R8E	80	34
R9E	80	33
R10E	60	33
R11E	60	31
R12E	60	33
R13E	40	26
R14E	40	28
R15E	40	29
R1E	20	17
R2E	20	18
R3E	20	16
R4E	-20	5
R5E	-20	4
R6E	-20	4

Specimen	Temperature [°C]	KV [J]
R7F	80	27
R8F	80	27
R9F	80	28
R10F	60	26
R11F	60	26
R12F	60	28
R13F	40	25
R14F	40	22
R15F	40	24
R1F	20	19
R2F	20	21
R3F	20	20
R4F	-20	7
R5F	-20	6
R6F	-20	4

As can be seen from the results, the structural steels show a ductile behaviour at room temperature and become brittle going down with the temperature. On the contrary the free-cutting steels at room temperature show an already low toughness level, the dissipated energy increased increasing the temperature level showing a transition to a ductile behaviour. In order to detect the DBTT (ductile-brittle transition temperature), the results of the tests have been graphically reported. Usually it is possible to recognize two side zones showing a small gradient in the energy level, corresponding to the brittle and ductile behaviour of the material, and a central part in which the dissipated energy decreases a lot decreasing the temperature. All the following curves represent the interpolation of the mean energy levels calculated for each temperature from the test results.
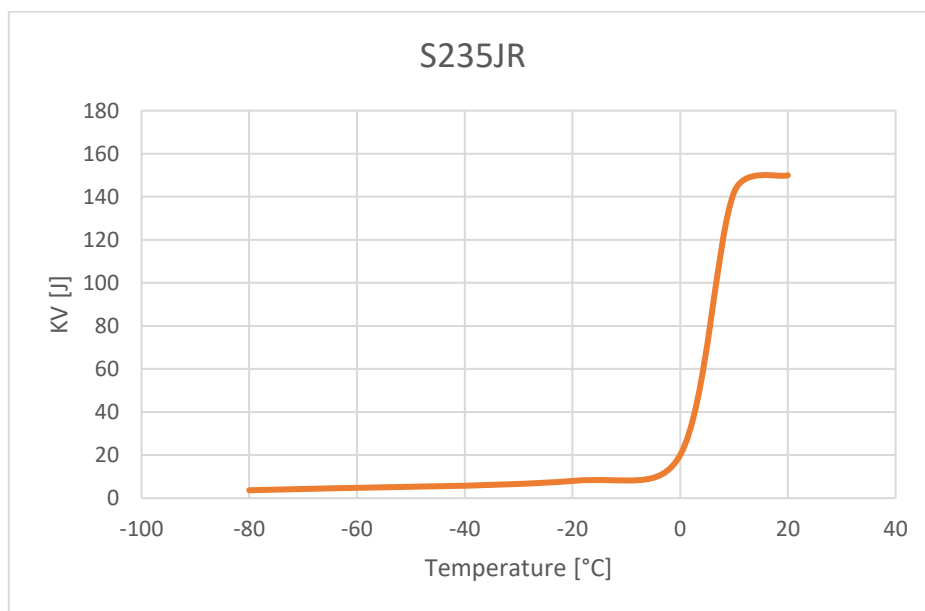
Figure 107 - Transition curve for the material S235JR
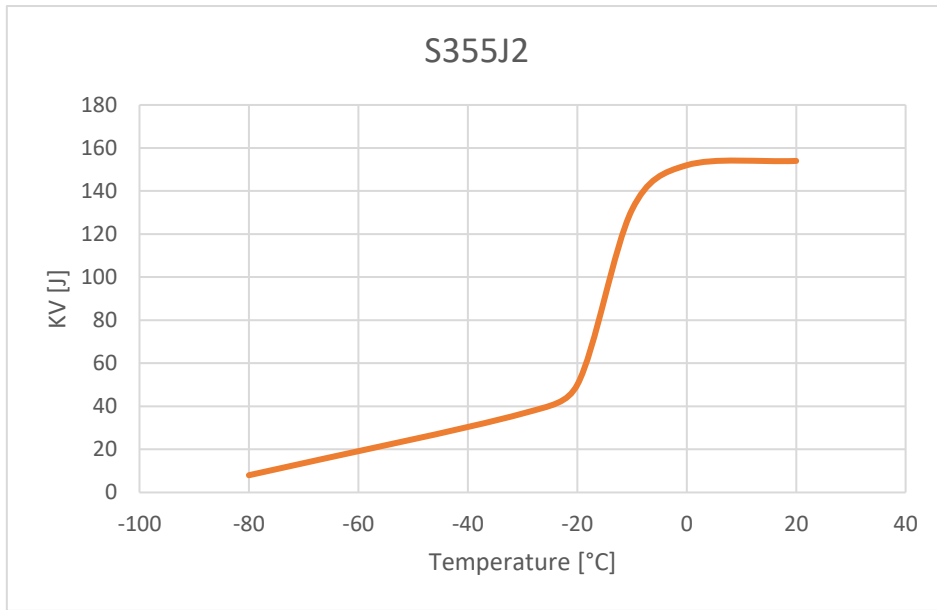
Figure 108 - Transition curve for the material S355J2

For the steel S235JR, the transition temperature can be taken at 5°C and it can be seen that it respects its designation for which it has to absorb at least 27J at 20°C (JR).

For the steel S355J2, the transition temperature is around -15°C and it respect its designation absorbing more than 27J at -20°C. The transition curve is almost complete, in that it is able to show the DBTT, detectable about -15°C, however there would be to test other specimens at lower temperature in order to find the limit for the brittle part of the curve.

As usual, the structural steels present a well-defined transition zone, with very high difference in the values of absorbed energy passing from ductile to brittle behaviour, the same cannot be said for the free-cutting steels.
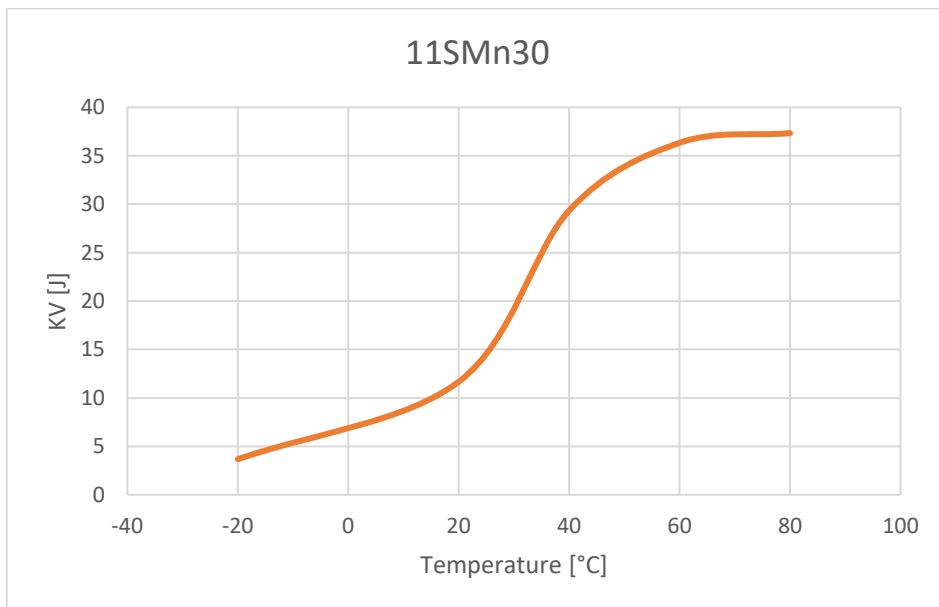
Figure 109 - Transition curve for the material 11SMn30

76
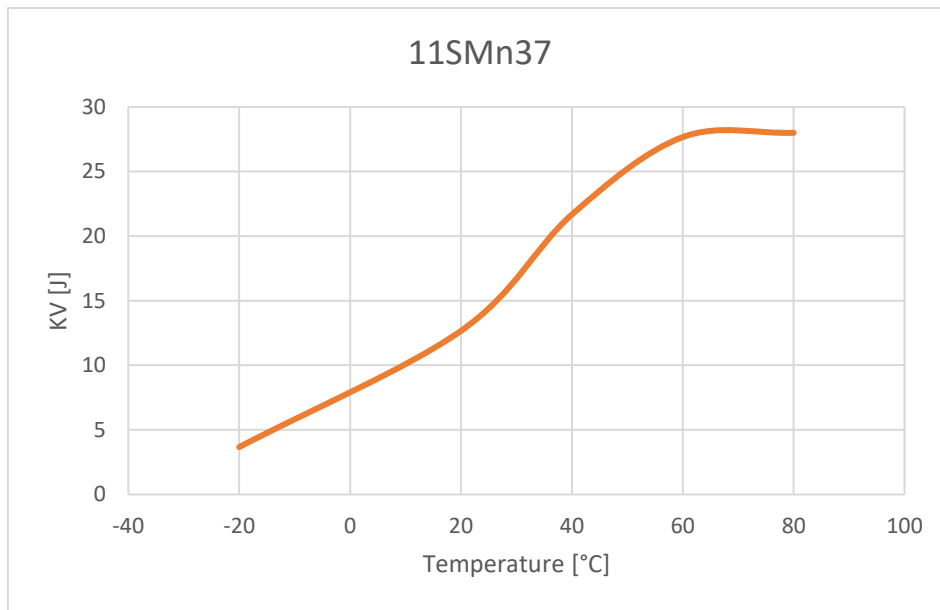
Figure 110 - Transition curve for the material 11SMn37

From the graphs, the transition from ductile to brittle behaviour is not so evident, this is due also to the not so high values of energy dissipated by the material even in the ductile case. The DBTT can be found as the temperature corresponding to the half of the maximum energy value registered. For the material 11SMn30 this temperature can be considered as around 30°C, while for the 11SMn37 it is fairly lower, abound 25°C.
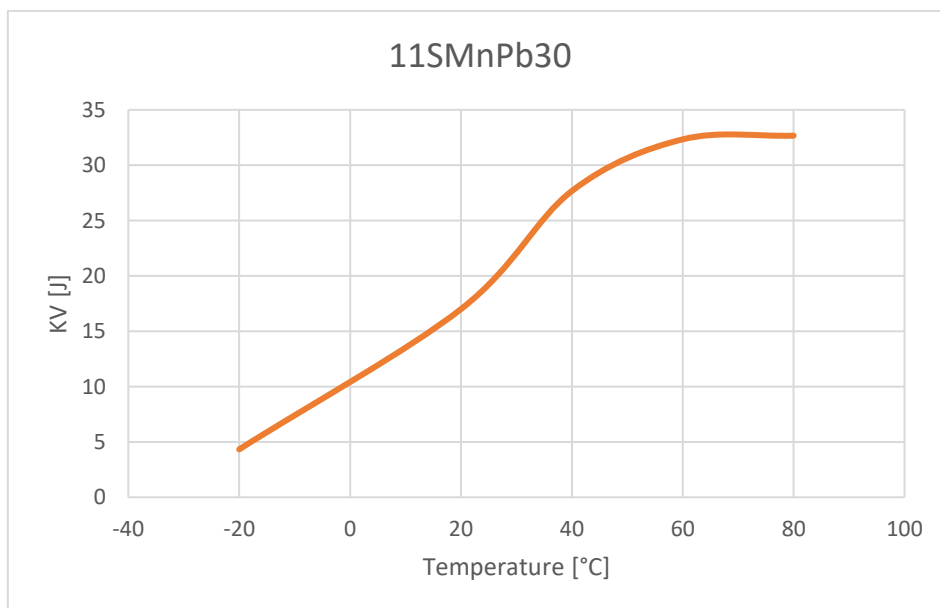
Figure 111 - Transition curve for the material 11SMnPb30
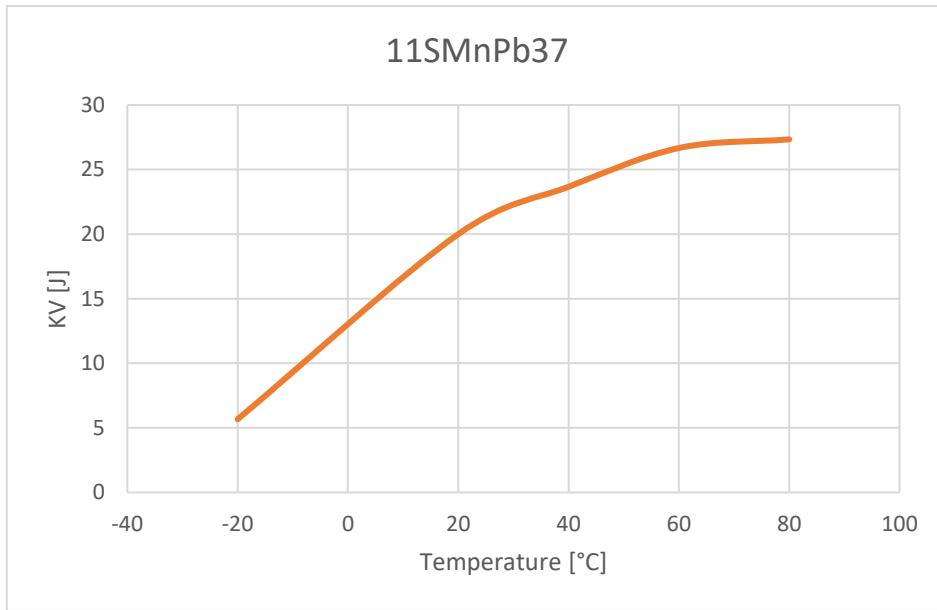
Figure 112 - Transition curve for the material 11SMnPb37

Using the same method, the DBTT for the material 11SMnPb30 can be evaluated about 20°C, while for the 11SMnPb37 it is about 5°C.

In order to evaluate the results and the effect of the different chemical compositions it is better to group the curves in a single graph.
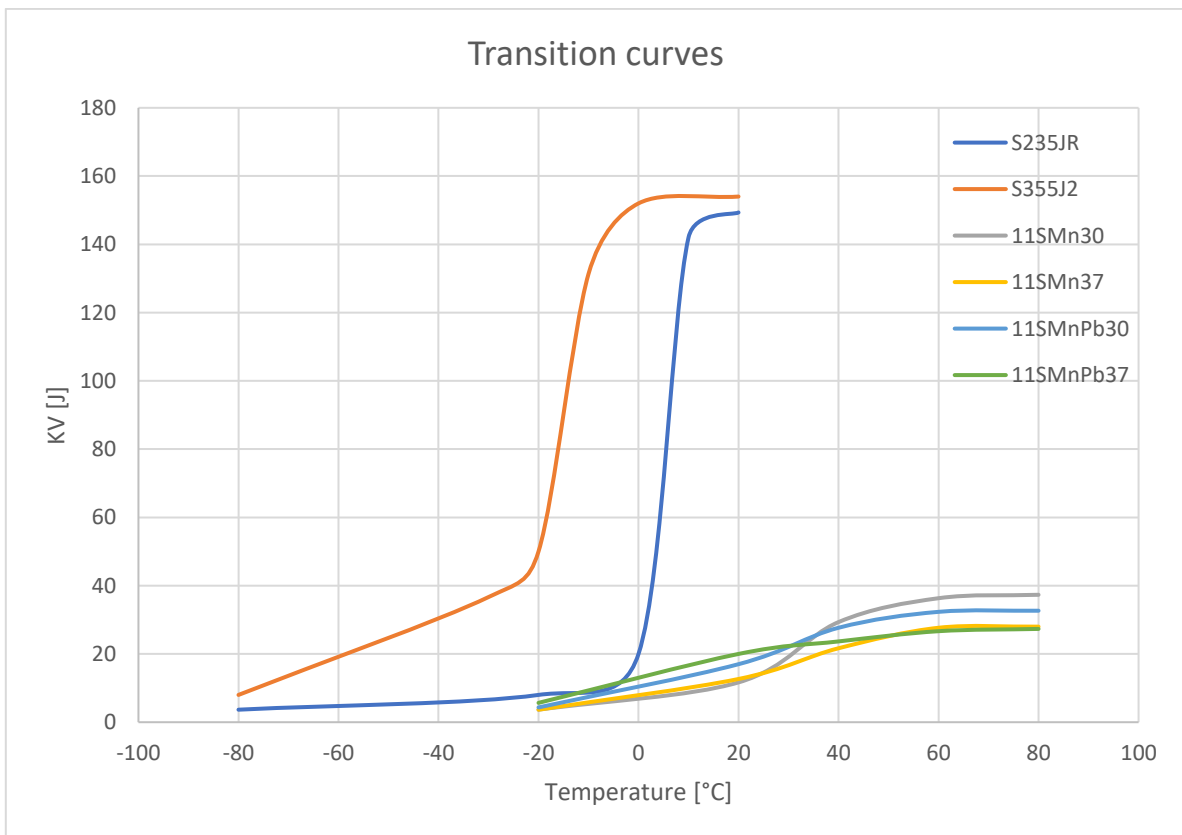
Figure 113 - Transition curves

From the graph it is evident the difference between the two kind of steels, both for the dissipated energy and for the transition temperature, they have clearly two different fields of application.

Comparing the two structural steels it is easy to see that at room temperature there are almost equal, while for lower temperature the S355J2 maintain a ductile behaviour mainly due to higher manganese content. For example, at 0°C the S235JR shows an already brittle behaviour, while the S355J2 is steel a ductile material.

For what concerns the free-cutting steels the factors under study are the sulphur content and presence of lead.
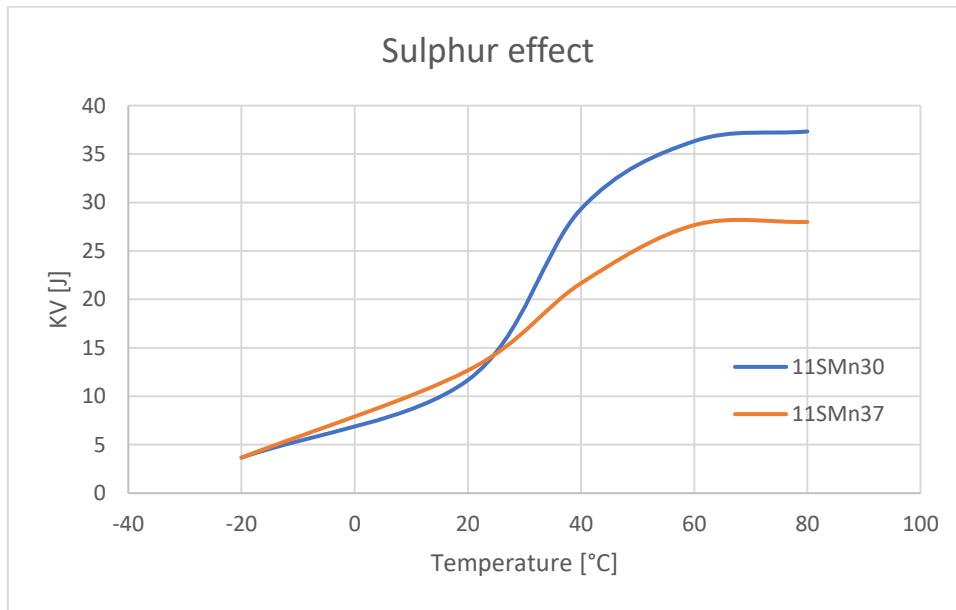
Figure 114 - Sulphur's effect on the transition curves

As can be seen, an increasing in the sulphur concentration leads to a lower energy dissipation in the ductile zone, so to an embrittlement of the material. The DBTT decreases, but not so evidently, while the brittle part zone of the curve does not seem to be affected.
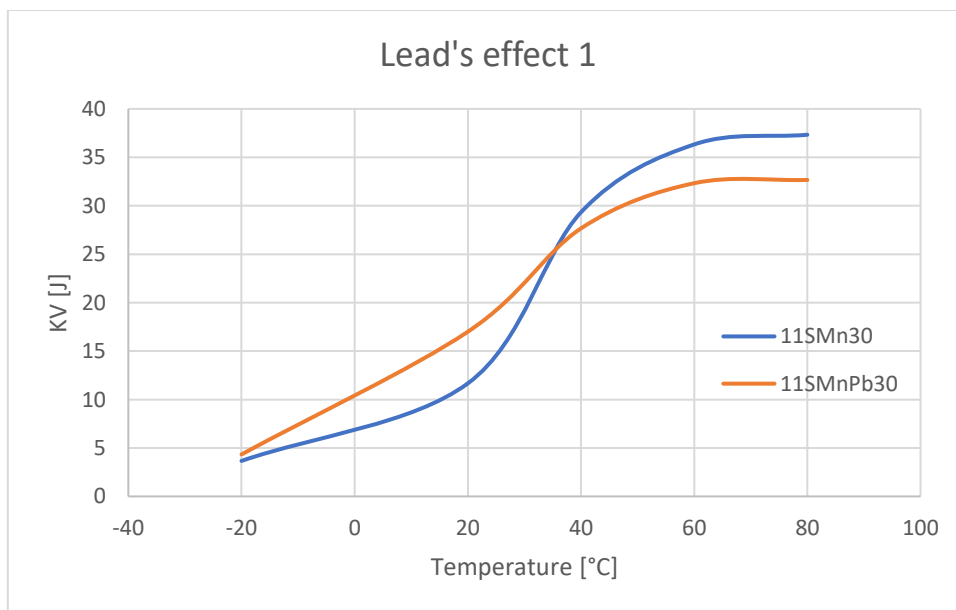
Figure 115 - Lead's effect with lower sulphur concentration

79
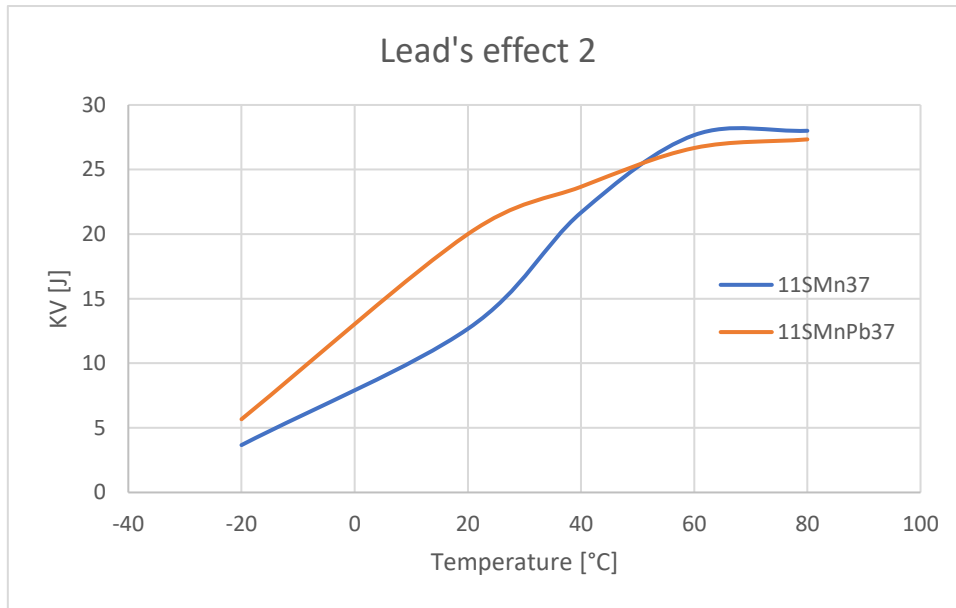
Figure 116 - Lead's effect with higher sulphur concentration

The presence of lead in the steels reduces a bit the DBTT enlarging the ductile field of the materials, but it also tends to reduce the energy absorption of the material in this area.

4.3.2 Macroscopic analysis of the fractures

For each material and for each temperature level a specimen was taken in order to compare the fractures appearance. From the macroscopic appearance of the fracture surface it is possible to identify the ductile and brittle zones and so to understand if at that temperature the behaviour of the material was completely ductile, brittle or both. The ductile zones appear darker, while the brittle ones present a lighter colour, this is due to the way in which the light is reflected from the surface.

From the macroscopic analysis, also the DBTT can be evaluated looking at the percentage of the fracture's area in which the material behaves in a brittle way. The transition temperature corresponds more or less to that temperature level at which the specimen presents a brittle fracture on half of its surface.

Key
1 notch
2 cleavage area (brittle)
3 shear area (dull)
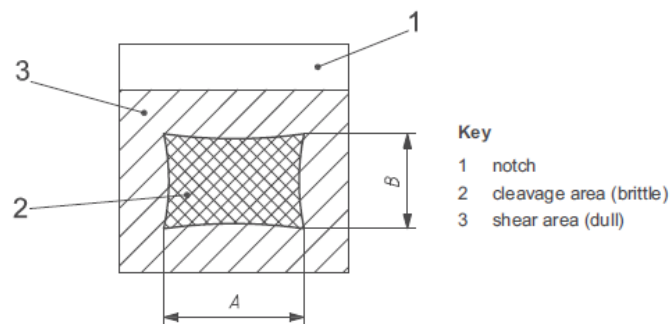
Figure 117 - Distinction between ductile and brittle area

Measuring "A" and "B" as indicated in the figure above and interpolating their values in the next table, the percentage of ductile area can be retrieved.

Table 19 - Per cent shear for measurements in millimetres

B mm	A mm																		
	1,0	1,5	2,0	2,5	3,0	3,5	4,0	4,5	5,0	5,5	6,0	6,5	7,0	7,5	8,0	8,5	9,0	9,5	10
	Per cent shear																		
1,0	99	98	98	97	96	96	95	94	94	93	92	92	91	91	90	89	89	88	88
1,5	98	97	96	95	94	93	92	92	91	90	89	88	87	86	85	84	83	82	81
2,0	98	96	95	94	92	91	90	89	88	86	85	84	82	81	80	79	77	76	75
2,5	97	95	94	92	91	89	88	86	84	83	81	80	78	77	75	73	72	70	69
3,0	96	94	92	91	89	87	85	83	81	79	77	76	74	72	70	68	66	64	62
3,5	96	93	91	89	87	85	82	80	78	76	74	72	69	67	65	63	61	58	56
4,0	95	92	90	88	85	82	80	77	75	72	70	67	65	62	60	57	55	52	50
4,5	94	92	89	86	83	80	77	75	72	69	66	63	61	58	55	52	49	46	44
5,0	94	91	88	85	81	78	75	72	69	66	62	59	56	53	50	47	44	41	37
5,5	93	90	86	83	79	76	72	69	66	62	59	55	52	48	45	42	38	35	31
6,0	92	89	85	81	77	74	70	66	62	59	55	51	47	44	40	36	33	29	25
6,5	92	88	84	80	76	72	67	63	59	55	51	47	43	39	35	31	27	23	19
7,0	91	87	82	78	74	69	65	61	56	52	47	43	39	34	30	26	21	17	12
7,5	91	86	81	77	72	67	62	58	53	48	44	39	34	30	25	20	16	11	6
8,0	90	85	80	75	70	65	60	55	50	45	40	35	30	25	20	15	10	5	0

100 % shear shall be reported when either *A* or *B* is zero.

Let's start analysing the fracture surfaces of the structural steels.
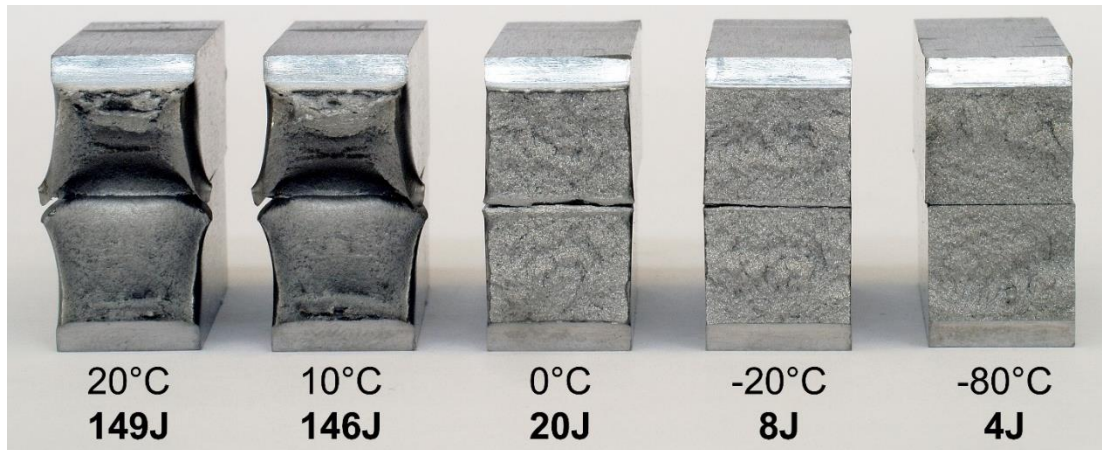
Figure 118 - Temperature's effect S235JR

It can be seen by eyes, comparing the fracture surfaces, that for what concerns the S235JR steel there are two completely different behaviours. In fact, this material presents a completely ductile fracture at room temperature and at 10°C, characterized by plastic deformations detectable also with in a very large side expansion. The specimen tested at 0°C presents an almost completely brittle fracture, apart from very small areas at the side that present a ductile behaviour. The specimens tested at negative temperatures present a completely brittle fracture keeping unmodified the dimensions of the cross area. The transition temperature, as suggested by the transition curve of the material, can be detected between 10°C and 0°C.

The specimens of the S355J2 steel were tested at very near temperature levels about the foreseen transition temperature, in order to better detect the change in the behaviour of the fracture. This choice limited the number of specimens for the brittle zone, but the ones tested at –80°C were sufficient in order to detect the completely brittle behaviour of the material.
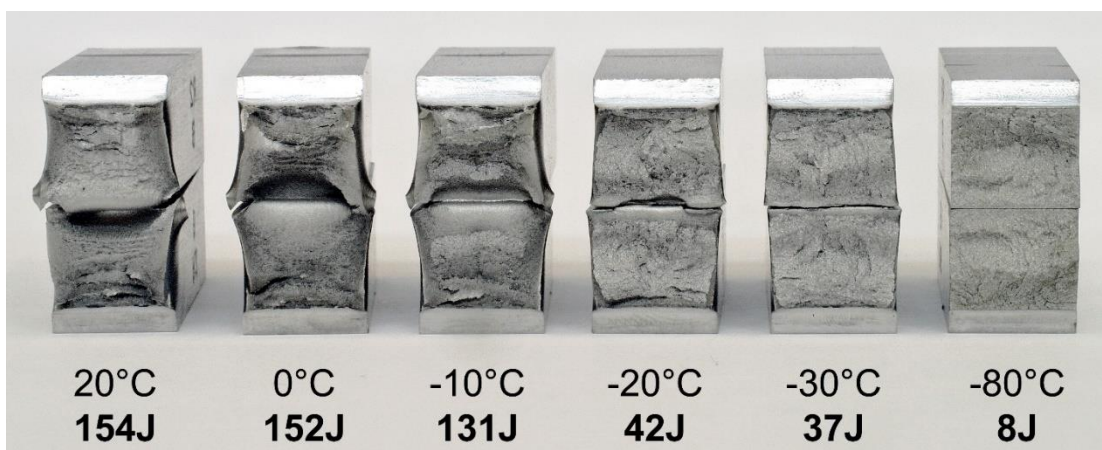
Figure 119 - Temperature's effect S355J2

The specimens tested at room temperature and at 0°C present a completely ductile behaviour, while a -10°C the fracture starts to behave in a brittle way at the centre of the specimen occupying the 10-15% of the area. The specimens tested at -20°C present an almost completely brittle fracture but characterized by small plastic

82

deformation zones at the sides and in the lower part, that in the opposite part in respect to the engraving. In this case the percentage of the area are inverted, the brittle fracture occupies the 90% of the area. At -30°C the fracture is completely brittle with a very small side deformations with a percentage of the ductile zone around the 1-5%. The last analysed case is that at -80°C that, as said before, shows a brittle fracture on the whole cross section of the specimen without any plastic deformation. For this material, looking at the percentage of the ductile and brittle areas, the transition temperature can be detected between -10°C and -20°C.

Let's now take in consideration the free-cutting steels, where the different colours of the fracture surface due to the oxidation of the material helps to easily identify the ductile zones from the brittle ones.
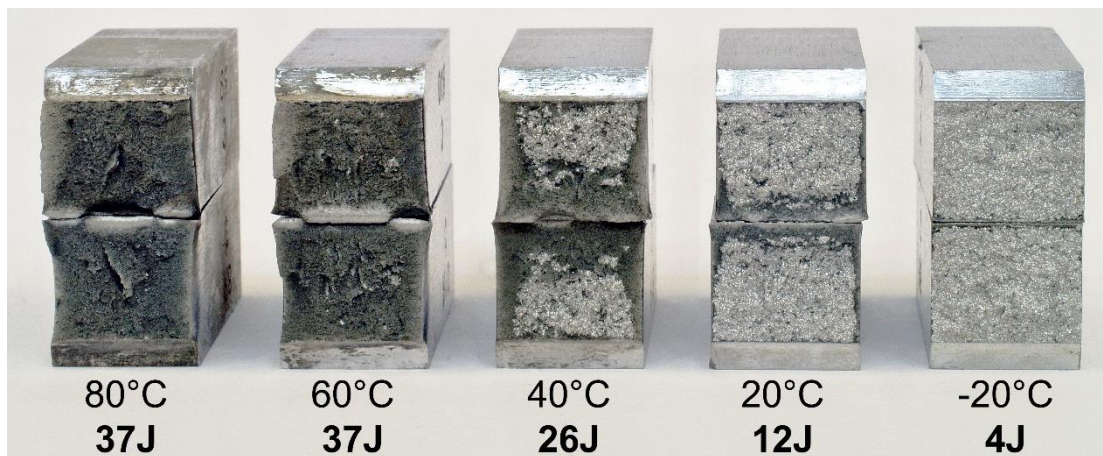
Figure 120 - Temperature's effect 11SMn30

For what concerns the11SMn30 steel, the specimens tested at 80°C and 60°C present a completely ductile behaviour also if the entity of the deformations is very small. This is due to the material itself that is not so ductile as the structural steels, as noticed during the tensile tests and from the maximum values of the absorbed energy. At 40°C the specimens present a brittle zone in the central part varying from the 40% to the 70% of the total cross section, so the transition temperature can be evaluated about this temperature level. The fracture surfaces of the specimens tested at 20°C show a very large brittle area with only the 20% of the cross section presenting a ductile behaviour, concentrated at the boundaries. At -20°C this material behaves in a completely brittle way without any deformation. In this last case, some very small parts show a different colour but, analysing them with the SEM, it was clear that also in these zones the fracture is completely brittle.
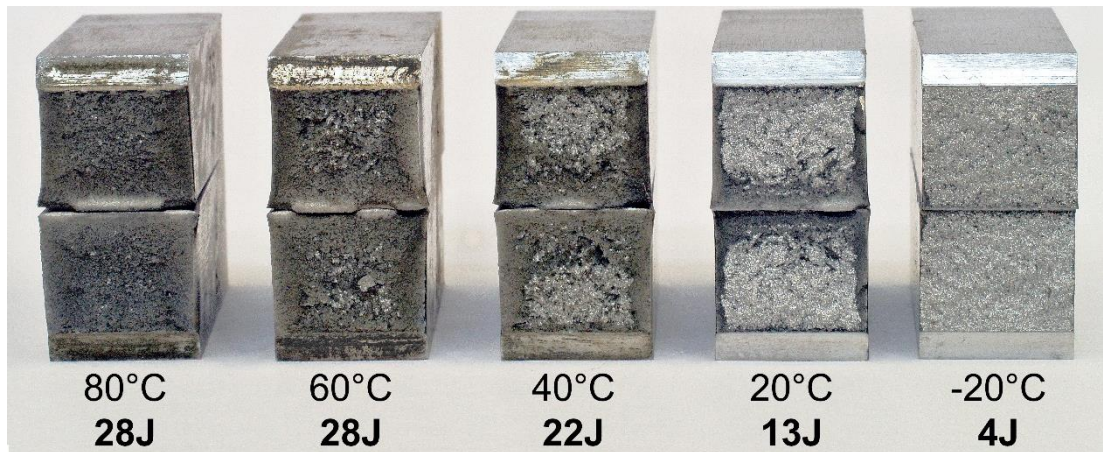
Figure 121 - Temperature's effect 11SMn37

The results obtained for the 11SMn37 steel are very similar to the ones presented before. The fractures of the specimens tested at 80°C and 60°C present a completely ductile behaviour. The scattered points that seem to present a brittle behaviour were analysed with the SEM and the above statement were confirmed. At 40°C the fractures present for the 60% a brittle behaviour, so the transition temperature has to be a little bit higher. For the last two temperature levels the considerations are the same made for the 11SMn30, the only small difference is that at 20°C this material presents a little bit higher percentage of ductile area.
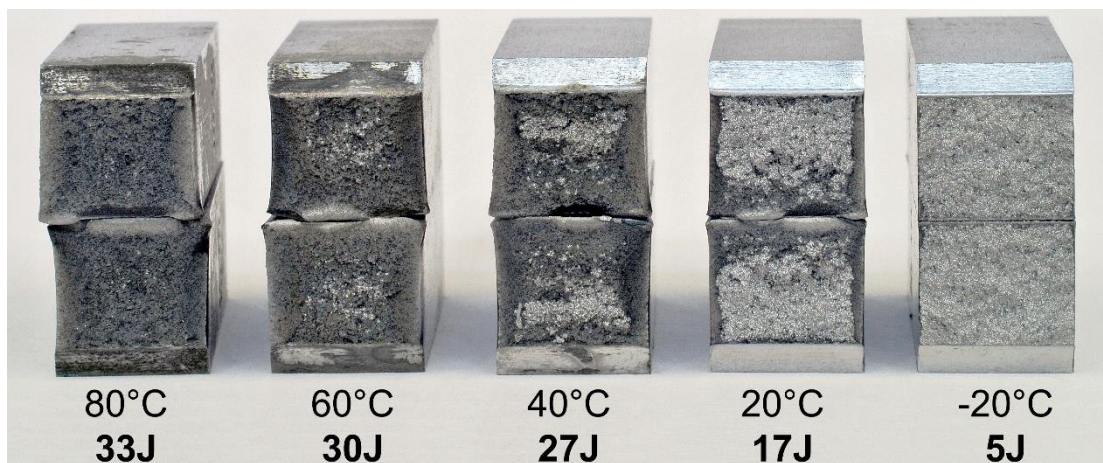
Figure 122 - Temperature's effect 11SMnPb30

As observed with the transition curves, the addition of lead doesn't change so much the properties of the material. The specimens tested at the two higher temperature levels present a completely ductile fracture, while at 40°C the ductile area is about the 60% of the total cross section. At 20°C the brittle area occupies about the 85% of the cross section, so the transition temperature can be detected between these last two temperature levels. As for the previous analysed materials, at -20°C the fracture is completely brittle. At each temperature level the values of absorbed energy are comparable, if not equal, to those observed for the 11SMn30 steel.
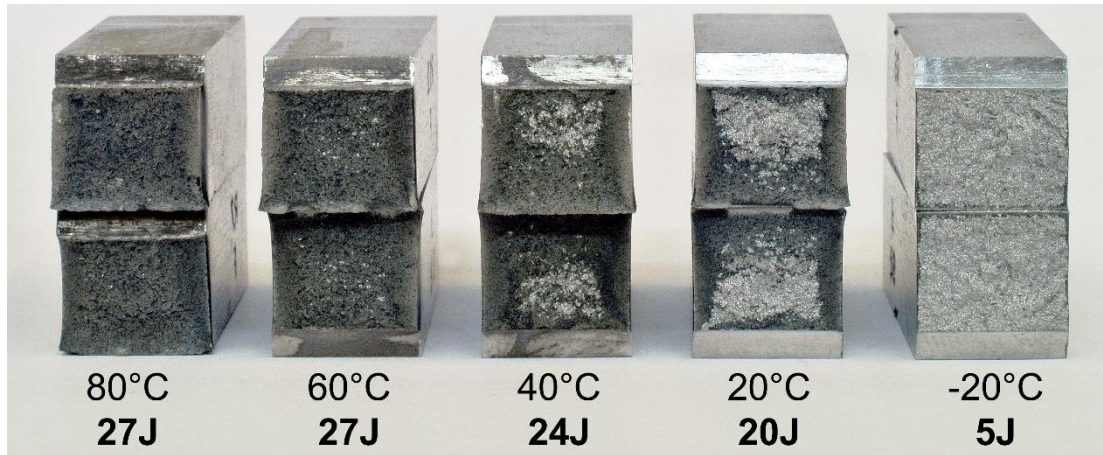
Figure 123 - Temperature's effect 11SMnPb30

In this last case, the situation is very similar to that observed with the correspondent material without lead. As in the previous case the greater difference stays in the appearance of the surfaces, but this can be due to the fact that lead promotes the macroscopic sliding of the material also when it presents a microscopic brittle behaviour. As for all the other materials, a microscopic analysis was carried out in order to check in a more precise way the behaviour of the material. The specimens tested at 80°C and 60°C present a completely ductile fracture with values of absorbed energy almost equal to those obtained by the 11SMn37 steel. At 40°C the brittle area is about the 30% of the cross section, while at 20°C it reaches the 80%, determining a transition temperature between these two temperature levels. As all the other free-cutting steels, at -20°C the specimens present a completely brittle fracture.

For what concerns the two methods used to find the transition temperature of the materials, it is evident that for both of them the results are more accurate increasing the number of temperature levels, but this imply a very high number of tests and so higher costs. Furthermore, as said previously, the DBTT is a qualitative indication about the material's behaviour, so its exact value isn't so important also because it varies according to the considered method acquiring a different definition.

4.3.3 Microscopic analysis of the fractures

After the macroscopic analysis, the fractures were observed with a SEM in order to check the correctness of the evaluations made about the percentage of the cross section presenting a brittle or ductile behaviour of the material, but also to be able to see how the different materials present a brittle behaviour and how their chemical composition influenced it.

Considering the structural steels, there's nothing in their chemical composition of particular importance for the microscopic analysis, the reported figures show the microscopic appearance of the fractures obtained at different temperatures where it is possible to recognize dimples, characteristic feature of a ductile behaviour, or the metallographic planes, characteristic feature of a trans-granular brittle behaviour
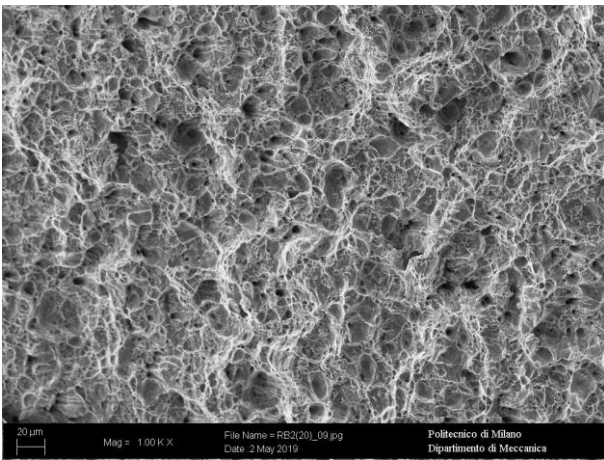
Figure 124 - S355J2 at 20°C 1000X
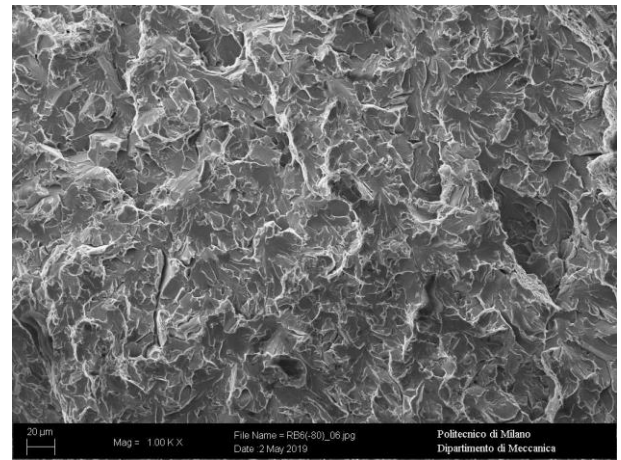
Figure 125 - S355J2 at -80°C 1000X

In the next figure it is possible to see both the two types of fracture, this is possible when the cross section presents both the two kind of behaviour, especially near the boundaries of the cross section.
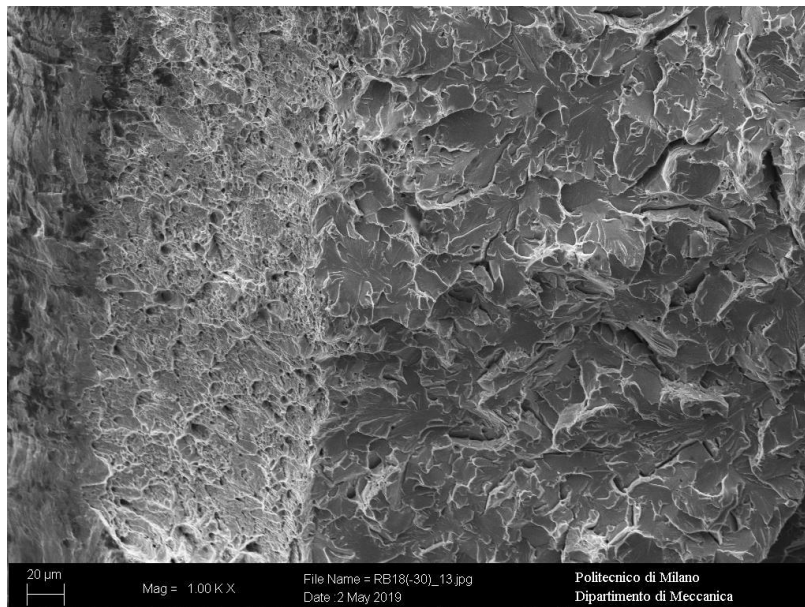
Figure 126 - S355J2 at -30°C 1000X

Dealing with the free-cutting steels, it is possible to see the manganese sulphides and their dimensions in relation to dimples and especially, in case of brittle fractures, in respect to grains.
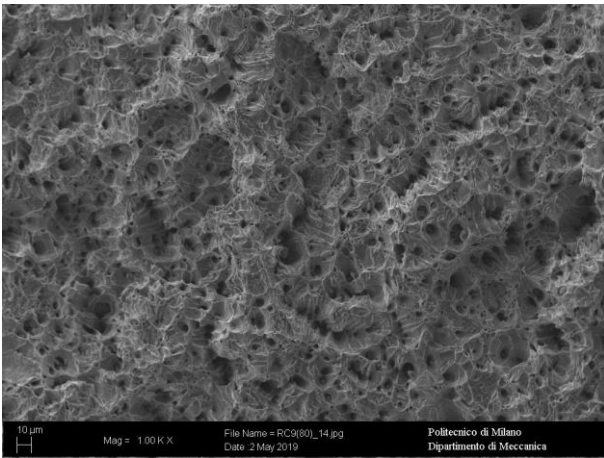
Figure 127 - 11SMn30 at 80°C 1000X
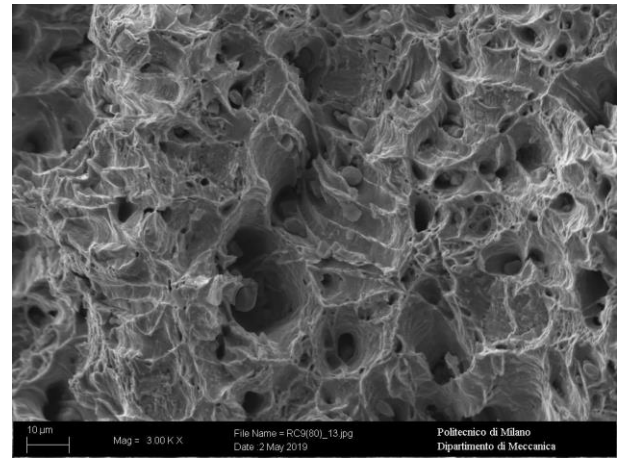
Figure 128 - 11SMn30 at 80°C 3000X

Looking at the figures above, it is possible to notice how the ductile behaviour of a free-cutting steel, seems different from the same behaviour of a structural steel, in that both present dimples, but those showed by the 11SMn30 steel appears smaller and more regular in respect to those showed by the S355J2 steel. This imply a macroscopic more brittle appearance of the fracture and it is due to the presence of the manganese sulphides that limit the sliding of the material.
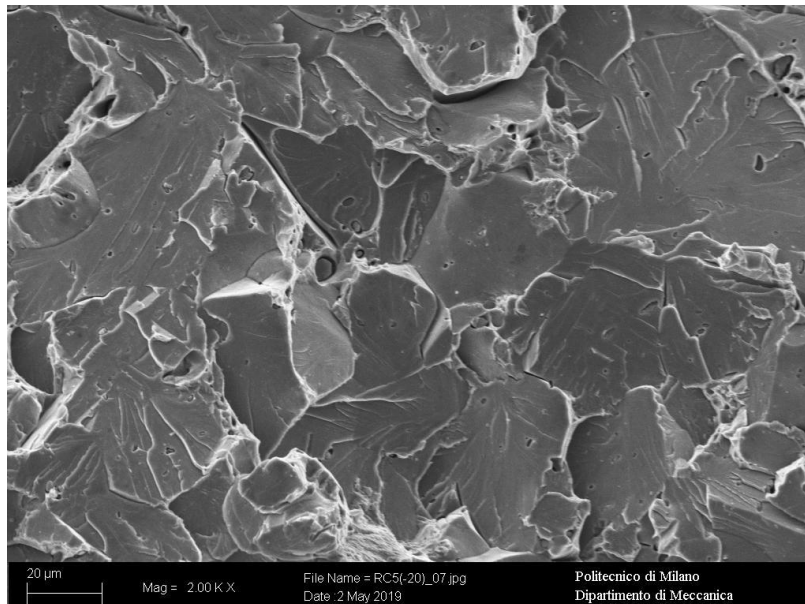
Figure 129 - 11SMn30 at -20°C 2000X

As can be seen from the figure, the brittle fracture of a free-cutting steel is not so different from that of a structural steel, but it is possible to individuate some very little "holes" on the planes created during the fracture or near their junctions. These holes are the signs leaved from the manganese sulphides, that are not visible because they are lost during planes separation.

In the next figure is possible to appreciate both the behaviours of the material, where the trans-granular fracture is surrounded by dimples, this is possible when the material starts to behave in a brittle way in the centre of the specimen.
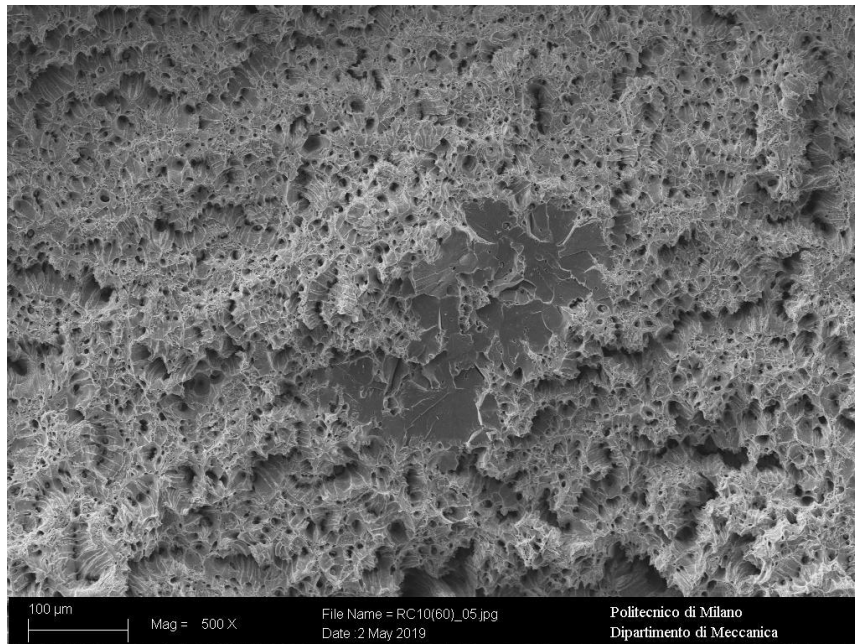
Figure 130 - 11SMn30 at 60°C 500X

In order to see the presence of lead in the material, also the 11SMnPb30 steel has been analysed.
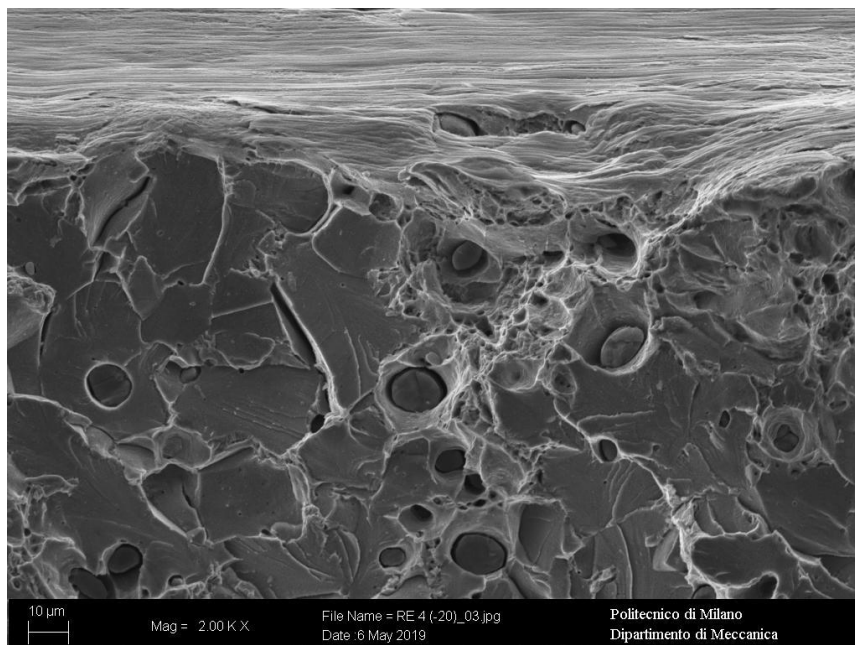
Figure 131 - 11SMnPb30 at -20°C 2000X

The appearance of the fractures isn't different from that of the 11SMn30 steel, but in the above figure it is possible to see both the ductile and brittle behaviours, containing very large manganese sulphides embedded in the structure.

The next figures show also the backscattered acquisitions that are the only ones that allow to see the lead and its distribution.
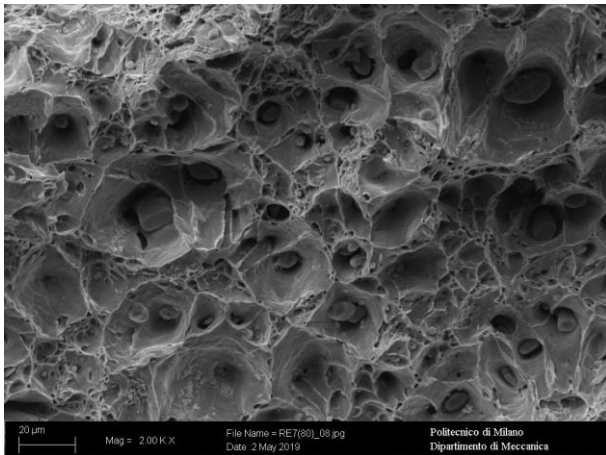
Figure 132 - 11SMnPb30 at 80°C 2000X
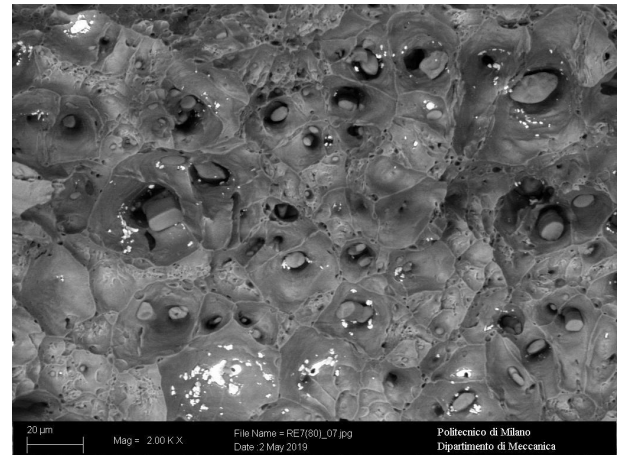
Figure 133 - 11SMnPb30 at 80°C 2000X (backscattered)
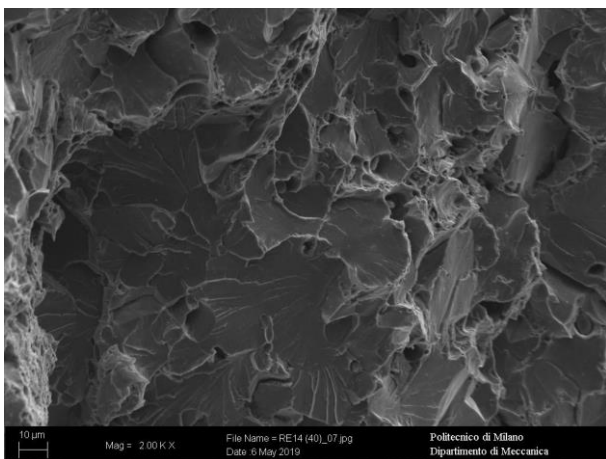
Figure 134 - 11SMnPb30 at 40°C 2000X
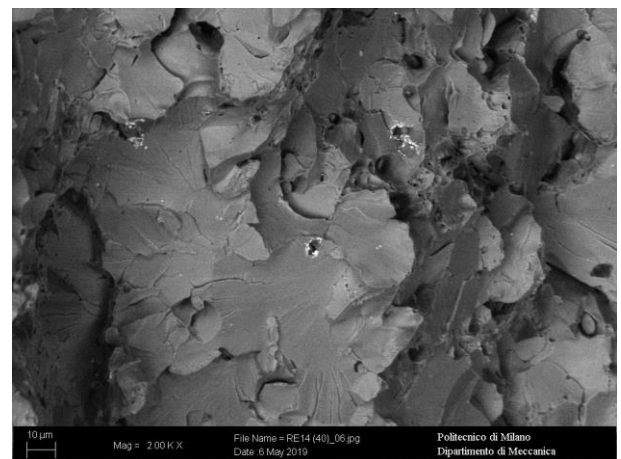
Figure 135 - 11SMnPb30 at 40°C 2000X (backscattered)

From the above figures it is clear that is possible to notice the presence of lead when the material behaves in a ductile way, but it is not so easy to detect it in case of brittle fracture. Just a little concentration of lead is evident in figure 135 in correspondence of a manganese sulphides. In the next figure, that is a magnification of the previous one, it is possible to appreciate how lead focuses its presence near a manganese sulphide.
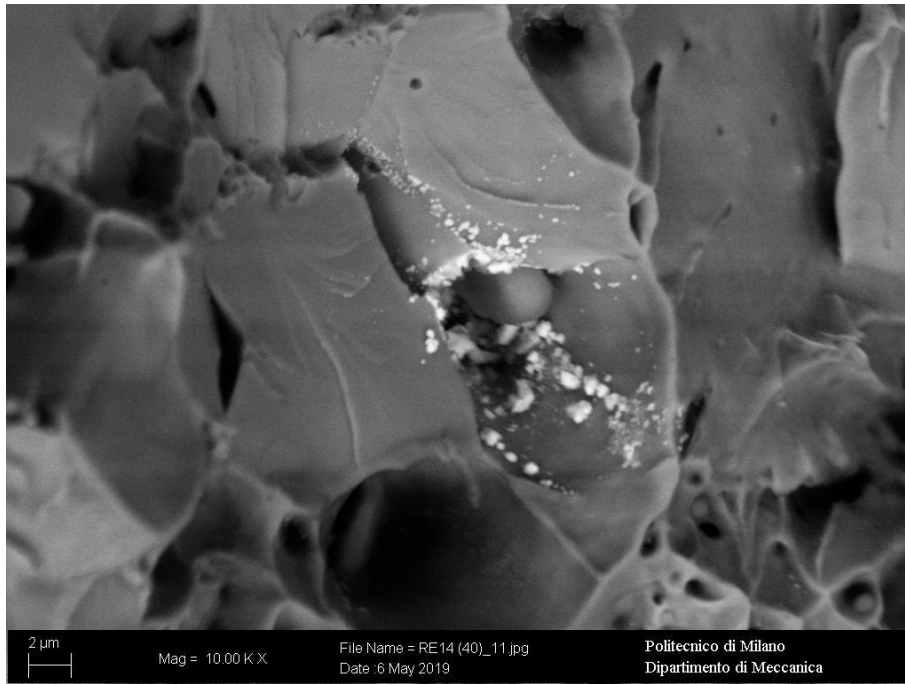
Figure 136 - Detail of a manganese sulphide surrounded by lead's particles 10000X (backscattered)

4.4 Rotating bending fatigue test

Fatigue tests were performed in the laboratories of Politecnico following the standard ISO 1143. Having only 8 specimens available for each material under study, it has been decided to use them to derive the fatigue limit using the Dixon method, leaving out the determination of the finite life of the materials, for which a higher number of specimens would have been needed.

Before proceeding with the tests, the specimens have been polished in the central part, were the cross section reduces, making the sample take on an hourglass shape. This operation is of great importance in that every little defect on the surface of the specimen could acts as initiation point for a crack, bringing to the failure of the piece in a very short time or with a very low applied load and so affecting the results of the test. In order to remove the signs left by the previous machining operations, some abrasives papers were used decreasing time to time the abrasive's dimensions (codes of the used papers: 40; 80; 120; 240; 400; 600). This operation was performed using a manual lathe on which a holder for the abrasive paper has been mounted, this device allowed to move and keep in contact the abrasive paper with the rotating specimen.

Figure 137 - Lathe used for polishing operations

Figure 138 - Detail of the paper's holder

After this polishing operation, another one was performed using a tumbler in order to obtain a smoother surface of the specimens. The functioning of this device is very simple, specimens are kept on a rotating holder that puts them in a contact with abrasive stones contained in a bin. Specimens undergo this treatment slowly rotating about their axis and about that of the holder device for almost twenty hours smoothing all the possible remaining defects on their surface.

Once obtained a good surface finishing, the specimens were examined using a profilometer in the Hammer's laboratory in Rho, in order to verify the absence of defects on the central part and to measure the mean diameter of the smallest cross section. This dimension is of fundamental importance for the test in order to calculate the correct load to be applied during the test and it must be measured after all the polishing operations that would reduce the specimen's cross section. In order to do that, five measurements were taken, and the mean diameter was calculated from them.

4.4.1 "Dixon" method ("UP-AND-DOWN" method)

Generally, the "Stair-case" method is used to estimate a quantity like in case of the fatigue limit, but it needs a large number of specimens (at least 50) leading to very high costs. For this reason, the "Dixon" method, that takes its name from W. J. Dixon, was chosen, in that it needs a limited number of specimens. The principle behind both the methods is the same, perform tests at different levels of applied load and determine by convergence the quantity of interest. The procedure starts choosing an initial value supposed near to that of interest that for bending fatigue can be estimated about the 50-55% of the ultimate tensile strength obtained by the tensile tests. A value for the interval between the two different load levels has to be decided, it is called "Δσ" and it must be constant for all the tests performed on a single material. The applied load to the subsequent specimen must be decreased of "Δσ" in case of failure, classified with letter "X", while it must be increased of the same value in case the tested specimen doesn't break after a predetermined number of cycles, in this case the test is classified with the letter "O". For each material, a series of 8 tests has been carried out, resulting in a sequence of "X" and "O". These sequences are composed by two parts divided by the first change of trend in the results, so the first part, composed by the test with equal response at the beginning of the sequence, can contain only one test or more tests that reported the same result "X" or "O", while the second part contains all the other tests. The number of tests present in the second part of the sequence determines two different methods proposed by Dixon. The first method proposed by W. J. Dixon must be used when the second part of the sequence contains 5 or less tests, while for a higher number of tests after the change of trend the second one must be used, let's now analyse them.

In the first case, so when the second part of the sequence contains at maximum 5 results, the following formula must be used:

$$\sigma_{lim} = \sigma_f + k \cdot \Delta\sigma$$

where "σ_{lim}" is the estimation of the fatigue limit of the material at which the 50% of the specimens will break, indicated in the "Dixon" method by LD_{50} (lethal dose for the 50% of the tests). The stress "σ_f" is the value of stress applied to the last specimen of the sequence, while "k" is a coefficient that can be retrieved from a table provided by Dixon in its standard that relates the first and second part of the sequence with this constant. As said before "Δσ" is the value of the interval between two levels of stress for the tests.

In this first case the table reporting the values of the coefficient "k" reports also an estimate of the standard error that can be used in order to retrieve the standard deviation.

N	Second Part of Series	k for Test Series Whose First Part is					Standard Error of LD₅₀
		O	OO	OOO	OOOO		
2	X	−.500	−.388	−.378	−.377	O	.88σ
3	XO	.842	.890	.894	.894	OX	.76σ
	XX	−.178	.000	.026	.028	OO	
4	XOO	.299	.314	.315	.315	OXX	.67σ
	XOX	−.500	−.439	−.432	−.432	OXO	
	XXO	1.000	1.122	1.139	1.140	OOX	
	XXX	.194	.449	.500	.506	OOO	
5	XOOO	−.157	−.154	−.154	−.154	OXXX	.61σ
	XOOX	−.878	−.861	−.860	−.860	OXXO	
	XOXO	.701	.737	.741	.741	OXOX	
	XOXX	.084	.169	.181	.182	OXOO	
	XXOO	.305	.372	.380	.381	OOXX	
	XXOX	−.305	−.169	−.144	−.142	OOXO	
	XXXO	1.288	1.500	1.544	1.549	OOOX	
	XXXX	.555	.897	.985	1.000+1	OOOO	
6	XOOOO	−.547	−.547	−.547	−.547	OXXXX	.56σ
	XOOOX	−1.250	−1.247	−1.246	−1.246	OXXXO	
	XOOXO	.372	.380	.381	.381	OXXOX	
	XOOXX	−.169	−.144	−.142	−.142	OXXOO	
	XOXOO	.022	.039	.040	.040	OXOXX	
	XOXOX	−.500	−.458	−.453	−.453	OXOXO	
	XOXXO	1.169	1.237	1.247	1.248	OXOOX	
	XOXXX	.611	.732	.756	.758	OXOOO	
	XXOOO	−.296	−.266	−.263	−.263	OOXXX	
	XXOOX	−.831	−.763	−.753	−.752	OOXXO	
	XXOXO	.831	.935	.952	.954	OOXOX	
	XXOXX	.296	.463	.500	.504+1	OOXOO	
	XXXOO	.500	.648	.678	.681	OOOXX	
	XXXOX	−.043	.187	.244	.252+1	OOOXO	
	XXXXO	1.603	1.917	2.000	2.014+1	OOOOX	
	XXXXX	.893	1.329	1.465	1.496+1	OOOOO	
		X	XX	XXX	XXXX	Second Part of Series	
		−k for Series Whose First Part is					

For what concerns the second case, so when the second part of the sequence contains more than 5 tests, the following formula must be used:

$$\sigma_{lim} = \frac{\sum_{i=1}^{N} \sigma_i}{N} + \frac{\Delta\sigma}{N} \cdot (A \cdot C)$$

where, as in the first case, "σ_{lim}" is the estimation of the fatigue limit of the material at which the 50% of the specimens will break. Considering N' the total number of tests composing a sequence, N is the total number of tests reduced by one less than the number of like responses at the beginning of the series. Consider the following series as example:

OOOXXOXO;

in this case N'=8 and N=6 (N is equal to the number of tests of the second part of the series plus one). In the formula are present also the sum of the last N levels "σ_i" tested in the sequence and the interval "$\Delta\sigma$". "A" and "C" are two coefficients provided by Dixon that are related to the last N responses of the series and can

be retrieved using the following table, where "n_O" and "n_X" are respectively the number of "O" and "X" responses present in the final N trials. When the first part of the sequence is composed by one response only ("X" or "O"), the coefficient "C" is equal to zero.

Table 21 - Table for retrieving the coefficients "A" and "C"

$n_o - n_x$	A	C for Test Series Whose First Part is			
		00	000	0000	00000
5	10.8	0	0	0	0
4	7.72	0	0	0	0
3	5.22	.03	.03	.03	.03
2	3.20	.10	.10	.10	.10
1	1.53	.16	.17	.17	.17
0	0	.44	.48	.48	.48
−1	−1.55	.55	.65	.65	.65
−2	−3.30	1.14	1.36	1.38	1.38
−3	−5.22	1.77	2.16	2.22	2.22
−4	−7.55	2.48	3.36	3.52	3.56
−5	−10.3	3.5	4.8	5.2	5.3
		XX	XXX	XXXX	XXXXX
$n_x - n_o$	$-A$	−C for Test Series Whose First Part is			

In this second case the "Dixon method" provides an estimation of the standard error equal to $\hat{\sigma} \cdot \sqrt{\frac{2}{N}}$.

In both cases the standard error can be calculated using the following formula:

$$std.\,error = \sqrt{\frac{\sum_{i=1}^{N}(\sigma_i - \sigma_{lim})^2}{N}}$$

Then can be used to retrieve the standard deviation "$\hat{\sigma}$" using its estimate in accordance with the type of sequence analysed.

4.4.2   Test's execution and analysis

For all the tests the same machine and the same parameters have been used in order to reduce as much as possible the variability of the results.

Figure 139 - Machine for the rotating bending fatigue test

The load applied on the bottom part of the machine generates a bending stress on the specimen and the rotation provided by the spindle transforms it in a rotating bending stress. The way in which the load is applied to the two spindles allows to have a constant bending moment along the specimen, so the highest stress is reached in the centre part, were the cross-section is smaller.
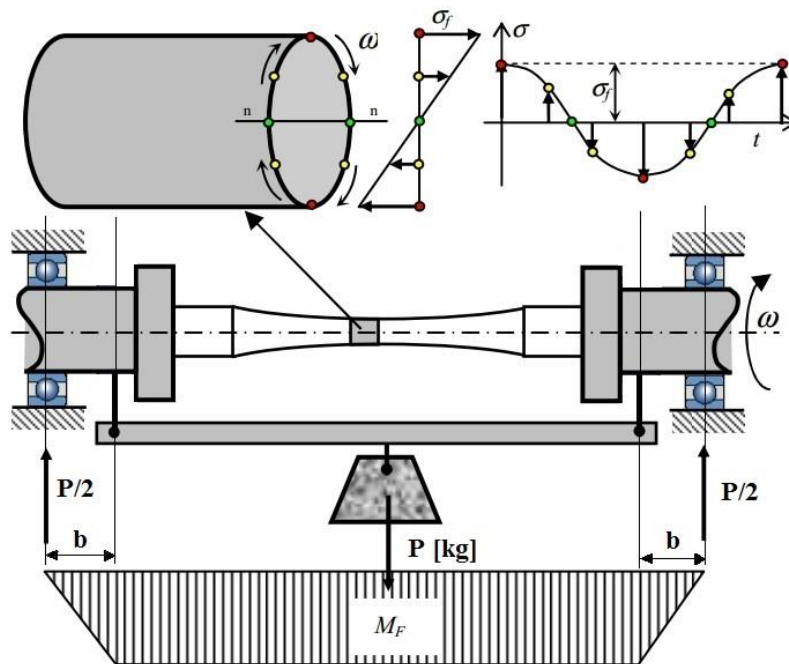
Figure 140 - Schematic of the machine

Once the stress that has to be applied to the specimen is known, the load that has to be carried on the machine can be calculated using the dimension of the smaller cross-section obtained from the measurements of the diameter carried out using the profilometer.

The following formulae have been used in order to calculate the load "P" for all the specimens:

- $\sigma_f = \dfrac{M_f}{w_f}$; $M_f = \dfrac{P \cdot g \cdot b}{2}$; $w_f = \dfrac{J \cdot 2}{d} = \dfrac{\pi \cdot d^3}{32}$

- $P = \dfrac{\sigma \cdot \pi \cdot d^3 \cdot 2}{b \cdot 32 \cdot g}$

Where:

- σ_f is the modulus of the alternated applied stress [MPa];
- M_f is the bending moment [MPa];
- J is the moment of inertia of the smaller cross section [mm⁴];
- d is the mean diameter of the specimen in correspondence of its smaller cross-section [mm];
- b is a characteristic measure of the machine [mm].

After the determination of all the parameters, the test can start, but here comes the most difficult part of the procedure, the assembly of the specimen on the machine.

Each specimen was initially positioned in both the spindles of the machine inserting it for almost all the length of the two external cylindrical part of the sample, then the spindles were tightened only by hand. In this condition a comparator was applied to one of the spindles in order to measure the eccentricity of the sample making it rotate at the minimum possible speed. The eccentricity was considered acceptable with a value lower than 0,05 mm, in that a large value of eccentricity could cause large vibrations during the test affecting the results.

In order to reach an acceptable value of eccentricity, the specimens have been dismounted from the spindle and rotated in respect to it, repeating the operation till reaching a good value. After fixing a side of the specimen, the same operation has been carried out on the other spindle. Once the correct eccentricity has been reached on both hands, the spindles were tightened using two appropriated wrenches.

Figure 141 - Comparator applied to the spindle

All the assembling operations were carried out without applying any load to the specimen, including the reaching of the determined rotating speed. The rotating speed has been set at 3000 rpm, only when the machine reached this value the calculated load was applied to the specimen, in order to avoid any vibration that could be generated during the transitory phase. The load consists of calibrated disks that allows to obtain a precision of a gram mounted on a pulley system provided by an unloading frame that have been used in order to apply all the load at the same time. After the application of the load, the cycle counter has to be reset and so the test starts.

Figure 142 - Load applied to the machine

As anticipated before, the test ends in two different cases, when the cycle counter reaches the number of cycles set as limit for the specimen or with the breakage of the specimen, that determines the stop of the machine thanks to a switch actuated by the free spindle itself.
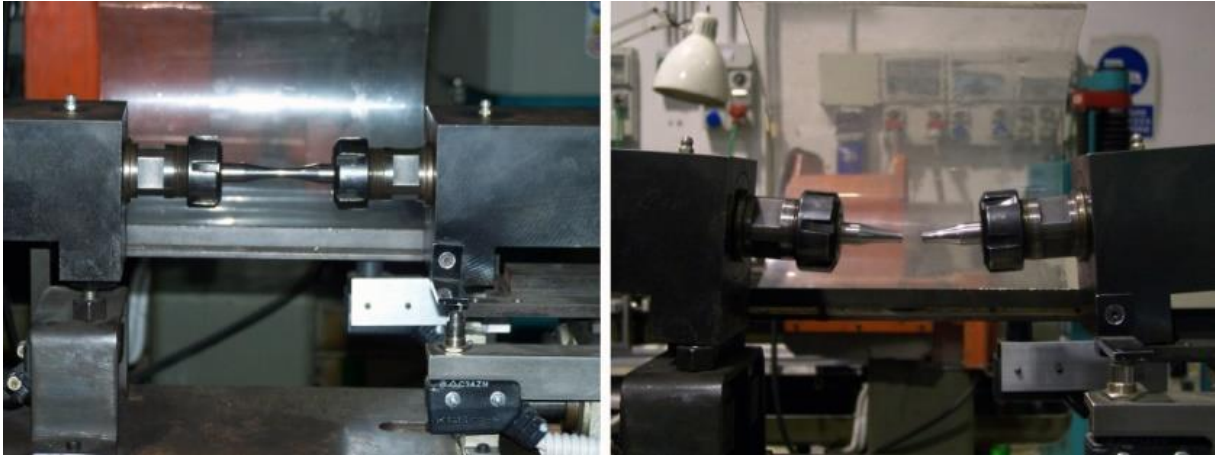
Figure 143 - Specimen on the machine: unbroken (left); broken (right)

For all the tests, the rotating speed has been set at 3000 rpm and the limit at $3x10^6$ cycles, so a test resulting in an unbroken specimen lasted 16,5 hours. Particular attention is needed also during the dismounting phase in case of broken specimen, in fact, unloading the machine, the two spindles tend to return in their initial position and the contact between the two fracture surfaces must be avoided in order to preserve them for the subsequent analysis.

Let's now analyse the results obtained from the tests for each material separately. In the following tables are reported also the principal data regarding the specimens and the parameters adopted during the tests. The order used in the tables is that in which the tests were carried out, reporting the exact sequences used for the "UP and DOWN" method to retrieve the results.

Table 22 - Rotating bending fatigue results for the material S235JR

Specimen	Material	d [mm]	Rm [MPa]	Δσ [MPa]	P [Kg]	σ [MPa]	rpm	O-X	Cycles	%Rm	A	C	σlim
F1A	S235JR	5,9096			8,796	298	3000	O	3000000	0,55			
F2A	S235JR	5,9684			9,669	318	3000	X	2191319	0,59			
F3A	S235JR	5,8702			8,621	298	3000	X	512958	0,55			
F5A	S235JR	5,8554	542	20	7,982	278	3000	O	3000000	0,51	3,2	0	311,1
F6A	S235JR	5,8064			8,343	298	3000	O	3000000	0,55			
F7A	S235JR	5,9298			9,482	318	3000	X	1780599	0,59			
F8A	S235JR	5,857			8,563	298	3000	O	3000000	0,55			
F4A	S235JR	5,895			9,317	318	3000	O	3000000	0,59			

The sequence obtained for the S235JR steel was "O|XXOOXOO" in which N=N'=8, so the second method proposed by Dixon have been used. So, from the coefficients "A" and "C" have been retrieved from the provided table.

$$\sigma_{lim} = \frac{\sum_{i=1}^{N} \sigma_i}{N} + \frac{\Delta\sigma}{N} \cdot (A \cdot C) = 311\ MPa \cong 0,57 \cdot \sigma_{UTS}$$

In order to calculate the standard deviation of the result, the RRSME must be calculated and then equated to the estimation for the standard error provided by Dixon. the specimens considered are the last N of the sequence, but in this case N=N'=8.

$$RRSME = \sqrt{\frac{\sum_{i=1}^{N}(\sigma_i - \sigma_{lim})^2}{N}} = 15,46 \ MPa$$

$$std.dev. = \hat{\sigma} = \frac{RRSME}{\sqrt{\frac{2}{N}}} = 30,92 \ MPa$$

The indication "LD$_{50}$" referred to "σ_{lim}" stays for "lethal dose for 50% of the specimens tested", so the fatigue limit calculated is an estimation of the applied stress that would bring to the fracture of the specimen with a probability equal to 50%.

The same procedure was used for all the materials under test.

Table 23 - Rotating bending fatigue results for the material S355J2

Specimen	Material	d [mm]	Rm [MPa]	Δσ [MPa]	P [Kg]	σ [MPa]	rpm	O-X	Cycles	%Rm	A	C	σlim
F1B	S355J2	5,8558			12,342	430	3000	X	270669	0,55			
F2B	S355J2	5,8004			11,437	410	3000	X	395988	0,52			
F4B	S355J2	5,7612			10,66	390	3000	O	3000000	0,50			
F5B	S355J2	5,6696	782	20	10,681	410	3000	X	534214	0,52	-1,53	-0,16	385,1
F6B	S355J2	5,8534			11,18	390	3000	X	954635	0,50			
F7B	S355J2	5,7108			9,85	370	3000	O	3000000	0,47			
F8B	S355J2	5,8254			11,02	390	3000	X	1058972	0,50			
F3B	S355J2	5,8252			10,454	370	3000	O	3000000	0,47			

The series for the S355J2 steel was "XX|OXXOXO", so N=7 and again the second method have been used.

$$\sigma_{lim} = \frac{\sum_{i=1}^{N}\sigma_i}{N} + \frac{\Delta\sigma}{N} \cdot (A \cdot C) = 385 \ MPa \cong 0,49 \cdot \sigma_{UTS}$$

$$RRSME = \sqrt{\frac{\sum_{i=1}^{N}(\sigma_i - \sigma_{lim})^2}{N}} = 15,87 \ MPa$$

$$std.dev. = \hat{\sigma} = \frac{RRSME}{\sqrt{\frac{2}{N}}} = 29,69 \ MPa$$

Considering the free-cutting steels, the idea was that the manganese sulphides present in the material would act as initiation points for the cracks on the surface of the specimens, lowering the fatigue limit of the material. For this reason, the first material of this kind was used as a test in order to check this intuition, starting from an initial value of the applied stress lower than the 50% of the maximum value of stress obtained in the tensile test. The starting value was fixed at 40% of the "σ_{UTS}", but the specimens didn't break till reaching a value higher than the 50% discarding the initial hypothesis.

Table 24 - Rotating bending fatigue results for the material 11SMn30

Specimen	Material	d [mm]	Rm [MPa]	Δσ [MPa]	P [Kg]	σ [MPa]	rpm	O-X	Cycles	%Rm	k	σlim
F1C	11SMn30	5,8318			6,605	233	3000	O	3000000	0,40		
F3C	11SMn30	5,8194			7,126	253	3000	O	3000000	0,43		
F5C	11SMn30	5,8172			7,681	273	3000	O	3000000	0,47		
F6C	11SMn30	5,8594	582	20	8,425	293	3000	O	3000000	0,50	0,741	308
F7C	11SMn30	5,8088			8,769	313	3000	X	1973034	0,54		
F8C	11SMn30	5,845			8,363	293	3000	O	3000000	0,50		
F2C	11SMn30	5,848			8,948	313	3000	X	1263874	0,54		
F4C	11SMn30	5,8132			8,227	293	3000	O	3000000	0,50		

The obtained series for the 11SMn30 steel was "OOOO|XOXO" in which N=5, so the first method proposed by Dixon have been used. In this case the load applied to the last specimen of the sequence must be used as "σ_f" and the coefficient "k" has to be retrieved from the provided table.

$$\sigma_{lim} = \sigma_f + k \cdot \Delta\sigma = 308 \ MPa \cong 0,53 \cdot \sigma_{UTS}$$

Using this method, the RRSME must be calculated considering all the trials of the sequence and equated to its estimation provided in the table, so $0,61 \cdot \hat{\sigma}$.

$$RRSME = \sqrt{\frac{\sum_{i=1}^{N}(\sigma_i - \sigma_{lim})^2}{N}} = 11,94 \ MPa$$

$$std.dev. = \hat{\sigma} = \frac{RRSME}{0,61} = 19,57 \ MPa$$

The test carried out on the 11SMn30 steel demonstrated that a free-cutting steel behaves in the same way as a structural steel, having the fatigue limit about the 50-55% of the maximum reached tensile stress, for this reason with the other materials the starting stress was maintained about this value, in order to reach as soon as possible the change in the trend.

Table 25 - Rotating bending fatigue results for the material 11SMn37

Specimen	Material	d [mm]	Rm [MPa]	Δσ [MPa]	P [Kg]	σ [MPa]	rpm	O-X	Cycles	%Rm	A	C	σlim
F1D	11SMn37	5,9192			8,7	293	3000	O	3000000	0,48			
F2D	11SMn37	5,9448			9,414	313	3000	O	3000000	0,51			
F3D	11SMn37	5,8946			9,763	333	3000	X	1599515	0,55			
F4D	11SMn37	5,9018	611	20	9,211	313	3000	O	3000000	0,51	1,53	0,16	332,5
F5D	11SMn37	5,9342			9,961	333	3000	X	2350479	0,55			
F6D	11SMn37	5,8798			9,108	313	3000	O	3000000	0,51			
F7D	11SMn37	5,9582			10,082	333	3000	O	3000000	0,55			
F8D	11SMn37	5,9664			10,731	353	3000	X	437692	0,58			

The sequence resulting for the 11SMn37 steel was "OO|XOXOOX" for which N=7, so returning to the second method "A" and "C" have been retrieved from the provided table.

$$\sigma_{lim} = \frac{\sum_{i=1}^{N}\sigma_i}{N} + \frac{\Delta\sigma}{N} \cdot (A \cdot C) = 332 \ MPa \cong 0,54 \cdot \sigma_{UTS}$$

$$RRSME = \sqrt{\frac{\sum_{i=1}^{N}(\sigma_i - \sigma_{lim})^2}{N}} = 14,8 \, MPa$$

$$std. \, dev. = \hat{\sigma} = \frac{RRSME}{\sqrt{\frac{2}{N}}} = 27,69 MPa$$

Table 26 - Rotating bending fatigue results for the material 11SMnPb30

Specimen	Material	d [mm]	Rm [MPa]	Δσ [MPa]	P [Kg]	σ [MPa]	rpm	O-X	Cycles	%Rm	A	C	σlim
F1E	11SMnPb30	5,8484			8,575	300	3000	O	3000000	0,50			
F2E	11SMnPb30	5,8586			9,195	320	3000	X	1999431	0,53			
F3E	11SMnPb30	5,8802			8,716	300	3000	O	3000000	0,50			
F4E	11SMnPb30	5,8756	600	20	9,276	320	3000	X	2450895	0,53	3,2	0	323
F5E	11SMnPb30	5,796			8,347	300	3000	O	3000000	0,50			
F6E	11SMnPb30	5,8684			9,242	320	3000	O	3000000	0,53			
F7E	11SMnPb30	5,8498			9,727	340	3000	X	832859	0,57			
F8E	11SMnPb30	5,8954			9,37	320	3000	O	3000000	0,53			

The series obtained for the 11SMnPb30 steel was "O|XOXOOXO", so N=N'=8 as in the first case.

$$\sigma_{lim} = \frac{\sum_{i=1}^{N}\sigma_i}{N} + \frac{\Delta\sigma}{N} \cdot (A \cdot C) = 323 \, MPa \cong 0,54 \cdot \sigma_{UTS}$$

$$RRSME = \sqrt{\frac{\sum_{i=1}^{N}(\sigma_i - \sigma_{lim})^2}{N}} = 14,79 \, MPa$$

$$std. \, dev. = \hat{\sigma} = \frac{RRSME}{\sqrt{\frac{2}{N}}} = 29,58 MPa$$

Table 27 - Rotating bending fatigue results for the material 11SMnPb37

Specimen	Material	d [mm]	Rm [MPa]	Δσ [MPa]	P [Kg]	σ [MPa]	rpm	O-X	Cycles	%Rm	A	C	σlim
F1F	11SMnPb37	5,9422			9,219	307	3000	O	3000000	0,50			
F2F	11SMnPb37	5,9182			9,7	327	3000	O	3000000	0,53			
F3F	11SMnPb37	5,9548			10,485	347	3000	X	936465	0,57			
F4F	11SMnPb37	5,956	615	20	9,887	327	3000	X	1820784	0,53	-1,55	0,55	327,3
F5F	11SMnPb37	5,8656			8,867	307	3000	O	3000000	0,50			
F6F	11SMnPb37	5,9516			9,865	327	3000	O	3000000	0,53			
F7F	11SMnPb37	5,9544			10,482	347	3000	X	642948	0,57			
F8F	11SMnPb37	5,8484			9,36	327	3000	X	872335	0,53			

The last series, that obtained for the 11SMnPb37 steel was "OO|XXOOXX", so N=7.

$$\sigma_{lim} = \frac{\sum_{i=1}^{N}\sigma_i}{N} + \frac{\Delta\sigma}{N} \cdot (A \cdot C) = 327 \, MPa \cong 0,53 \cdot \sigma_{UTS}$$

$$RRSME = \sqrt{\frac{\sum_{i=1}^{N}(\sigma_i - \sigma_{lim})^2}{N}} = 13,09 \, MPa$$

$$std. \, dev. = \hat{\sigma} = \frac{RRSME}{\sqrt{\frac{2}{N}}} = 24,49 MPa$$

In conclusion, considering the fatigue limit in respect to the maximum tensile stress, the behaviour between different materials is very similar and looking at the limits retrieved for the free-cutting steels demonstrate that the presence of lead doesn't affect the resistance of the material nether in this kind of test.

4.4.3 Macroscopic analysis of the fractures

The fracture surfaces generated by a fatigue test must be firstly analysed by eyes, because the light helps a lot in recognizing the two main part of the fracture. In fact, the part appearing smooth and plane represents the growing of the crack, this area presents a higher and more uniform reflection of the light appearing shiny, while the zone characterised by a darker colour, due to the less uniform reflection of the light, presents the final and sudden brittle rupture of the cross-section.

The macroscopic analysis allows to detect if the expansion of these two areas respects the applied load or if any defect has affected the result. Considering a load higher than the fatigue limit, the specimen would reach the fracture in less cycles, determining a smaller growth of the crack and so a wider area subjected to the sudden rupture. Usually, the macroscopic analysis of the fracture surface allows also to detect the position of the initiation point of the crack and the point of intersection between different fracture planes if any.
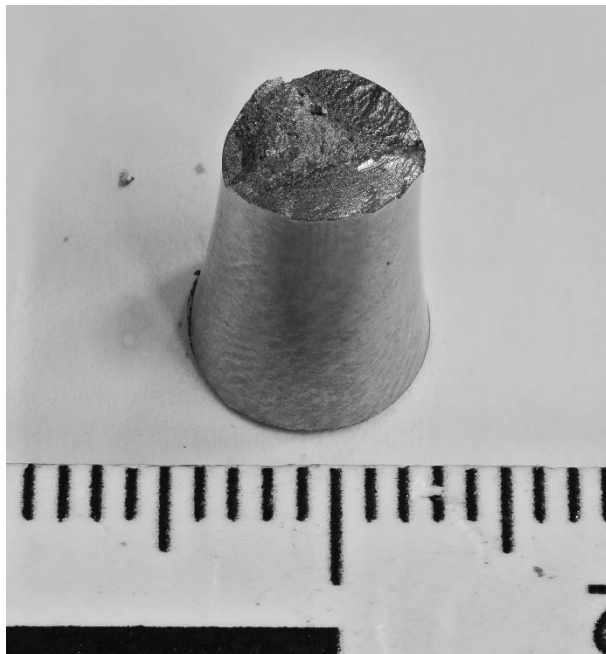

Figure 144 - Fracture surface of specimen F6B (S355J2)

In the above figure it is possible to see a fracture in which there is only one plane of growing of the crack (on the right), easily distinguishable from the final fracture part (on the left). This is due to the fact that the entity of the applied load was very near to the value of the fatigue limit found for this material. For this reason, the fracture starts from only one initiation point and propagates till reaching a dimension larger enough to bring the specimen to its breakage. In the next picture a specimen of the same series is reported, but in this case the applied load was very high, and this allowed every little defect present on the surface to behave as initiation point for a crack. This is the reason why the surface presents a lot of plane intersections, that represent the point in which two cracks, laying on different planes, encounter each other.

102

Figure 145 - Fracture surface of specimen F1B (S355J2)

Another example of this effect can be observed in the next figure, that present a wider propagation area on the right-bottom part of the cross-section and a smaller propagation area on the left. The final rupture happened in the almost in the centre of the specimen, while on the upper-right part there is a zone presenting some feature of both behaviours, so presenting very small propagation of some cracks, but with a part that breaks suddenly presenting some sharpen crests.

*Figure 146 - Fracture surface of specimen F7E (11SMnPb37)*

For all the specimens, the exact position of the initiation points cannot be identified due to the fact that the defect from which starts the crack is too small and there are not the beach-marks on the surface due to the fact that the test is carried out without any stops.

4.4.4 Microscopic analysis of the fractures

As for the other tests, the SEM was used to acquire images of the surfaces at different magnifications. The microscopic analysis on this kind of fractures revealed that all the materials under study are very deformable in fact, in the propagation zone of the cracks, where the two sides of the fracture hit continuously one against the other during the test, the material was completely pressed and it was impossible to see its structure presenting a classic brittle behaviour. The two following figures show an example of this feature detectable for all the other samples, in figure 149 it is possible to see the initiation point of the crack.
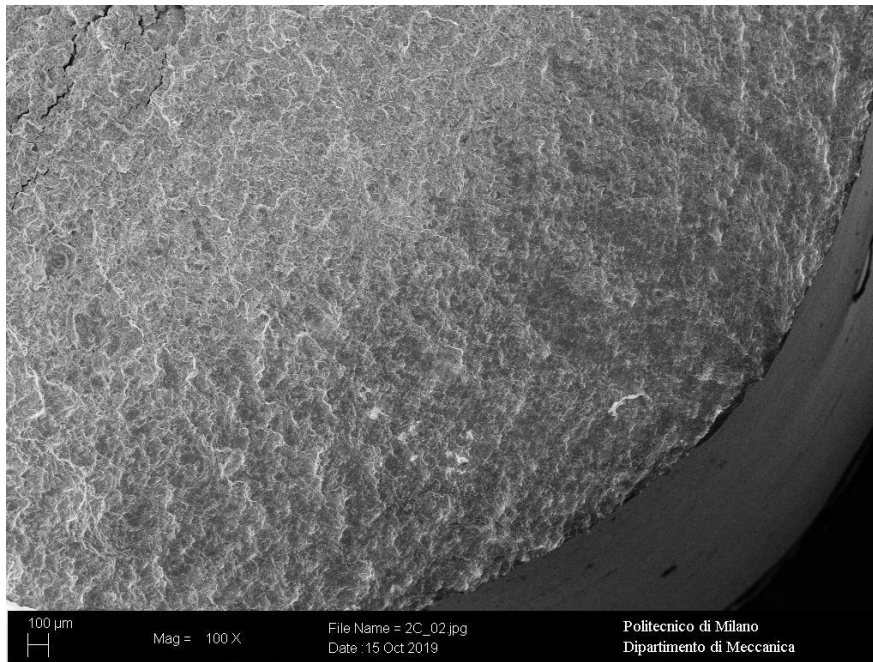

Figure 147 - 11SMn30 specimen 100X
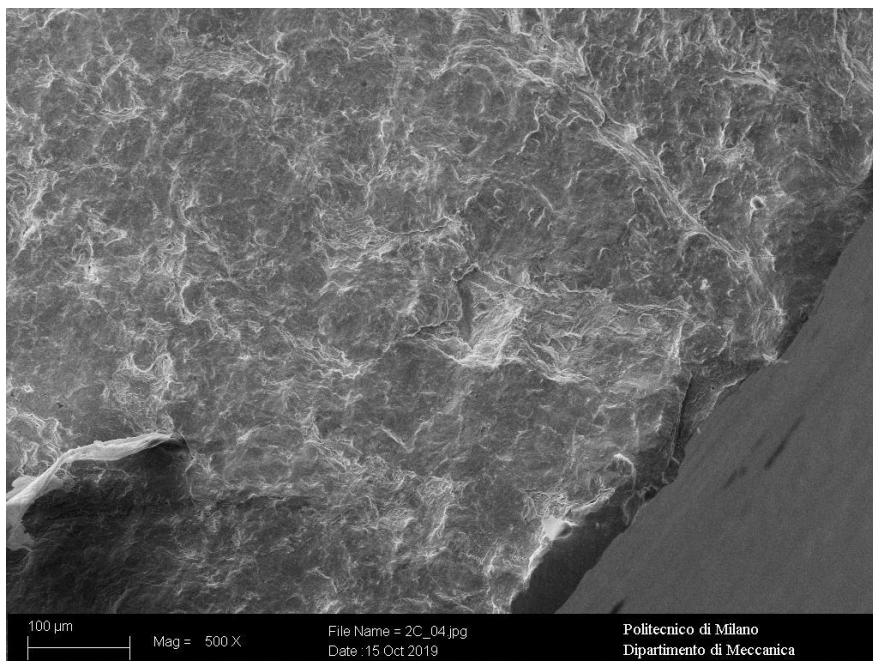
Figure 148 - 11SMn30 specimen 500X

The microscopic analysis carried out on the final resistant part of the section, so that subjected to the sudden breakage, showed the ductile behaviour of the materials. In fact, all the materials present dimples in this zone as noticed also in the fractures obtained with the other tests, but here they are very regular in shape and dimensions due to the type of fracture that doesn't allow the sliding of the material.
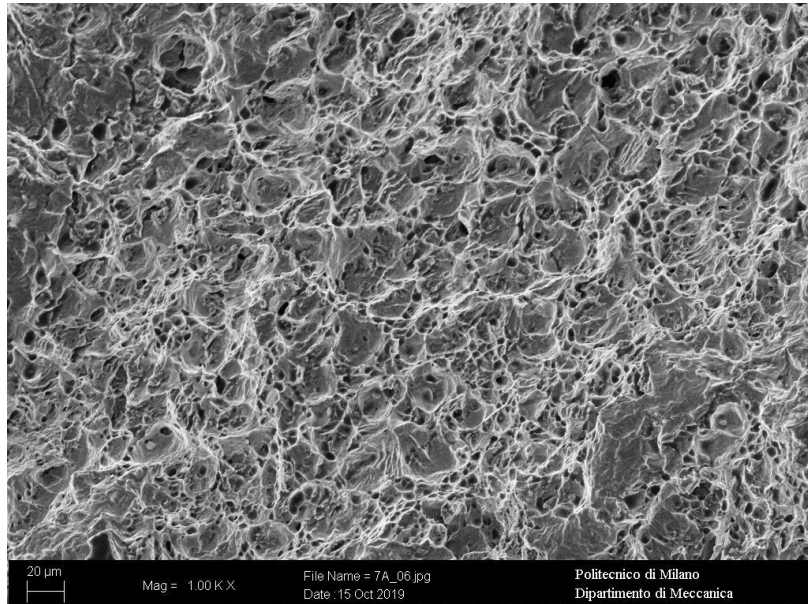

*Figure 149 - Dimples in the fracture of specimen F7A (S235JR) 1000X*
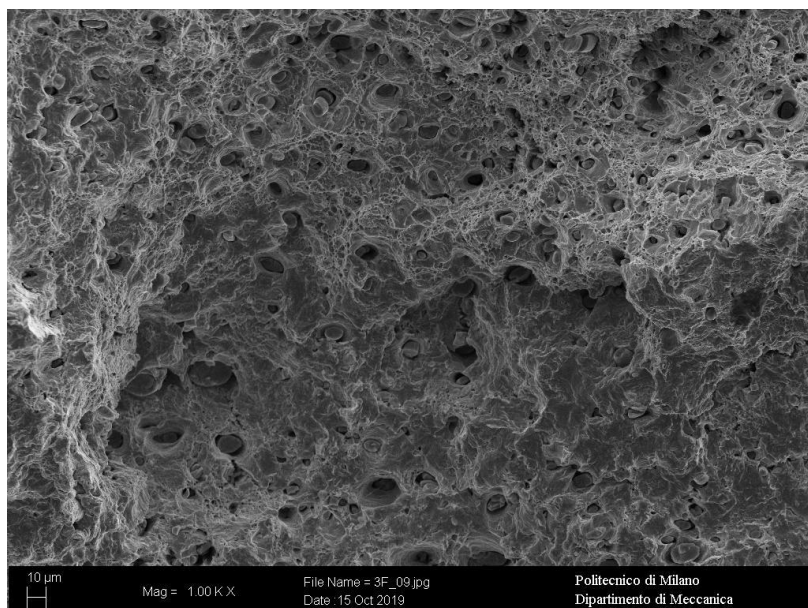
Figure 150 - Dimples in the fracture of specimen F3F (11SMnPb37) 1000X

In figure 151 it is possible to see manganese sulphides present in the dimples of the material and in the following figure it is possible to notice how the fracture acted also on these compounds breaking them in a very sharpen way, due also to their brittleness.
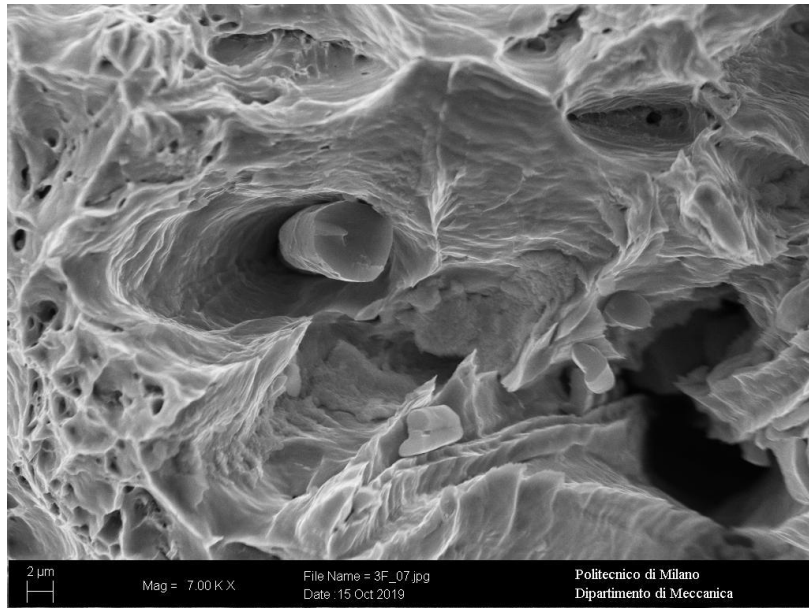
Figure 151 - Detail of a broken manganese sulphide 7000X

The same pic acquired in backscattered modality reveals the presence of lead near the manganese sulphide as noticed in the other tests.
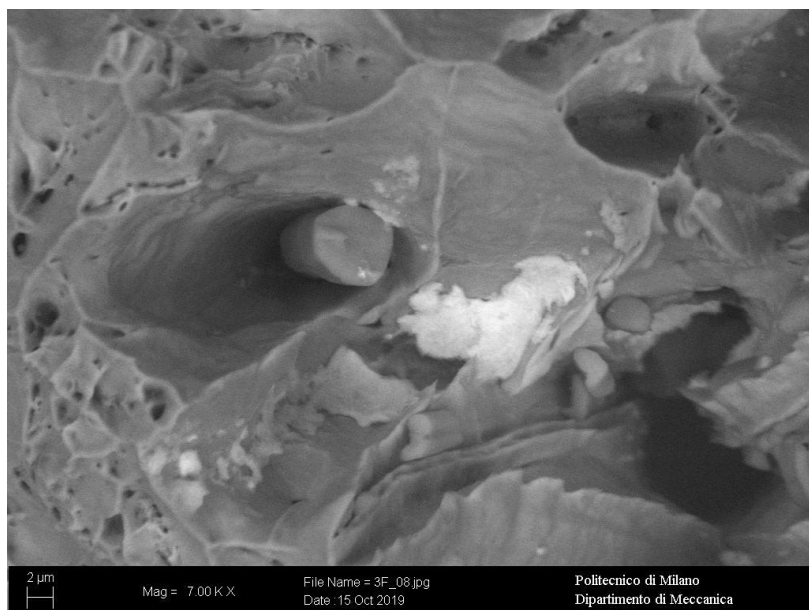
Figure 152 - Detail of a broken manganese sulphide with lead 7000X (backscattered)

4.5 Vickers hardness test

For each material the hardness has been measured on the same samples created and used for the metallographic analysis following the standard UNI EN ISO 6507 in the laboratory of Politecnico di Milano. In order to obtain a better estimation of the value, 10 measurements were carried out both on the orthogonal and longitudinal plane of the original bars. The test takes the name of micro-hardness Vickers test due to the very small load applied to the penetrator and in consequence to the small mark obtained. In this case the penetrator, that is made from diamond, has a pyramidal shape with a square base and an angle at the top of 136°. This test exploits the dimensions of the diagonals of the square mark left on the specimen in respect to the applied load in order to calculate the hardness of the material following this formula:

$$HV = \frac{P \cdot 0{,}102 \cdot 9{,}81}{\dfrac{d^2}{2 \cdot \sin\left(\dfrac{136}{2}\right)}}$$

where "P" is the applied load expressed in kg and "d" is the arithmetic mean of the diagonals measured on the material in millimetres, while 0,102 is a constant used in this calculation and 9,81 is the gravity acceleration.
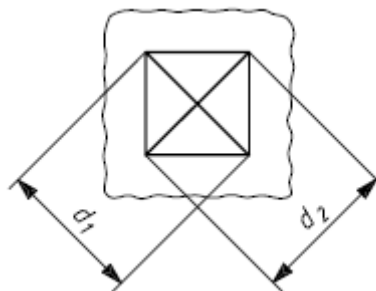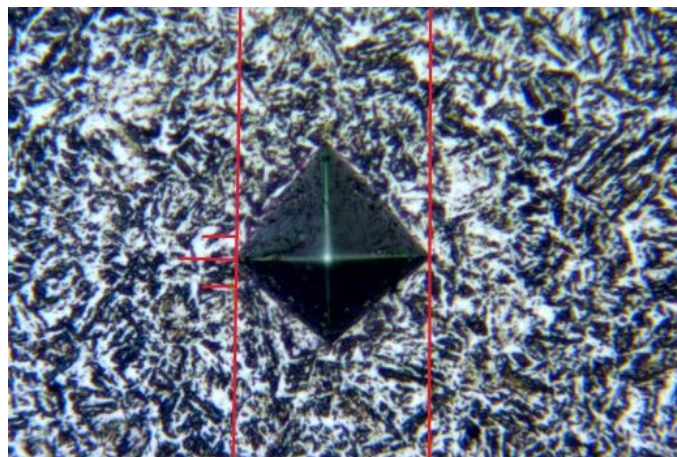

Figure 153 - Schematic of a mark left during a Vickers hardness test

The durometer used to execute this test calculates itself the hardness value, the only data that it needs are the applied load, that must be set by a selector, and the measure of the diagonals, that must be measured by an ocular viewer provided of an electronic measuring system. The procedure starts switching on the durometer, then the load must be selected, and the specimen can be positioned on the clamp of the machine. Once the specimen has been clamped, it is possible to focus its surface using the microscope of which is provided the machine, increasing time to time the magnification in order to better individuate the correct position on which the test will be carried out, for this reason, the machine is also provided with two micrometric screws that allow to move the specimen with high accuracy. Once the specimen has been correctly positioned the test can be carried out pushing the starting button, in this way the durometer automatically selects the penetrator in respect to the set load and press it against the specimen. Once the test is finished, the durometer will automatically return to the "microscope modality", allowing the measurement of the diagonals through the ocular viewer. The electronic system of this machine allows to measure the distance between two parallel lines present in the ocular viewer that can be moved thanks to a screw and aligned with the vertex of the mark left

on the surface, obtaining so the length of a diagonal. Pressing a button, the measure of this distance is stored in the durometer and giving it also the second one, it automatically returns the value of hardness of the material following the formula reported above.

Figure 154 - Durometer for Vickers hardness tests

Figure 155 - Example of a mark left during a Vickers hardness test

Due to the very small dimensions of the mark, the place in which the test is done assume a very important role, because when the material presents two or more different structures, the risk of carrying out the measure of the hardness of one of this structure instead of the whole material is high. For this reason, the test must be done involving all the possible structures present (e.g. the manganese sulphides present in the free-cutting steels are very hard in respect to ferrite).

The measurements have been taken along all the two sections, from the external part to the centre in order to compensate the strain hardening suffered by the bars during cold drawing operations.

Table 28 - Vickers hardness test results

Specimen	1	2	3	4	5	6	7	8	9	10	HV	std.dev.
A-long	179	196	189	191	192	197	191	193	200	186	191	5,64
A-orth	183	193	198	195	197	195	210	190	191	194	195	6,53
B-long	266	251	230	242	237	223	241	246	228	236	240	11,82
B-orth	253	254	227	231	282	265	252	260	238	255	252	15,52
C-long	196	213	200	200	233	208	200	211	204	199	206	10,33
C-orth	224	208	212	212	207	198	212	212	208	202	210	6,59
D-long	205	222	219	210	201	215	208	213	213	213	212	5,92
D-orth	210	214	223	212	211	214	208	214	221	219	215	4,65
E-long	210	224	201	209	209	217	204	209	226	224	213	8,41
E-orth	204	218	212	214	205	220	221	225	217	210	215	6,55
F-long	214	216	217	205	207	207	218	208	220	222	213	5,83
F-orth	222	221	223	220	227	225	228	233	211	230	224	5,85

In the above table the results obtained are reported, keeping the coding used for the material under study. All the results have been rounded to the nearest integer, the mean value "HV" and its standard deviation "$\hat{\sigma}$" have been calculated for both the directions (orthogonal and longitudinal) for each material.

It is visible that values are almost constant among measures taken in different points and in different directions, as indicated also by low standard deviations, so materials properties were not highly affected by strain hardening due to cold drawing operations.

The obtained results follow the same order of those obtained with the tensile tests, the harder material is the S355J2 steel, due to its higher carbon content and so to a higher percentage of pearlite in the structure in respect to ferrite (pearlite shows higher mechanical properties). The free-cutting steel show more or less the same hardness, that is higher than that showed by the S235JR steel due to the presence of manganese sulphides in the structure that are very hard.

It is normal to obtain a correspondence between the results of this test and those retrieved by the tensile tests, in fact it also possible to obtain an estimation of the maximum tensile stress "σ_{UTS}" of a material starting from its hardness calculated in "HV". The procedure is very simple because there is direct proportionality between these two values:

$$\sigma_{UTS} \cong K \cdot HV \quad where \ 3 < K < 3,3$$

5 Conclusions

The tests carried out during this work have been chosen in order to retrieve the principal mechanical properties of the materials under study. The tensile test allowed to define the ultimate tensile stress and the yielding stress; two fundamental parameters widely used for designing purposes. The Charpy pendulum test provided the transition curve of each material; a very important information in order to understand the behaviour of the material at different temperatures. By means of the rotating bending fatigue test, it was possible to retrieve the fatigue limit of the materials; a crucial property for mechanical applications, where the components are usually subjected to alternated stresses. The Vickers hardness test allowed to calculate the hardness of different materials, checking also their state in terms of strain hardening after plastic deformation applied to the bars during production processes. In the table below are reported the principal results obtained during this work.

Table 29 - Summary table

Material	R_m [MPa]	R_{P02} [MPa]	$KV_{20°C}$ [J]	DBTT [°C]	σ_{lim_f} [MPa]	HV
S235JR	542	517	149	$10 \div 0$	311	193
S355J2	782	640	154	$-10 \div -20$	385	246
11SMn30	582	545	12	$45 \div 35$	308	208
11SMn37	611	584	13	$50 \div 30$	332	213
11SMnPb30	600	565	17	$40 \div 20$	323	214
11SMnPb37	615	577	20	$40 \div 20$	327	218

Looking at the obtained results, it is clear that the great differences between the structural and the free-cutting steels derive from the presence of sulphur. The results obtained by the tensile tests show that in static applications the free-cutting steels have performances that are similar to those of a structural steel with a low carbon content, reaching values of stress comparable and even higher in respect to those of the S235JR steel. This can be mainly a consequence of the high content of manganese that helps to compensate the low percentage of carbon but can also depend in part from a higher level of strain hardening due to larger deformations applied during production processes. At the same time, the brittleness given to the material by the presence of manganese sulphides affect the resistance of the material in case of dynamic loads, leading to very different values of toughness and to higher DBTTs. This last information is very important to define the field of application of these materials in respect to the behaviour that is needed and the temperature at which the material has to work. From the fatigue test it is evident that the presence of such brittle compounds in the

materials doesn't affect their resistance to alternated loads, in spite of what one might think. The results retrieved from the hardness tests follow the same trend of those derived by the tensile tests, there aren't larger differences between the free-cutting steels and the structural one with the lower content of carbon, while the S355J2 steel shows higher values both in terms of hardness and tensile stresses due to a high percentage of carbon.

The differences between the two kind of materials are due to their chemical composition and respect their different fields of application. Components realised with structural steels must resist mainly to heavy and almost static loads showing a general ductile behaviour, while free-cutting steels are used for little mechanical components mainly used for connections in mass production fields as in case of automobile industries or households appliances, and so that are not subjected to particular states of stress. The presence of manganese sulphides allows to keep high the cutting speed, due to the easier breakage of the produced chips, and low the consumption of the machining tools leading to lower production costs. The presence of lead doesn't seem to affect the results of the tests, so it can be added in order to enhance the machinability of the material as it acts as solid lubricant.

It was not possible to perform fracture's mechanic tests but, like in the Charpy pendulum tests, the presence of manganese sulphides would lead to higher brittleness and so to an easier crack propagation in the free cutting steels in respect to the structural ones.

6 Appendix A
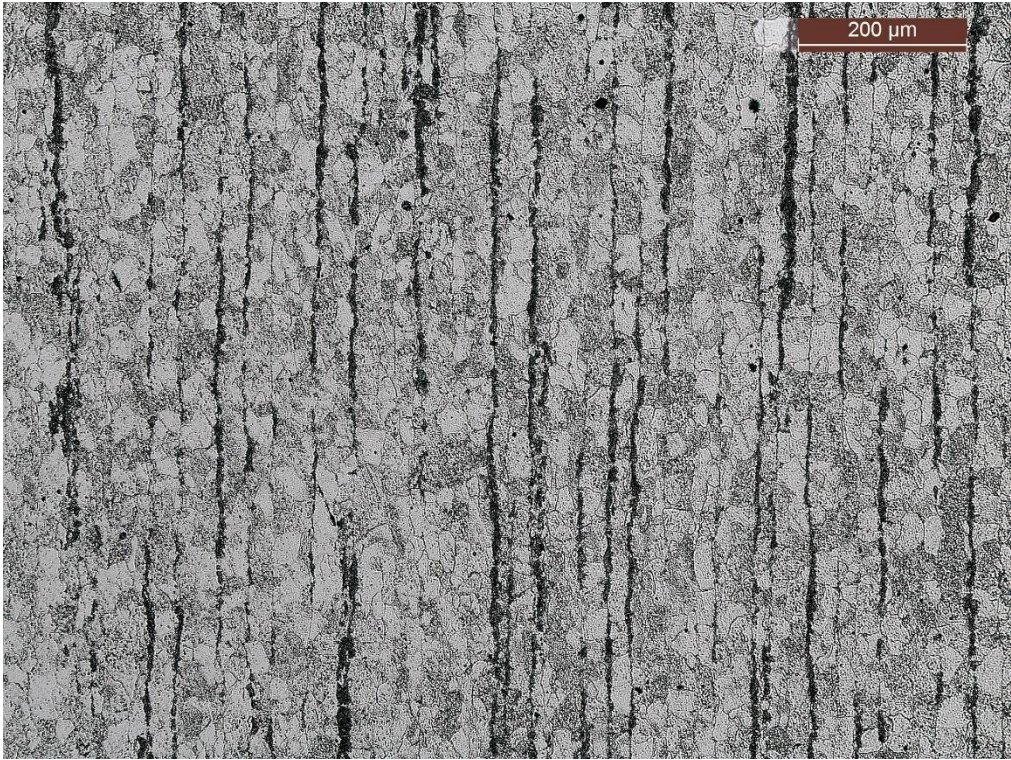
Figure 156 - S235JR longitudinal 100X

Figure 157 - S355J2 longitudinal 100X

Figure 158 - 11SMn30 longitudinal 100X
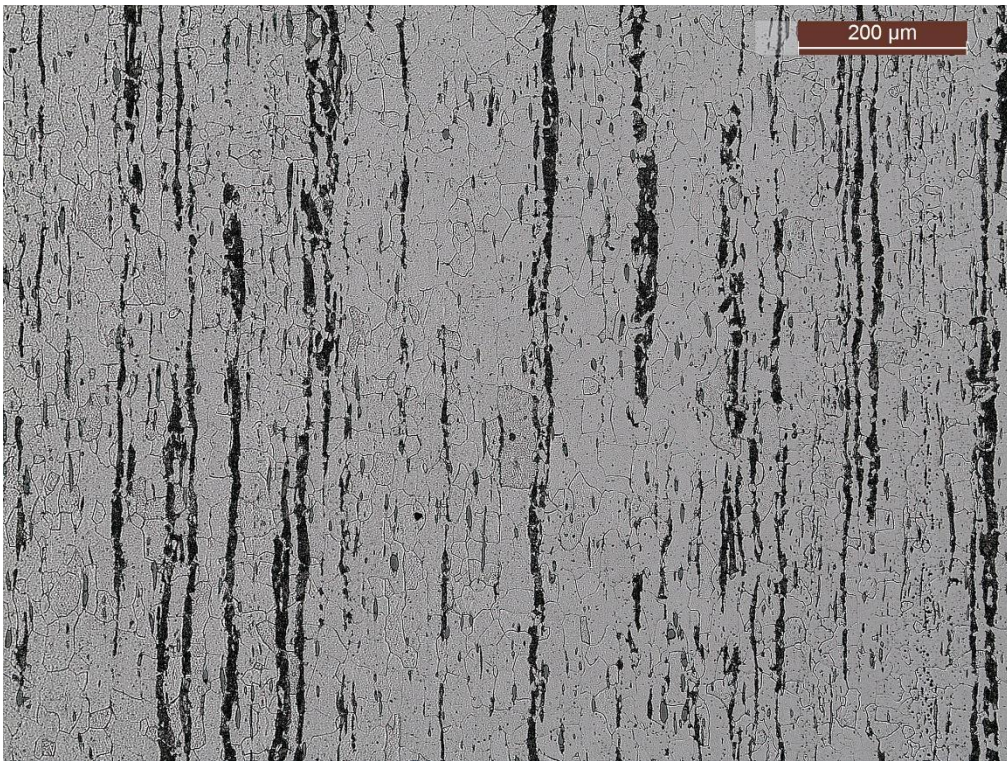
Figure 159 - 11SMn37 longitudinal 100X

116

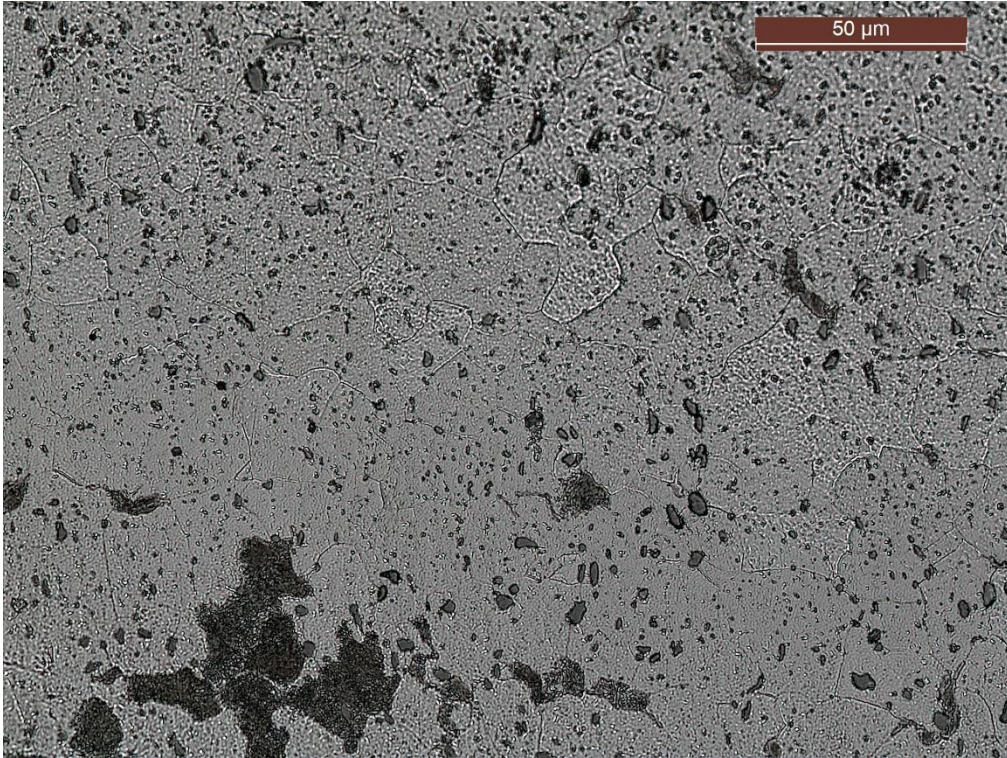*Figure 160 - 11SMnPb30 longitudinal 100X*
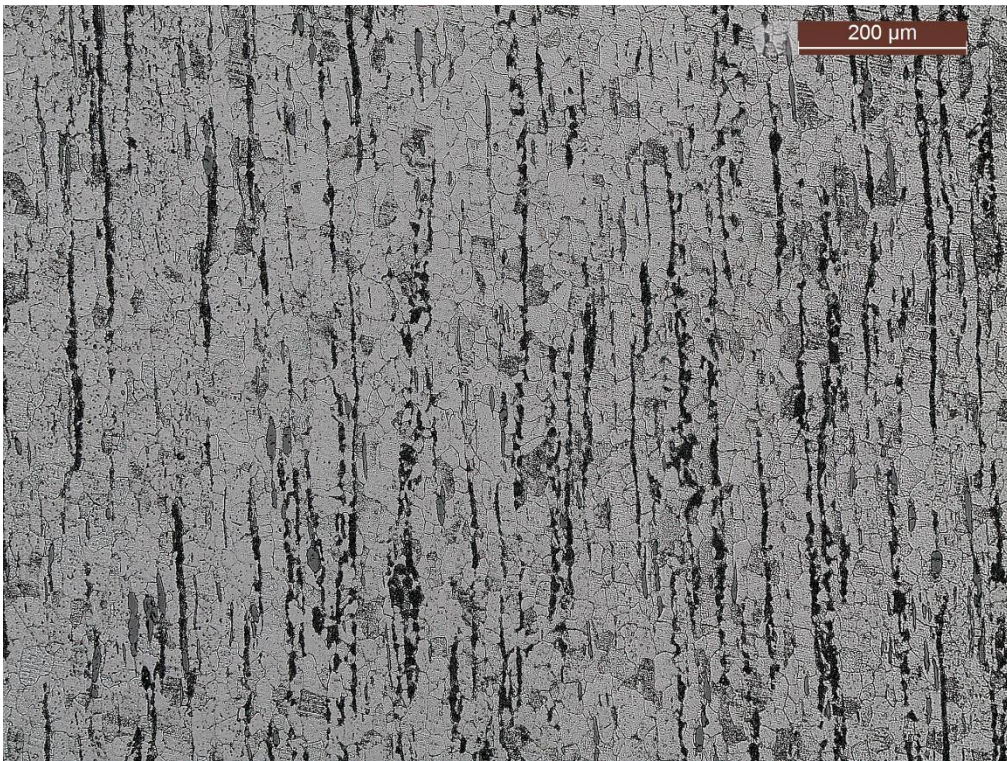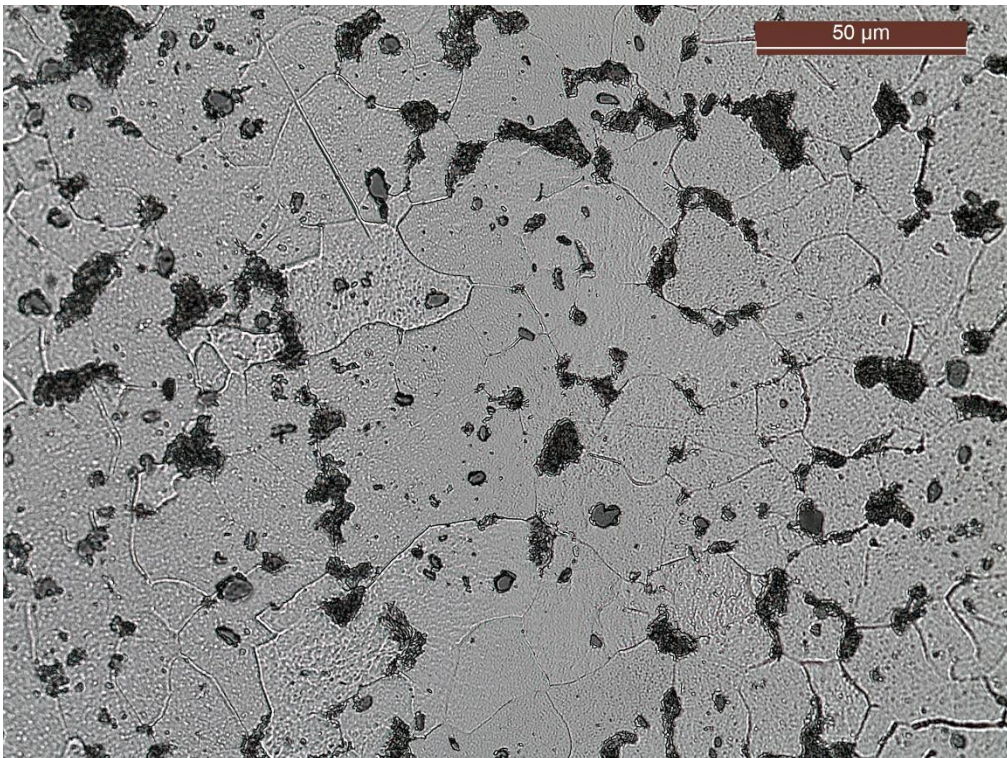

Figure 161 - 11SMnPb37 longitudinal 100X
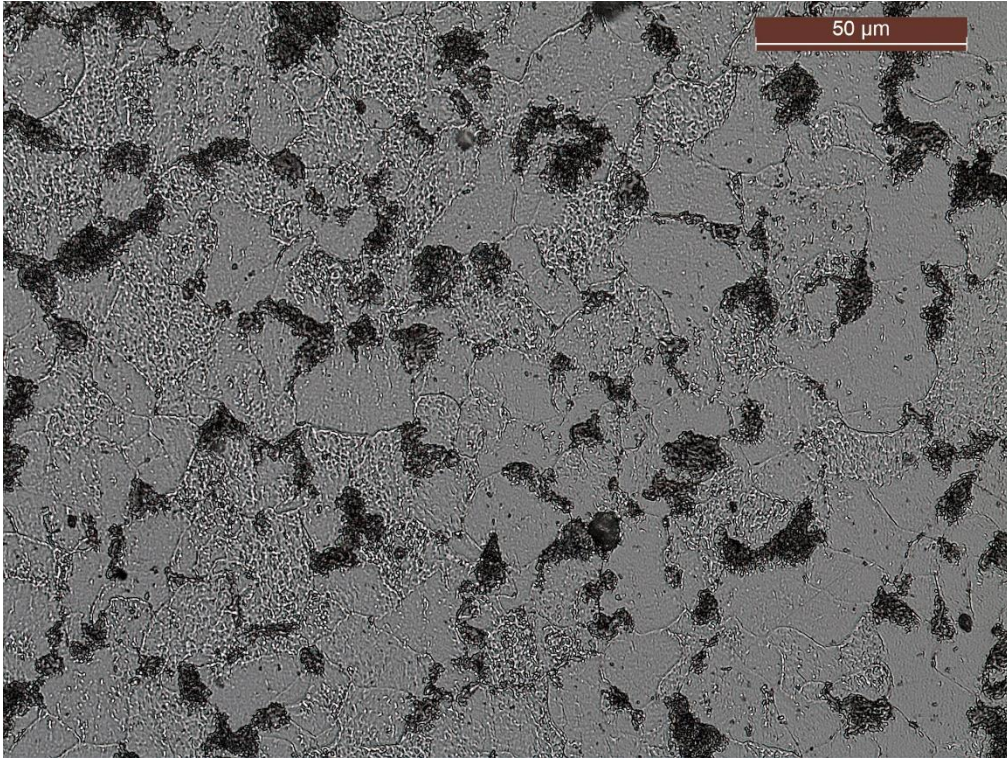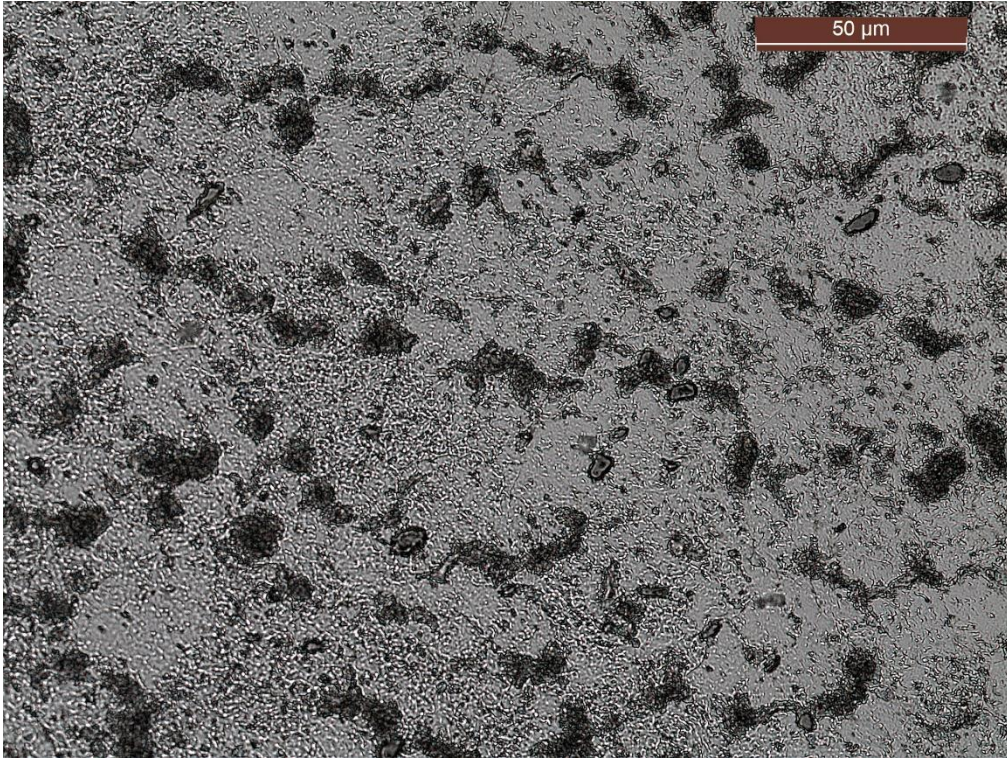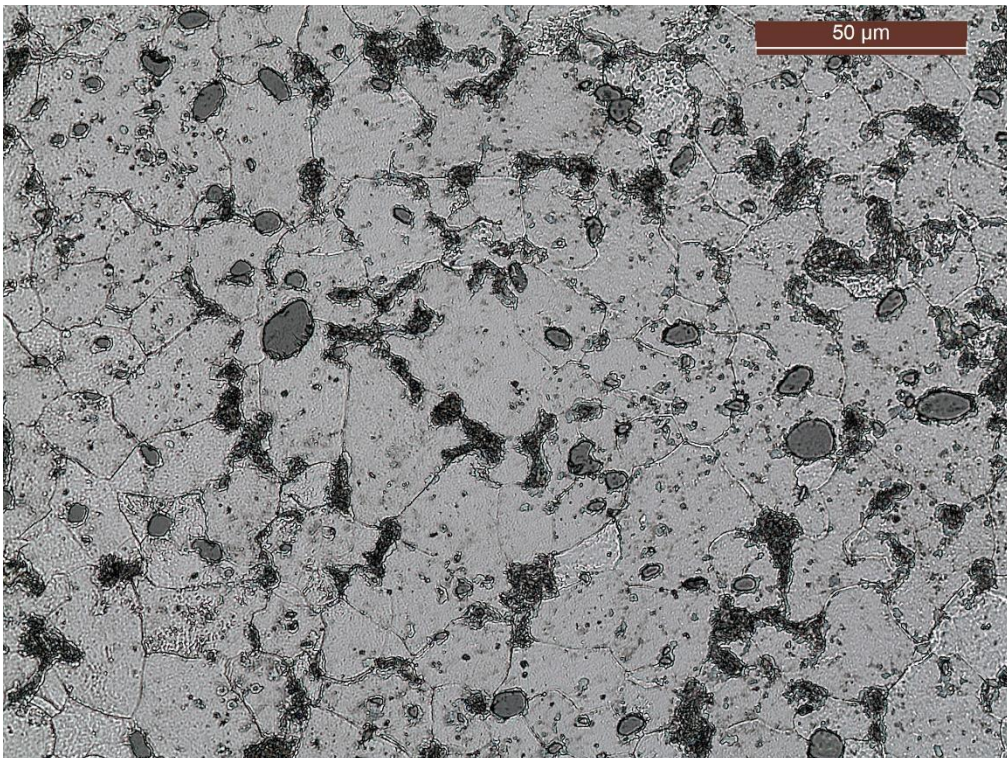
Figure 162 - S235JR transversal 500X
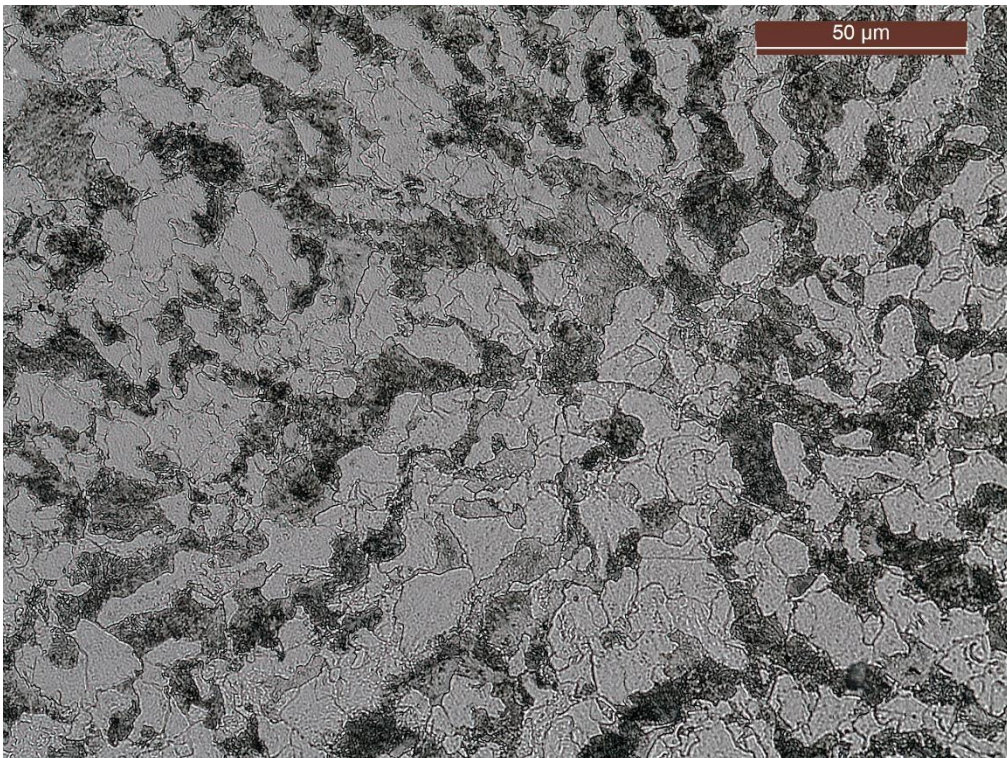
Figure 163 - S355J2 transversal 500X

Figure 164 - 11SMn30 transversal 500X
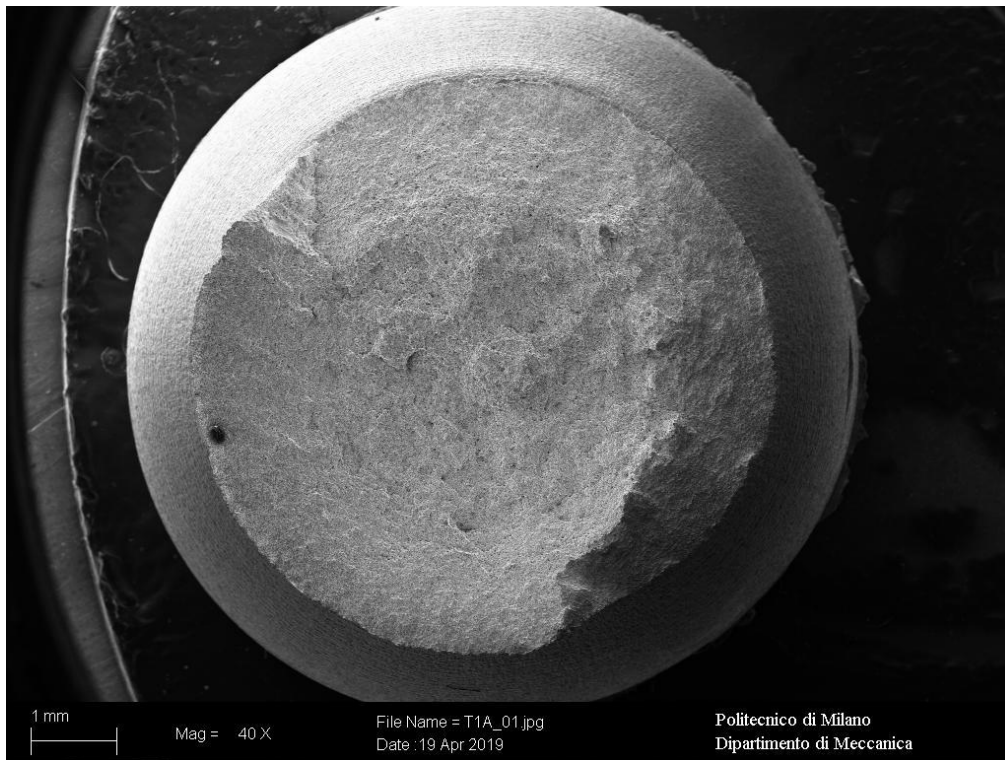

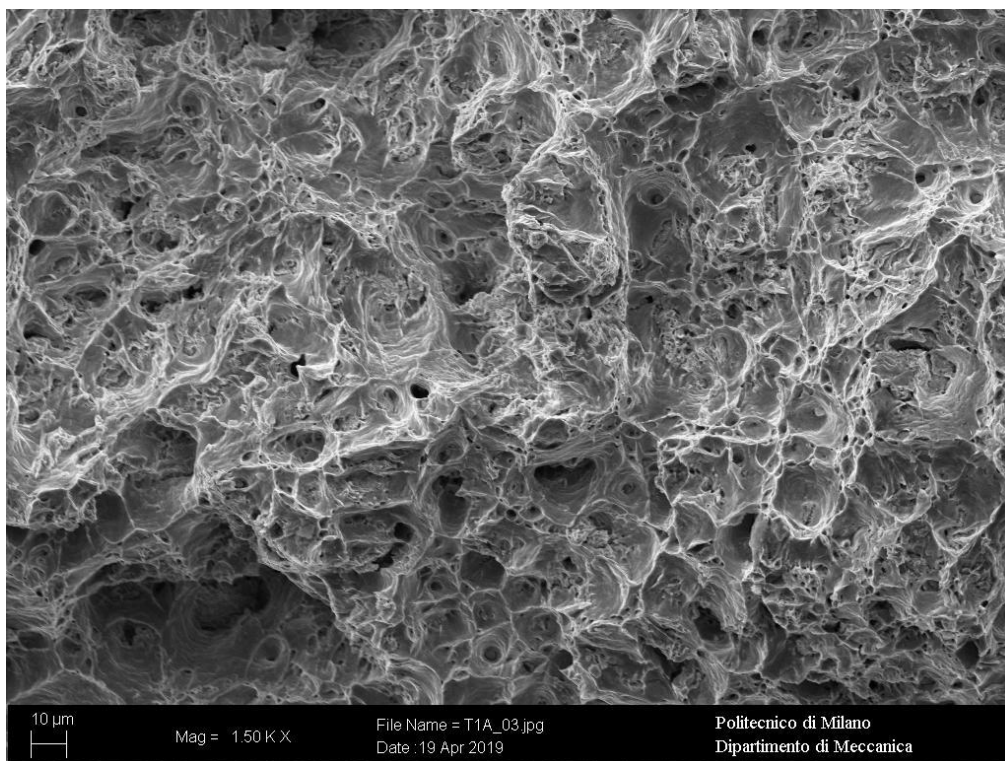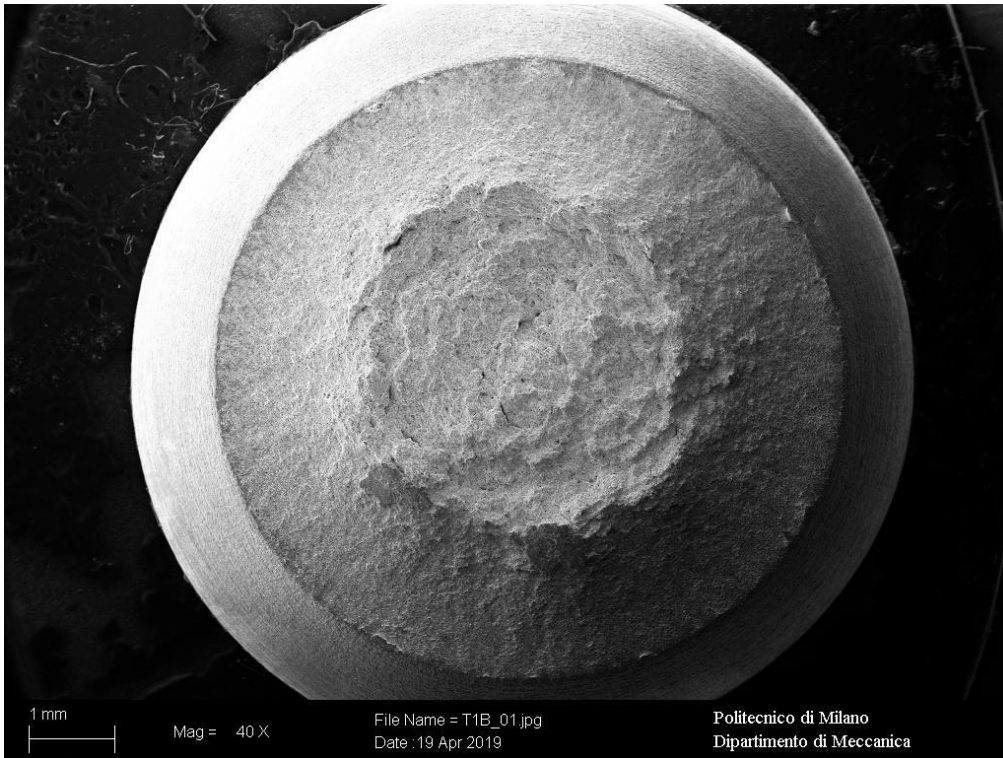*Figure 165 - 11SMn37 transversal 500X*

Figure 166 - 11SMnPb30 transversal 500X

Figure 167 - 11SMnPb37 transversal 500X

120

7 Appendix B

Figure 168 - S235JR tensile test sample 40X

Figure 169 - S235JR tensile test sample 1500X
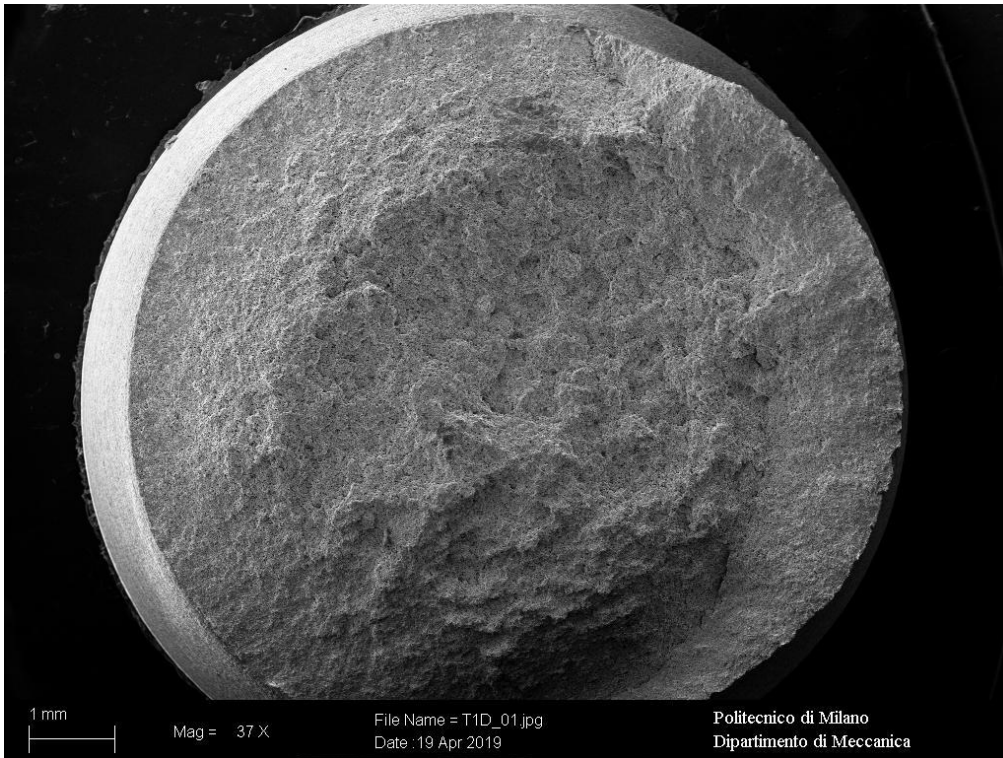
Figure 170 - S355J2 tensile test 40X
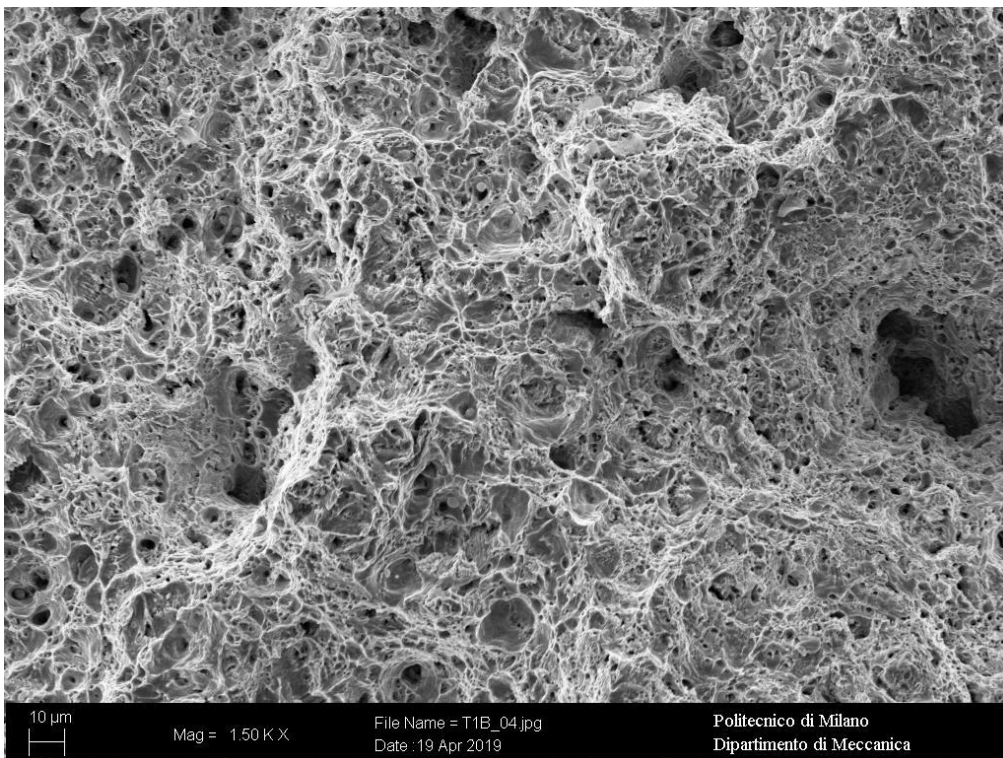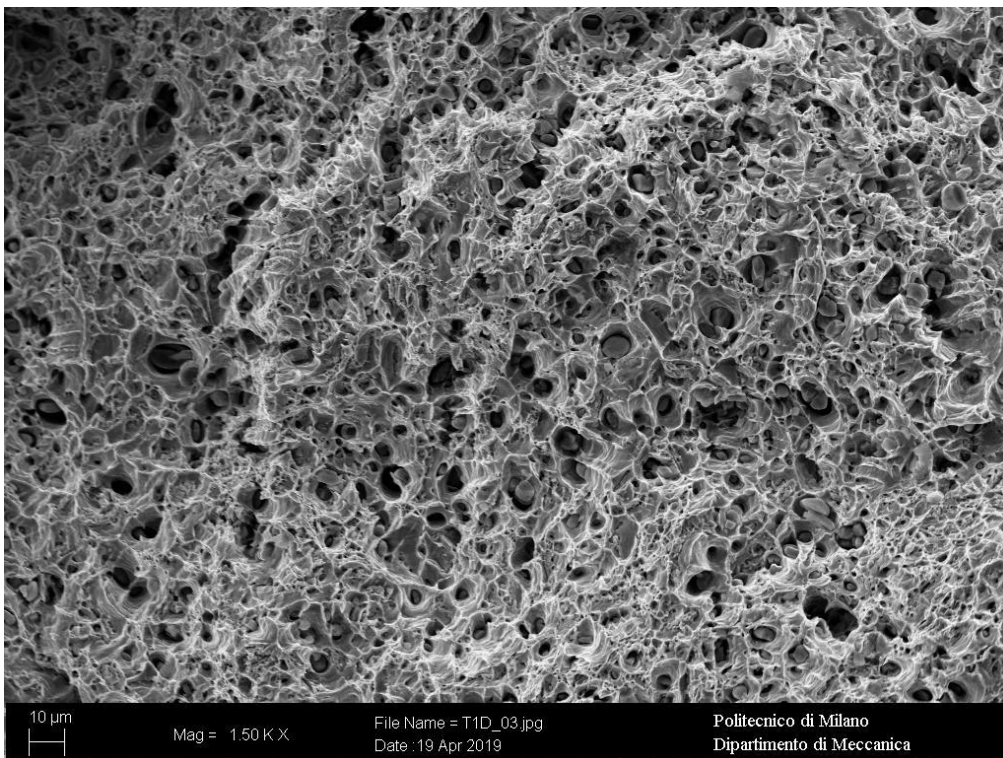

Figure 171 - S355J2 tensile test sample 1500X
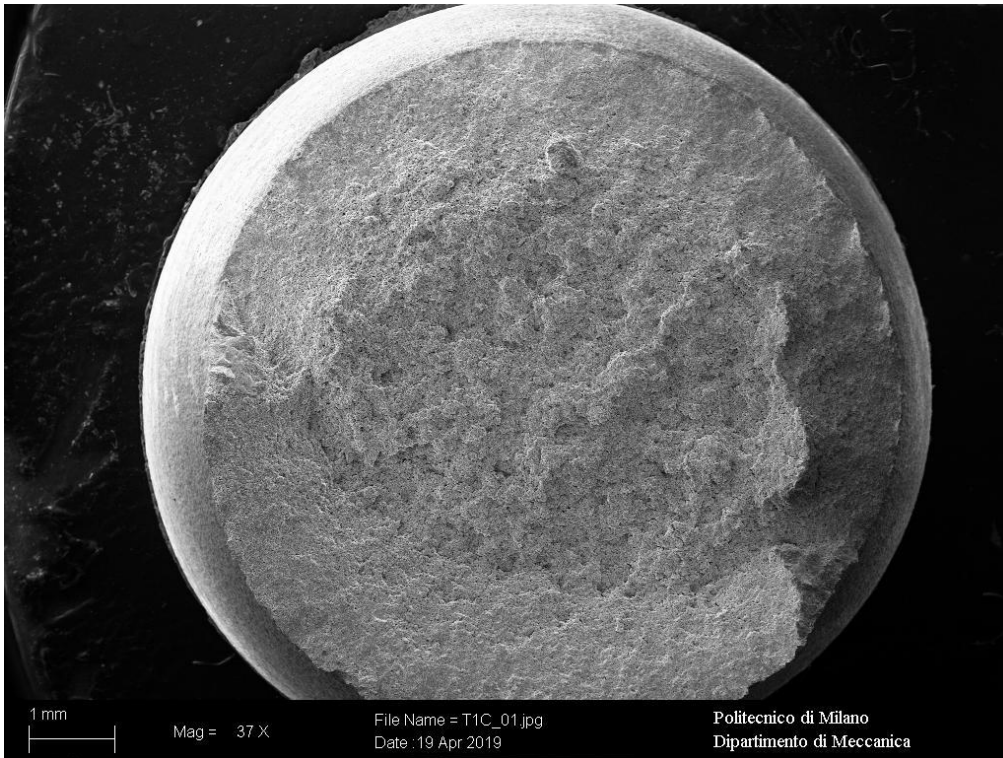
Figure 172 - 11SMn30 tensile test sample 37X
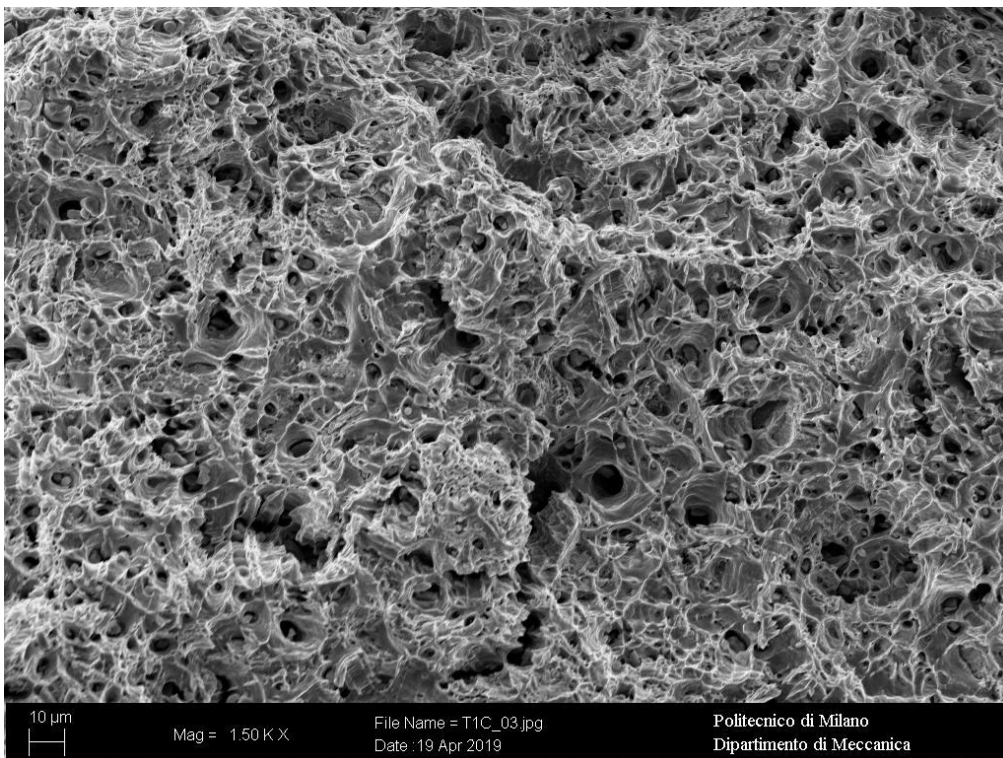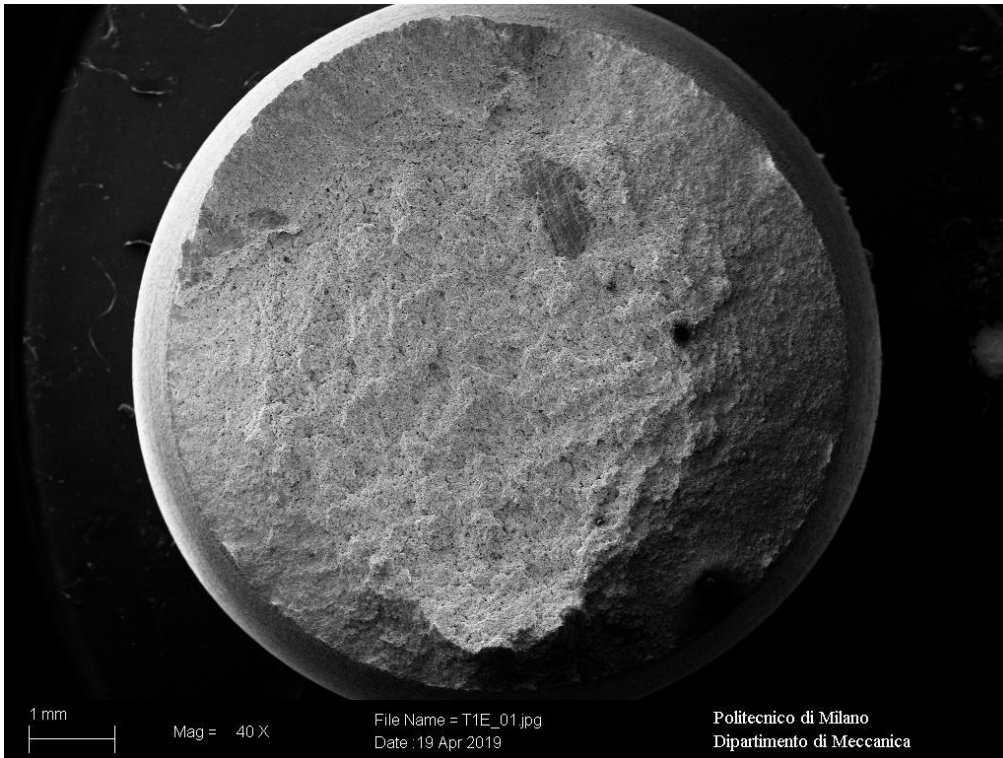

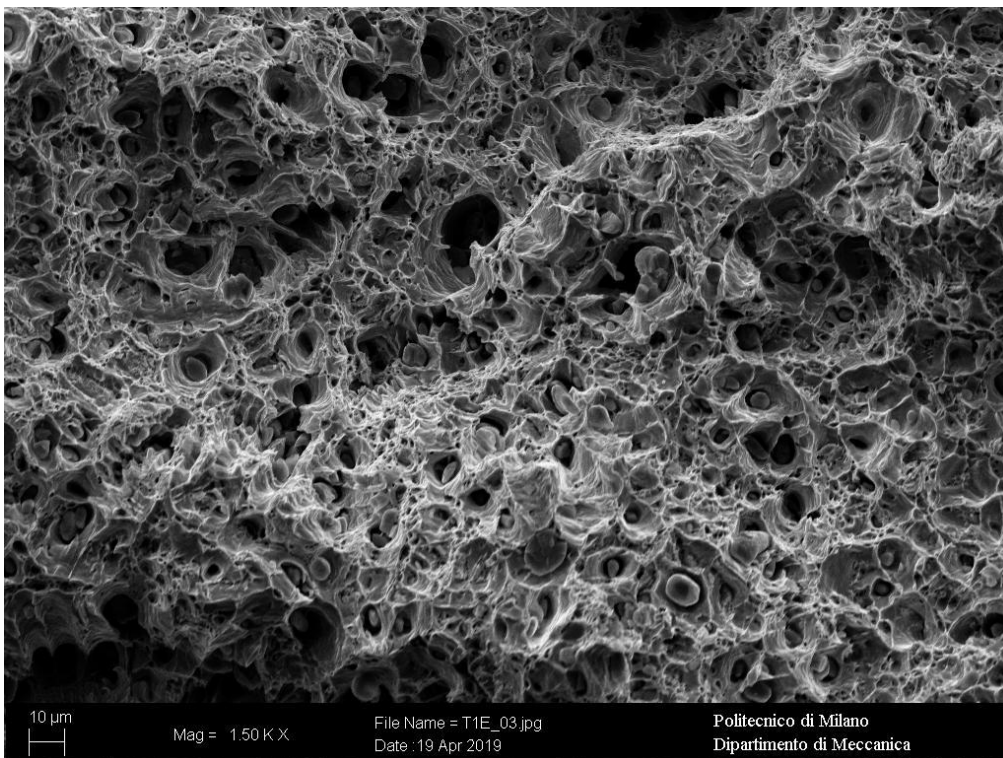*Figure 173 - 11SMn30 tensile test sample 1500X*

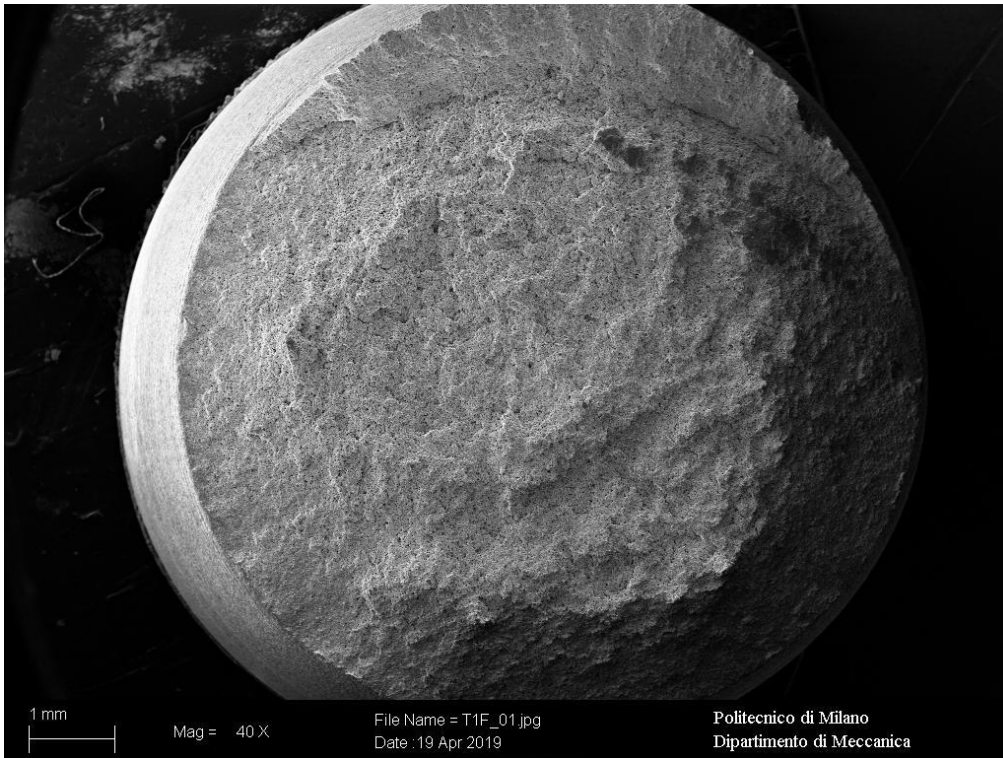*Figure 174 - 11SMn37 tensile test sample 37X*

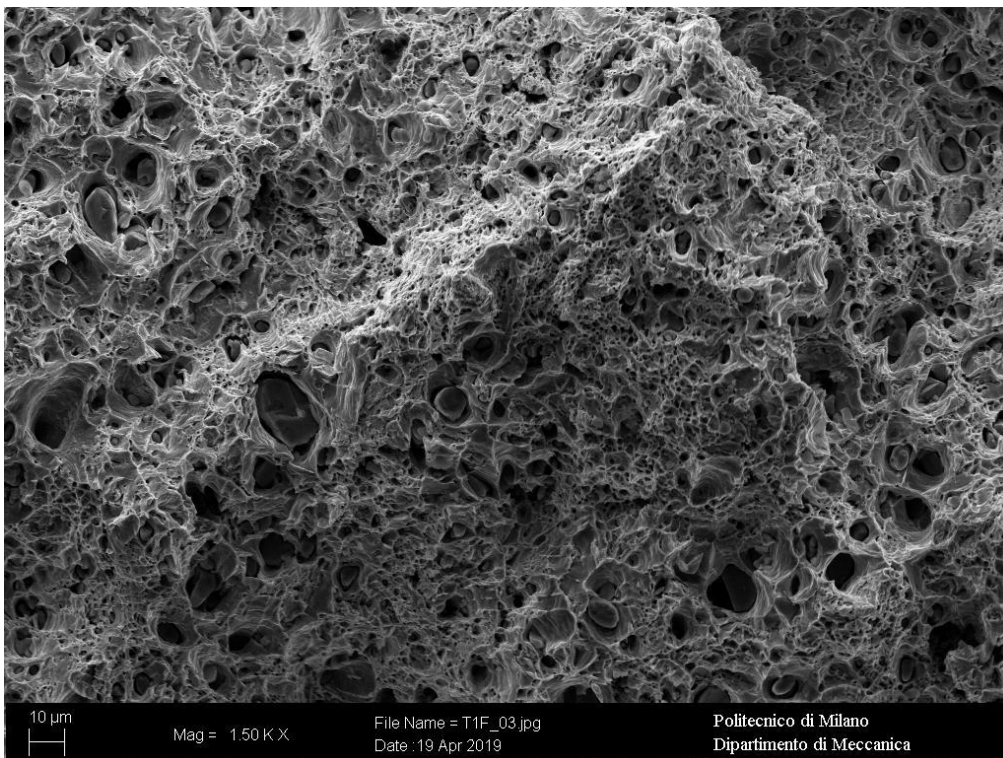*Figure 175 - 11SMn37 tensile test sample 1500X*

Figure 176 - 11SMnPb30 tensile test 40X

Figure 177 - 11SMnPb30 tensile test sample 1500X

Figure 178 - 11SMnPb37 tensile test sample 40X

Figure 179 - 11SMnPb37 tensile test 1500X

8 Bibliography

- *Metallurgia*, W. Nicodemi, Zanichelli, 2000;

- *Acciai e leghe non ferrose*, W.Nicodemi, Zanichelli, 2000;

- *Manuale di meccanica*, L. Caligaris, S. Fava, C. Tomasello, HOEPLI, 2006;

- *Siderurgia*, W. Nicodemi, C. Mapelli;

- *Sistemi di designazione degli acciai*, EN 10027-2006;

- *Design and analysis of experiments*, Douglas C. Montgomery, Eighth edition;

- *Bright steel products - Technical delivery conditions - Part 2: Steels for general engineering purposes*, EN 10277-2-2008;

- *Bright steel products - Technical delivery conditions - Part 3: Free-cutting steels*, EN 10277-3-2008;

- *Metallic materials - Tensile testing - Part 1: Method of test at room temperature*, EN 6892-1-2009;

- *Metallic materials - Charpy pendulum impact test - Part 1: Test method*, EN 148-1-2011;

- *Metallic materials - Rotating bar bending fatigue testing*, ISO 1143-2010;

- *Metallic materials - Vickers hardness test - Part 1: Test method*, EN 6507-1-2006;

- *The Up-and-Down Method for Small Samples*, W. J. Dixon, American statistical association journal, 1965;

- *Lead-free free-cutting steels as modern environmentally friendly materials*, Dragana Živkovića, Nada Štrbaca, Sabahudin Ekinovićb, Edin Begovićb, 2011;

- *Steel and its heat treatment*, Author: Karl-Erik Thelning;

- *Correlation of yield strength and tensile strength with hardness for steels*; E.J Pavlina, ASM International, 2008;